N72-15271

NASA TECHNICAL TRANSLATION NASA TT F-14066

TESTING AT S1.MA FOR BASIC INVESTIGATIONS ON JET INTERACTIONS. DISTRIBUTION OF PRESSURES AROUND THE JET ORIFICE

A. Soullier

Translation of "Essais à S1.MA Pour Recherches de Base Sur Les Interactions de Jet - Répartition des pressions autour de l'orifice du jet," Office National d'Etudes et de Recherches Aerospatiales, Chatillon, Document 1/253 GY, Part No. 1/5, April 1968, 97 pages

CASE FILE COPY

NATIONAL AERONAUTICS AND SPACE ADMINISTRATION
WASHINGTON, D. C. 20546 JANUARY 1972

ABSTRACT: This installment of report 1/253 GY provides findings concerning the distribution of pressures around an orifice through which a jet is discharged perpendicular to a flow.

TABLE OF CONTENTS

		Page
1.	Summary	1
2.	Notations and Conventions	1
3.	Background	3
4.	Testing Goal	3
5.	Identification of Testing Equipment	3
6.	Testing Configuration	4
7.	Methods and Testing Techniques	5
8.	Testing Results	9
9.	Conclusion	12

TESTING AT S1.MA FOR BASIC INVESTIGATIONS ON JET INTERACTIONS DISTRIBUTION OF PRESSURES AROUND THE JET ORIFICE

1. Summary

This installment, 1/5 of report 1/253 GY, provides findings concerning the distribution of pressures on a plate around an orifice through which a jet is discharged perpendicular to a flow. /3*

Installment 3/5 provides the numerical results and installment 2/5 provides the results of measurements carried out in the jet.

Installments 4/5 and 5/5 show the flow visualization of the jet and on the plate around the jet.

2. Notations and Conventions

2.1. Quantities relative to the wind tunnel:

No: number of the measuring point.

pa: atmospheric pressure at the level of the test section axis, in kg/m^2.

pi: stagnation temperature of the wind tunnel, in kg/m^2.

p : static reference pressure, in kg/m^2.

Ti: stagnation temperature of the wind tunnel, in °K.

M : reference Mach number, deduced from pi and p.

$V = M \sqrt{\gamma RT}$: true testing velocity, in m/s.

$\frac{1}{2} \rho V^2 = \frac{1}{2} \gamma p M^2$: kinetic reference pressure, deduced from pi and p, in kg/m^2.

2.2. Quantities relative to the jet: (see installment 2/5) /4

pj: stagnation pressure of the jet, in kg/m^2.

Tj: stagnation temperature of the jet, in °K.

Mj: Mach number of the jet at the discharge orifice, deduced from pj and p.

$Vj = Mj \sqrt{\gamma jRTj}$: velocity of the jet at the discharge orifice, in m/s.

$\frac{1}{2} \rho j V_j^2 = \frac{1}{2} \gamma j p M_j^2$: kinetic pressure of the jet at the discharge orifice, in kg/m^2.

---

* Numbers in the margin indicate pagination in the foreign text.

pt: stagnation pressure at a point of the jet, measured by the total pressure probe of the rake, in kg/m^2.

ps: static pressure at one point of the jet, calculated from measurements taken by the clinometric probe of the rake, in kg/m^2.

$\left(\frac{\rho V^2}{2pt}\right)_j$: kinetic pressure at one point of the jet reduced to pt.

Mn: Mach number at a point of the jet deduced from pt and ps.

Tn: stagnation temperature at a point of the jet measured by the temperature probe of the rake, in °K.

k^2: coefficient of utilization of the clinometric probe.

i : angle of the projection of the velocity vector at one point of the jet, on a vertical plane passing through the axis of the clinometric probe, with the axis of this probe, in degrees.

j : angle of the projection of the velocity vector at one point of the jet, on a horizontal plane passing through the axis of the clinometric probe, with the axis of this probe, in degrees.

2.3. Quantities relative to the plate:

r and d: radius and diameter of the discharge orifice of the jet, in meters.

x, y, z: coordinates of one point with respect to axes coming out of the jet orifice, in meters (Figure 3). 5

α: angle of a generating line with respect to the longitudinal axis of the plate, in degrees.

pn: static pressure measured by pressure sensor n of the panel, in kg/m^2.

$Kp_n = \frac{pn - p}{\frac{\rho V^2}{2}}$: coefficient of pressure relative to pressure sensor n.

Δ Cz : coefficient of lift induced by the jet on the plate (positive direction opposite to the direction of the jet, see Figure 3).

Δ Cm : coefficient of the pitch moment induced by the jet on the plate with respect to the transverse axis passing through the center of the jet orifice (positive direction: stalling when considering the plate as a wing from which the jet comes out from the lower surface, see Figure 3).

2.4. Constants:

$R = 287\ m^2/s^2$.

$r = d/2 = 0.06$ meters.

$\gamma = 1.4$

$\gamma_j = 1.4$ for testing in the cold state.

3. Background

/6

3.1. The origin of this testing dates back to September 1965, the first document being research requests GSMA No. 865,401 of 23 September 1965. The order form from the aeronautical technical service was confirmed by letter 32166 of 23 February 1967.

3.2. The test equipment arrived in Modane at three different times: 3 April, 29 May, and 28 June 1967.

3.3. Preliminary testing began on 29 June 1967. The tests took place from 11 July 1967 to 12 September 1967, and from 17 October 1967, to 20 October 1967.

The total period for spinning was 20 hours 56 minutes during which 104,750 m^3 of water were centrifuged.

4. Testing Goal

The testing goal subject of the present report is:

the study of interaction on a flat plate of a jet discharging perpendicularly to this plate and located perpendicularly to a flow (present installment);

the study of a jet located in a flow perpendicular to its discharge orifice (installment 2/5).

The above research carried out with a nozzle simulating the output nozzle of a lift engine as well as those with a high-temperature jet (973°K) will form the subject of another report.

5. Identification of Testing Equipment

/7

5.1. The assembly used allows production of a jet with a 120 mm diameter at the orifice and whose velocity can vary up to one Mach number equal or greater than 1.

5.2. An appreciably square wooden panel (2510 x 2520 mm) containing the discharge nozzle of the jet is fastened on the vertical wall located in the experimental test section of carriage III (Figures 1 and 2).

The panel is equipped on the upper half with 337 static pressure sensors distributed over 19 generating lines (Figure 3).

The nozzle is supplied with compressed air by the installation at 9 bars from the testing center. Two interchanged nozzles can be tried:

one so-called "ideal" nozzle (Figure 2);
one type "RB162" nozzle representing in scale the discharge from the Rolls Royce RB162 lift engine (the results concerning the tests carried out with this nozzle form the subject of a separate report).

A kerosene burner located upstream from the nozzle allows carrying out testing in a heated state up to a temperature of approximately 973°K (the findings concerning these tests in a heated state form the subject of a separate report).

5.3. A rake including total pressure sensors and clinometer as well as a temperature probe can be attached on the panel and be shifted into the jet field in the three directions in order to scan the jet (Figure 4). The results of these measurements are recorded in installment 2/5 of the present report.

6. Testing Configurations /8

The following table provides the list of the various configurations tested:

TABLE.

Date	Point no.	M	$\frac{Mj}{M}$	Observations
29.6.67	1 to 6	0 to 0.27	0	Test without jet. Adjustment of the panel.
30.6.67	7 to 19	0 to 0.27	0	Test without jet. Adjustment of the panel.
11.7.67	20 to 25	0 to 0.27	0	Measurement of pressures.
8.9.67	79 to 83	0		Measurement of total jet pressure with A13 recorder.
11.9.67	84 to 89	0.27	2 to 4	Visualization using wool threads.
17.10.67	920 to 943	0.09 to 0.27	2 to 10	Measurement of pressures on the plate.
17.10.67	944 to 949	0		Fixed point. Measurement of pressures.
20.10.67	950 to 954	0.09 to 0.27	4 to 11	Measurement of fluctuations of static pressures measured by L1 and M1 sensors.

7. Methods and Testing Techniques

7.1. Installation

The panel including the jet orifice is fastened on the vertical wall set up in carriage III (Figure 2).

The pneumatic circuits end up with pressure switches located behind the vertical wall and fastened by means of rubber supports as are the pressure sensors.

The compressed air pipe supplying the nozzle is connected to the air inlet at 9 bars supplying the S1.MA wind tunnel and whose flow is adjustable using a hand valve as well as a remote controlled by-pass.

7.2. Definition of the Test References

The testing conditions relative to the wind tunnel are defined by:

the stagnation pressure pi measured by a probe installed according to the axis of the test section at the entry point of the convergent;

the stagnation temperature Ti obtained by means of a thermocouple installed near the preceding probe;

the static reference pressure p. This pressure is measured by the F1G sensor located on the wall left of the test section in the median horizontal plane at a distance of 5125 mm from the entry point of the carriage.

The pressures pi, p, as well as the atmospheric pressure pa (measured at the level of the axis of the test section) are switched in with the reference balances of the wind tunnel which are connected to a central measuring station delivering a punched tape.

7.3. Measurement of pressures on the plate around the jet /10

The pressure sensors Nos. 1 to 15 of generating lines A to R are connected to six pressure switches each with 48 channels, numbered sca. 1 to 6 (Figure 3). Each switch is connected to a Statham pressure sensor ±2.5 psi (±17,200 Pascal).

In order to remove the risks of error owing to fluctuations of pressure for some sensors, the pneumatic circuits connecting these sensors to the pressure switch were supplied with a dash pot (inside diameter 0.2, length 20 mm) and with a capacity made up by a vinyl slot with an inside diameter of 8 mm and a length of 2 meters.

The other pressures (generating line S and sensors whose numbers are greater than 15) are measured using a water multimanometer, switchable with mercury and photographed.

The measuring chain in connection with the pressure switches (Figure 5) furnishes a punched tape.

7.4. Measurement of the jet's velocity

A pressure rake including three total pressure sensors and one static pressure sensor is located in the 215 mm diameter section between the burner and the nozzle. These pressures are measured using manometers with a Wallace and Tierman dial. The knowledge of the total pressure in the jet and the static pressure in the test section allows calculation of the Mach number of the jet at the discharge orifice.

7.5. Measurement of temperatures

A total temperature probe fitted out with a chromel-alumel thermocouple is placed in the direct proximity of the rake referred to in 7.4. The readings of the thermocouple are recorded on a MECI potentiometer.

7.6. Analysis of the measurements

The calculations relating to the pressures are carried out in the Modane computer center according to chain No. 329,211.

For one measuring point the tabulated results give:

pn pn/pi kpn = $\frac{pn - p}{\frac{1}{2} \rho V^2}$ for each pressure sensor and the dynamic pressure, test section velocity as well as the lift coefficients and pitch moment induced for each measuring point. /11

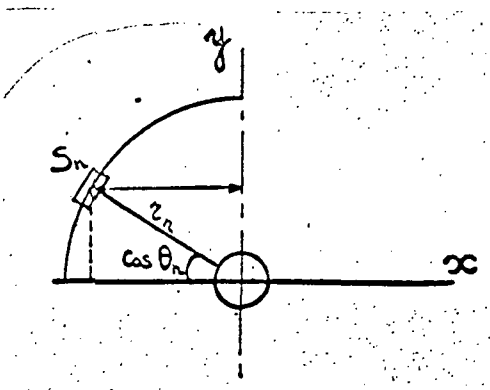

The induced lift coefficient is obtained by integration of local pressure coefficients:

$$\Delta C_z = \frac{\Delta F_z}{\frac{\rho V^2}{2} S} = \frac{\sum (p_n - p) S_n}{\sum \frac{\rho V^2}{2} S_n} = \frac{\sum K p_n \cdot S_n}{\sum S_n}$$

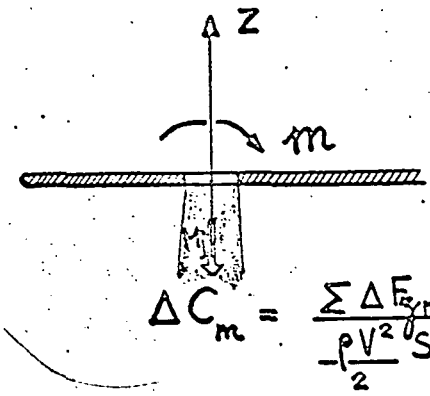

The pitch moment coefficient induced with respect to the transverse axis of the plate passing through the orifice of the jet is obtained by:

$$\Delta C_m = \frac{\Sigma \Delta F_{zn} . d_n}{\frac{\rho V^2}{2} S . l} = \frac{\Sigma (p_n - p) S_n . r_n . \cos\theta_n}{l \Sigma \frac{\rho V^2}{2} S_n} = \frac{\Sigma K p_n . S_n . r_n . \cos\theta_n}{l \Sigma S_n}$$

at the same time considering θ_n as varying from 0 to π (direction the reverse of the trigonometric direction).

The sign convention shown on the figure opposite agrees well: $Kp_n < 0$ leading to $\Delta Cz < 0$.

These calculations of ΔCz and ΔCm were carried out by considering several integration surfaces (causing the radius to vary) in such a way as to recognize the effect of the jet as a function of the distance.

7.7. Measurements carried out in the jet

The description of these measurements is given in installment 2/5 of the present report.

7.8. Criterion of similitude accepted /12

In order to carry out a valid comparison of the various tests with each other, we shall consider the value of the thrust coefficient of the jet C_μ and the comparable tests should have the same value of this coefficient

$$C_\mu = \frac{Q_j V_j}{\frac{\rho V^2}{2} S_j}$$

Qj being the mass flow from the jet or $Q_j = \rho_j V_j S_j$ hence,

$$C_\mu = \frac{\rho_j V_j^2 S_j}{\frac{\rho V^2}{2} S_j} = 2 \frac{\rho_j V_j^2}{\rho V^2}$$

since

$$\rho V^2 = \gamma p M^2 \qquad C_\mu = 2\,\frac{\gamma_j\, p_j\, M_j^2}{\gamma\, p\, M^2}$$

The static pressure from this jet is that of the flow into which it sprays, hence pj = p and $C_\mu = 2\,\frac{\gamma_j}{\gamma}\left(\frac{M_j}{M}\right)^2$

Therefore, in order to produce equality of the C_μ values, we shall take the equality of the quantities $\frac{M_j}{M}\sqrt{\frac{\gamma_j}{\gamma}}$

During the mutual comparison of tests carried out at the same temperature we shall take as a criterion the ratio Mj/M, whereas the comparison of tests in the heated state with tests in the unheated state will have to take into account the corrective term $\sqrt{\frac{\gamma_j}{\gamma}}$, a term, furthermore, quite close to 1; indeed, the maximum temperature of the jet being around 950°K, $\gamma_j = 1.34$.

$$\sqrt{\frac{\gamma_j}{\gamma}} = \sqrt{\frac{1.34}{1.4}} = 0.98$$

7.9. Reynolds number of the jet

Figure 6 provides the value of the Reynolds number of the jet at the discharge orifice as a function of the jet velocity for tests in the unheated state, the goal of the present report. This number varies from approximately $0.5 \cdot 10^6$ to $2.6 \cdot 10^6$.

8. Testing Results

8.1. Behavior of the equipment

On the whole, the behavior of the equipment was satisfactory.

8.2. Results of the tests

8.2.1. Tests without jet, orifice closed off

These tests were carried out in order to better adjust the position of the plate in the blast.

After adjustment, the position used gave, on the two generating lines A and S, the results shown in Figure 7.

It may be noted that generating line A retains the effect from the leading edge of the plate, whereas, in the case of generating line S, there may be noted, on the sensor located directly alongside the orifice, a reduced pressure caused undoubtedly by a very slight project in the closure of the jet orifice.

8.2.2. Pressures induced by the jet

Figures 8 to 58 provide the distribution of the coefficients of pressure along each generating line for the three blast velocities scanned and for different ratios of velocity Mj/M.

In order not to overload the figures, we only connected by curves some of the configurations of velocity Mj/M.

Figures 59 to 61 provide the comparison for three generating lines of the the points of intersection. It should be noted that these intersections are especially favorable.

Figures 62 to 72 provide the distributions of pressures on the plate in the form of isobaric curves (iso-coefficients of pressure). On these figures, the distributions of pressure are corrected for the distribution without jet. /14

It is advisable to note that the testing without blast provided inconclusive results as a consequence of the interaction of the test section wall opposite the jet.

8.2.3. Effect of the velocity of flow

The comparison of results obtained at different velocities is made on Figure 73 for Mj/M = 2 and on Figure 74 for Mj/M = 3.

It should be noted that, upstream from the jet, its effect increases with the velocity. This is because the zones of overpressure are more extended. On the other hand, the zones of reduced pressure are very close to one another without a specific tendency revealed.

The differences ascertained upstream are reflected on the coefficients of lift and pitch moment which have been induced (cf. 8.2.5).

8.2.4. Effect of the discharge velocity of the jet

On Figures 62 to 66 relating to the lowest wind tunnel flow velocity, it is possible to follow the gradual development of the isobars from a ratio Mj/M = 2

(low jet velocity) to Mj/M = 10 (high jet velocity).

In the case of low jet velocities, there should be noted an obstruction effect with overpressure in front of the jet and reduced pressure behind it. Proportionally, as the relative jet velocity increases, the suction effect becomes preponderant and the zone of reduced pressure is extended forward. This transformation is shown clearly on Figure 75 and on Figure 76 on which it is possible to compare the ratios Mj/M = 2 and Mj/M = 10.

In the case of this latter ratio, it may be noted that the zone of effect of the jet is much greater and that the greater zone of reduced pressure is extended forward, whereas the zone of overpressure has practically disappeared.

8.2.5. Induced lift and pitch moment

In order to study the induced lift and pitch moment, we have related the forces and moments calculated to the section of the jet as well as to its diameter. /15

$$\Delta C_z = \frac{2\Delta F_z}{\frac{\rho V^2}{2} \cdot \frac{\pi d^2}{4}}$$

and

$$\Delta C_m = \frac{2\Delta m}{\frac{\rho V^2}{2} \cdot \frac{\pi d^2}{4} \cdot d}$$

at the same time considering that the integration of the pressures provides ΔFz and ΔM with only half of the plate.

In the computer-derived results, ΔCz and ΔCm are given related to the total surfaces taken into consideration for the integration. A simple rule of three allows coordinating coefficients calculated in this way with those related to the section and diameter of the jet.

Figures 77 and 78 provide the results obtained in the form of numerical tables.

Figures 79 and 80 show the gradual development of the ΔCz and ΔCm coefficients as a function of the ratio of the velocity of the jet to the velocity of the wind tunnel.

Examination of these figures allows the following observations to be made:

in the case of the two smallest integration surfaces (x/r = 5 and 10), the induced lift tends toward a practically constant value beginning from a specific jet velocity whereas the pitch moment continues to develop. This means that, beginning from a specific jet velocity, the increase in this velocity while at the same time changing the distribution of pressures, does not change their total value in the surfaces located in the proximity of the jet orifice;

the points obtained at different wind tunnel velocities (and for the greatest integration surface x/r = 15) reflect the comments of paragraph 8.2.3;

the increase in overpressures upstream from the jet slightly decrease the induced lift and increase the stalling moment;

the gradual development of the induced pitching moment is quite consistent with the gradual development of the distribution of pressures on the plate when the relative velocity of the jet increase. The transport of the zones of reduced pressure in the direction upstream of the jet with increase in velocity (Figures 75 and 76) causes the sign of the induced moment to be changed.

9. Conclusion

The tests forming the subject of this report have allowed:

determination of the distribution of pressures induced on a plate around the orifice of a large-sized jet located perpendicularly to a flow;

determination, as a function of the surface considered around the orifice of the jet and the relative velocity of the jet with respect to that of the flow, of the lift and pitch moment induced by the presence of the jet.

These results have clearly revealed the reversal in direction of the pitch moment during variation of the relative velocity of the jet with respect to the velocity of flow.

Listing of Figures

		Figure No.
Jet interaction test panel		1
Test section installation		2
Position of pressure sensors		3
Jet scanning rake		4
Pressure measuring chain		5
Reynolds number of the jet		6
Pressure distribution in unheated state		7
Pressure coefficients along the different generating lines	M = 0.09	8 to 24
" " " "	M = 0.18	25 to 41
" " " "	M = 0.27	42 to 58
Comparison of points of intersection		59 to 61
Distribution of pressures on the plate -	M = 0.09	62 to 66
	M = 0.18	67 to 70
	M = 0.27	71 and 72
Effect of wind tunnel velocity		73 and 74
Effect of jet velocity		75 and 76
Tables of numerical results: induced lift and pitch moment		77 and 78
Induced lift and pitch moment		79 and 80

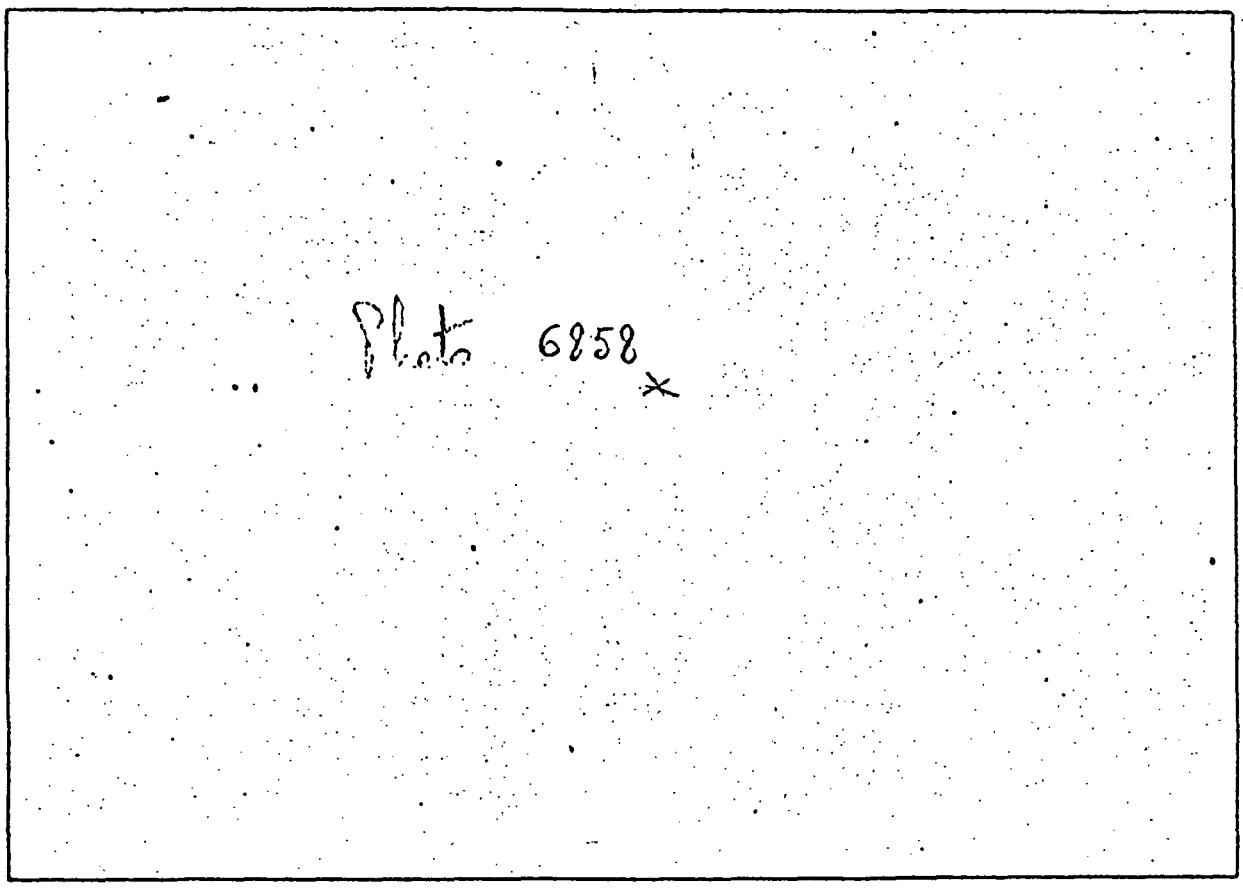

Figure 1. Jet interaction test panel.

* Figure not available.

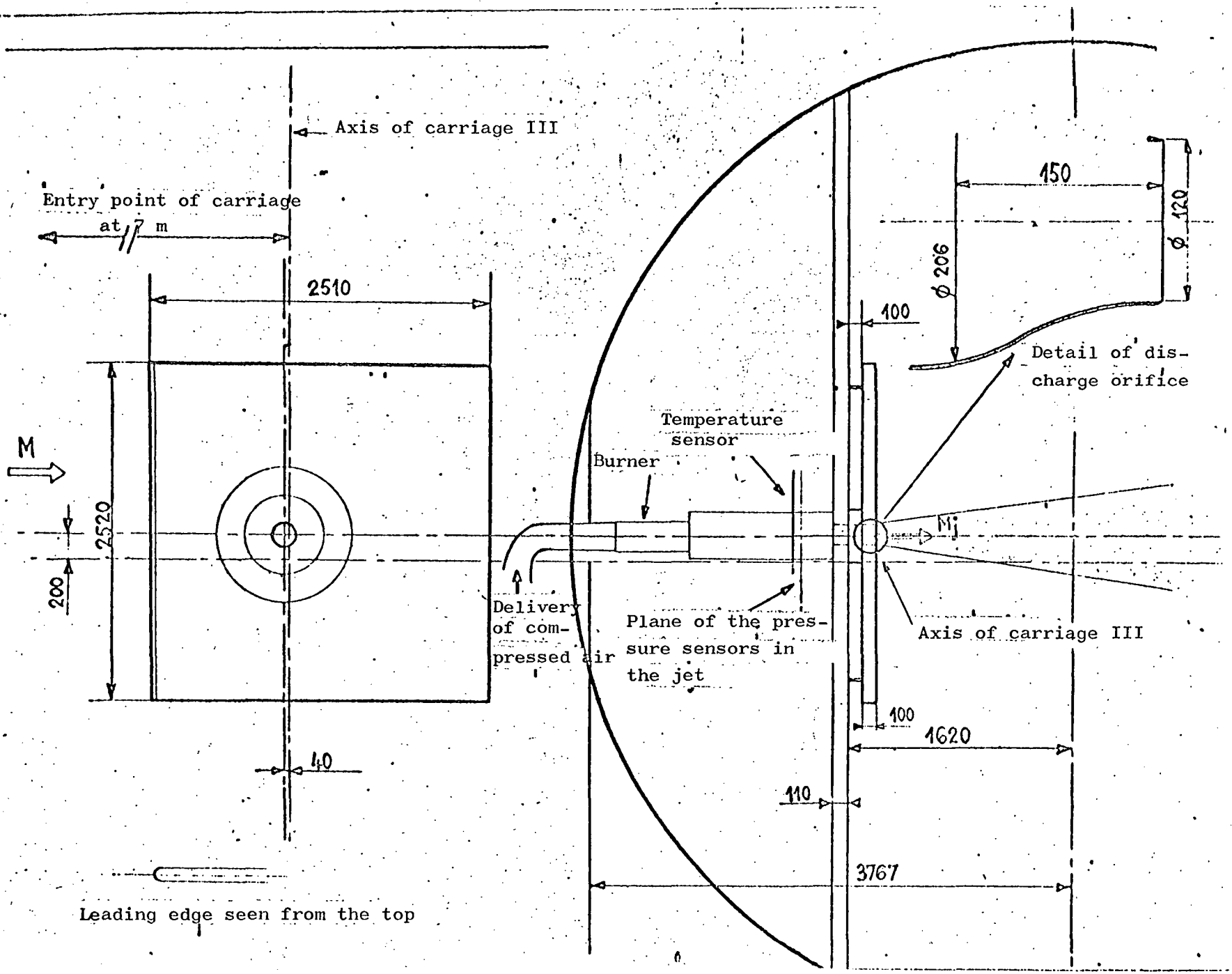

Figure 2. Test section installation.

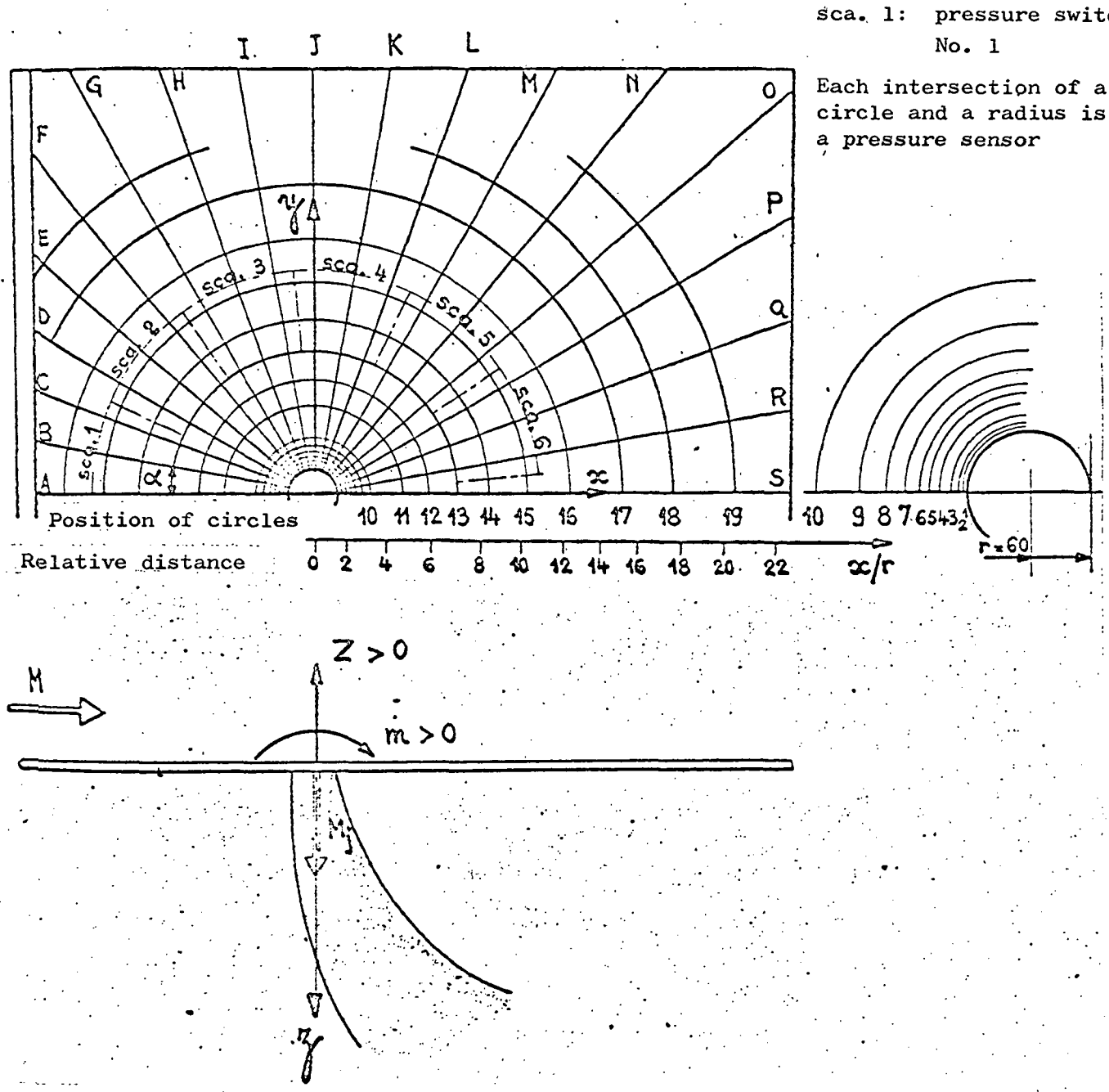
sca. 1: pressure switch No. 1
Each intersection of a circle and a radius is a pressure sensor
I J K L
G H M N O
F P
E Q
D R
C
B
A S
sca. 1
sca. 2
sca. 3
sca. 4
sca. 5
sca. 6
Position of circles 10 11 12 13 14 15 16 17 18 19
Relative distance 0 2 4 6 8 10 12 14 16 18 20 22 x/r
10 9 8 7 6 5 4 3½
r = 60
M
Z > 0
ṁ > 0

Figure 3. Position of pressure sensors.

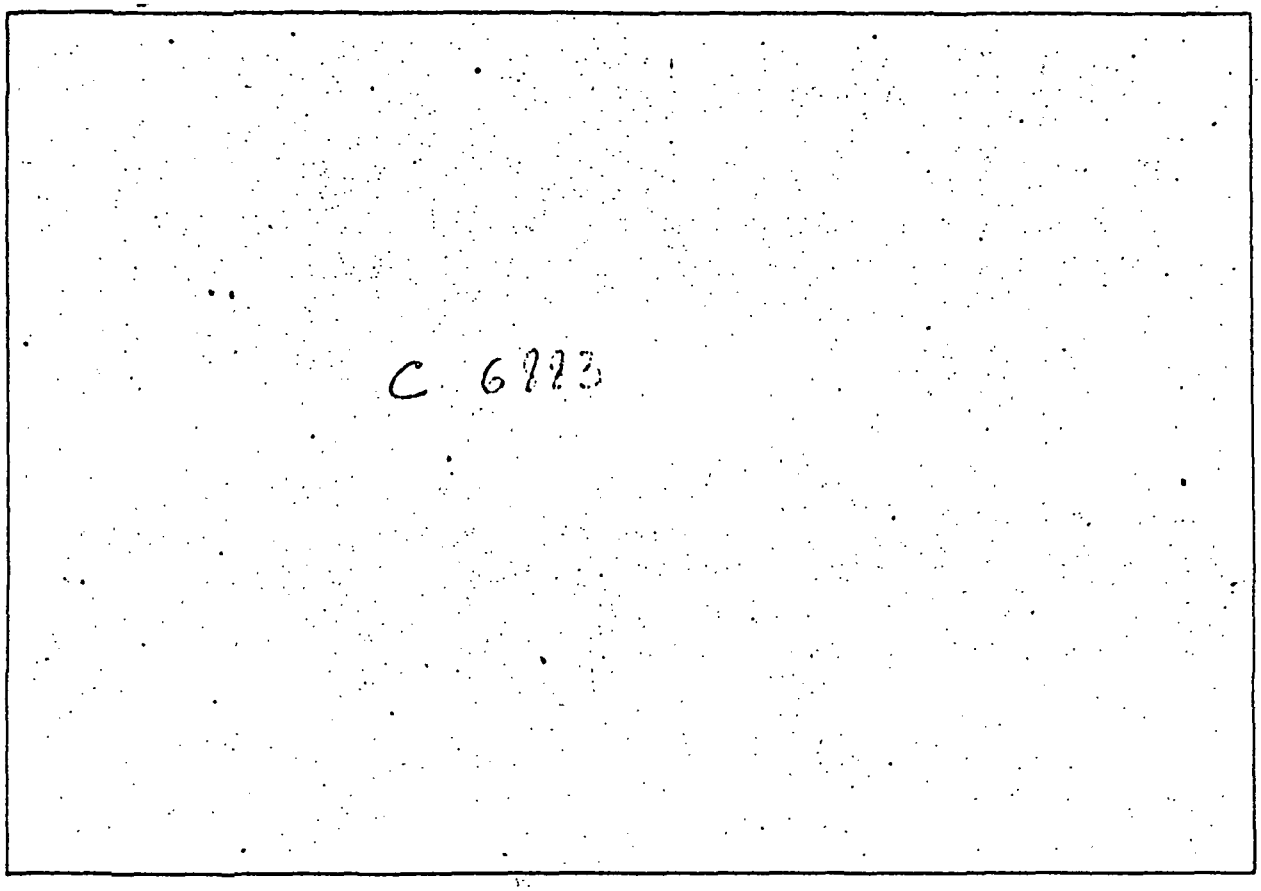

Figure 4. Jet scanning rake.

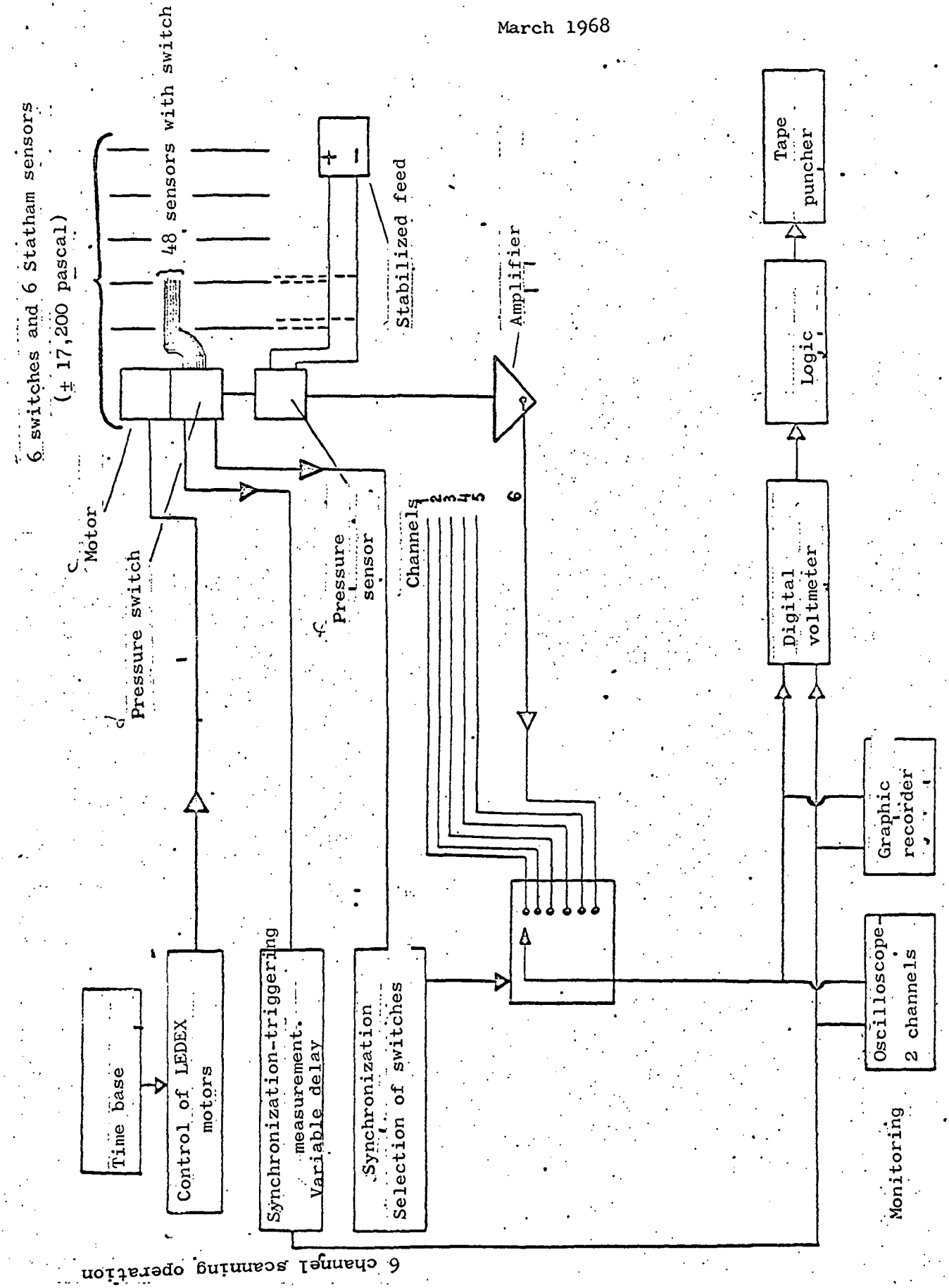

Figure 5. Pressure measuring chain.

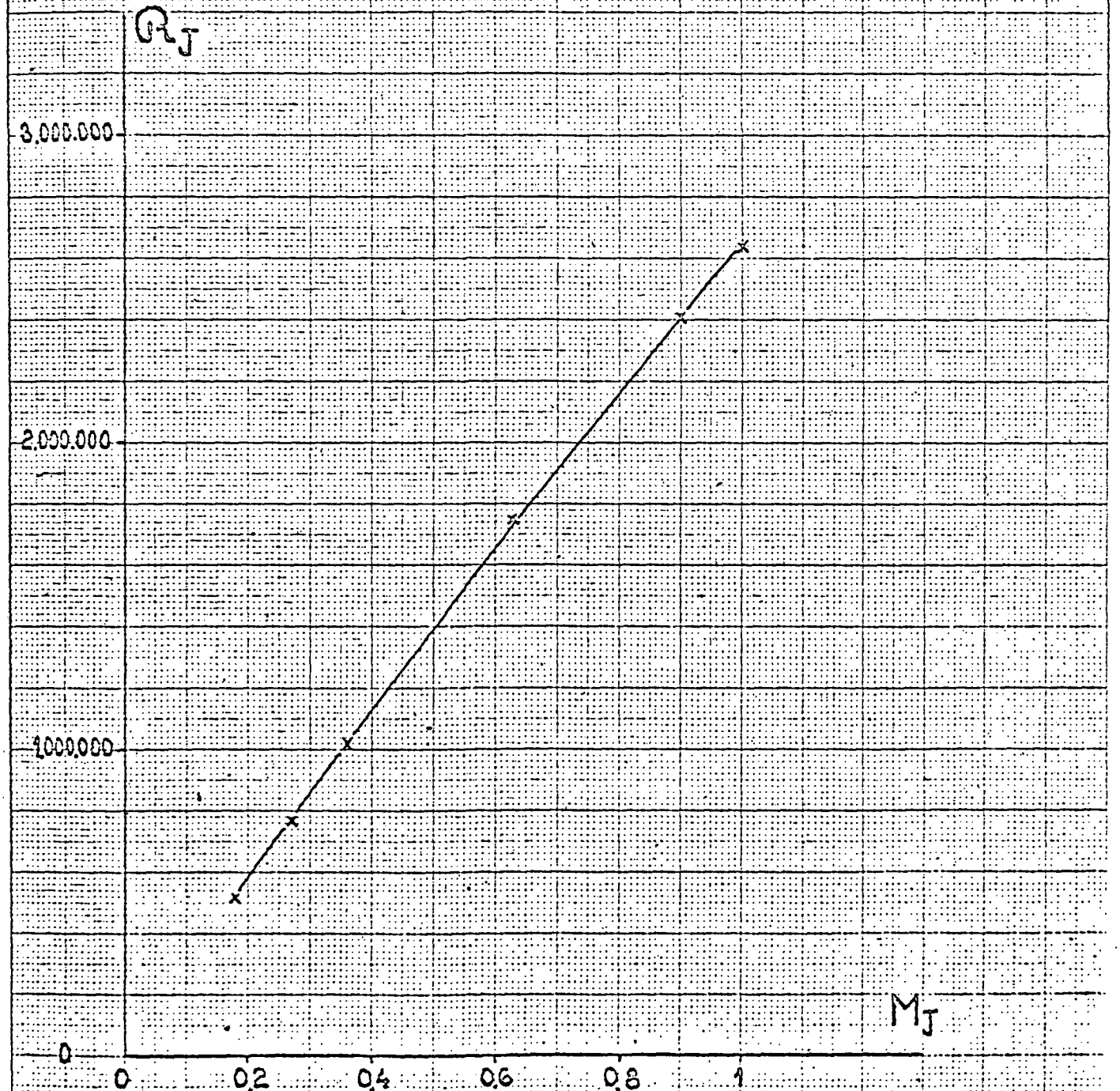

Figure 6. Reynolds number of the jet.

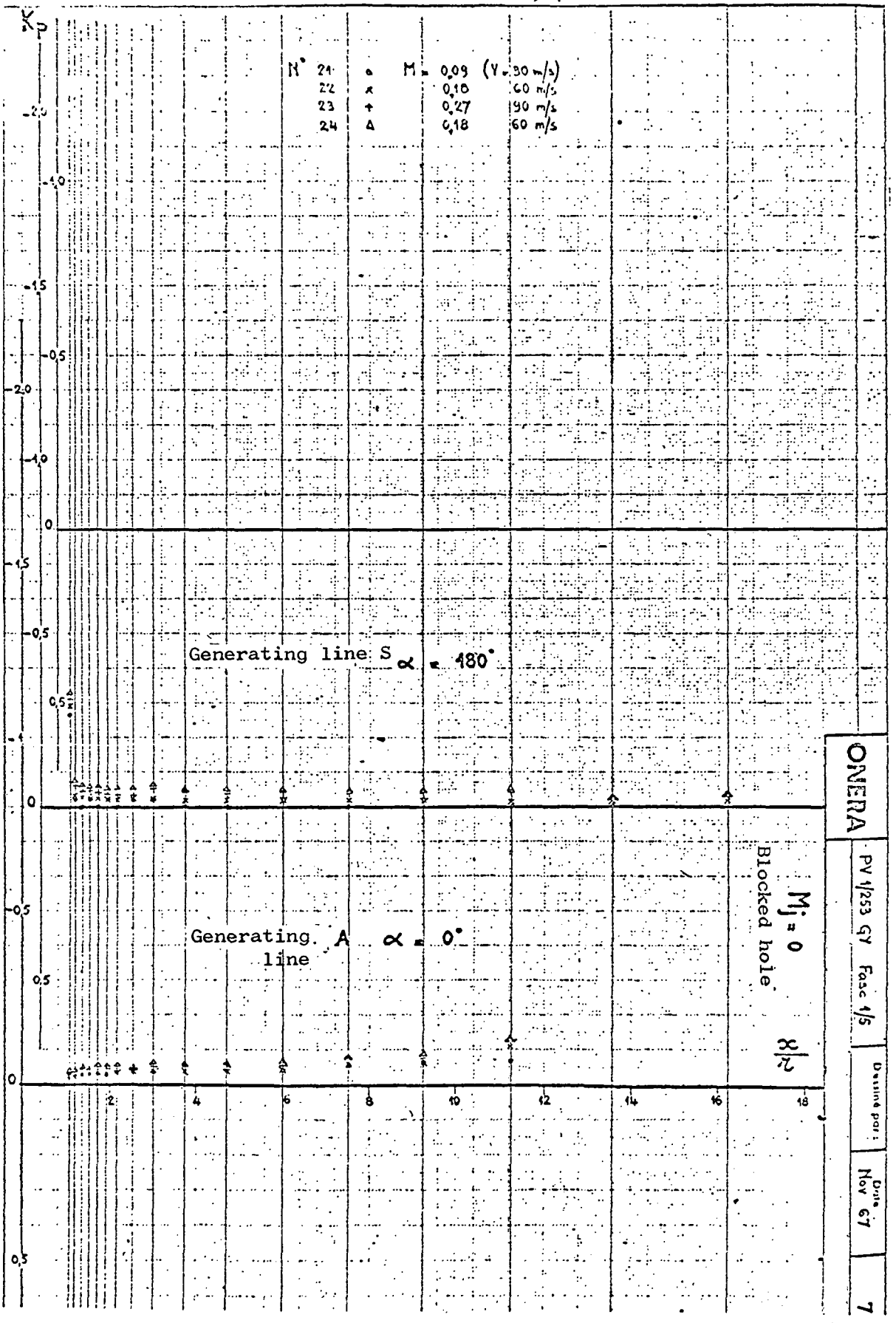
N° 21 ○ M = 0,09 (V = 30 m/s)
22 × 0,10 60 m/s
23 + 0,27 90 m/s
24 Δ 0,18 60 m/s
Generating line S α = 180°
Generating line A α = 0°
Mj = 0
Blocked hole
ONERA
PV 1/253 GY Fasc 1/5
Dessiné par :
Date Nov 67
7

Figure 7. Jet interaction. Test in unheated state.

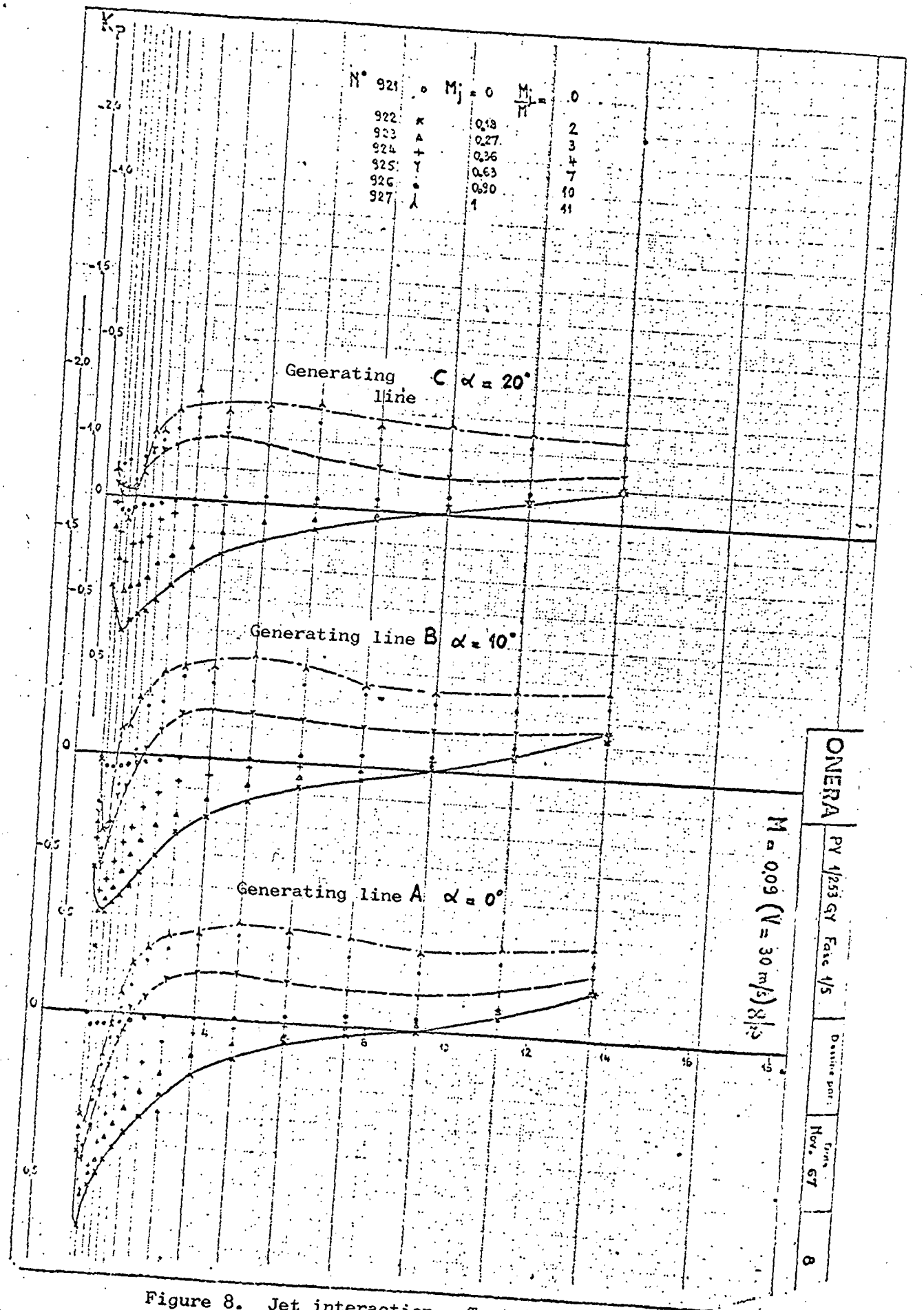
Kp
N° 921 ○ Mj = 0 Mj/M = 0
922 × 0,18 2
923 Δ 0,27 3
924 + 0,36 4
925 Y 0,63 7
926 • 0,90 10
927 λ 1 11
Generating line C α = 20°
Generating line B α = 10°
Generating line A α = 0°
M = 0,09 (V = 30 m/s)
ONERA
PY 1/253 GY Fasc 1/5
Nov. 67
8

Figure 8. Jet interaction. Test in unheated state.

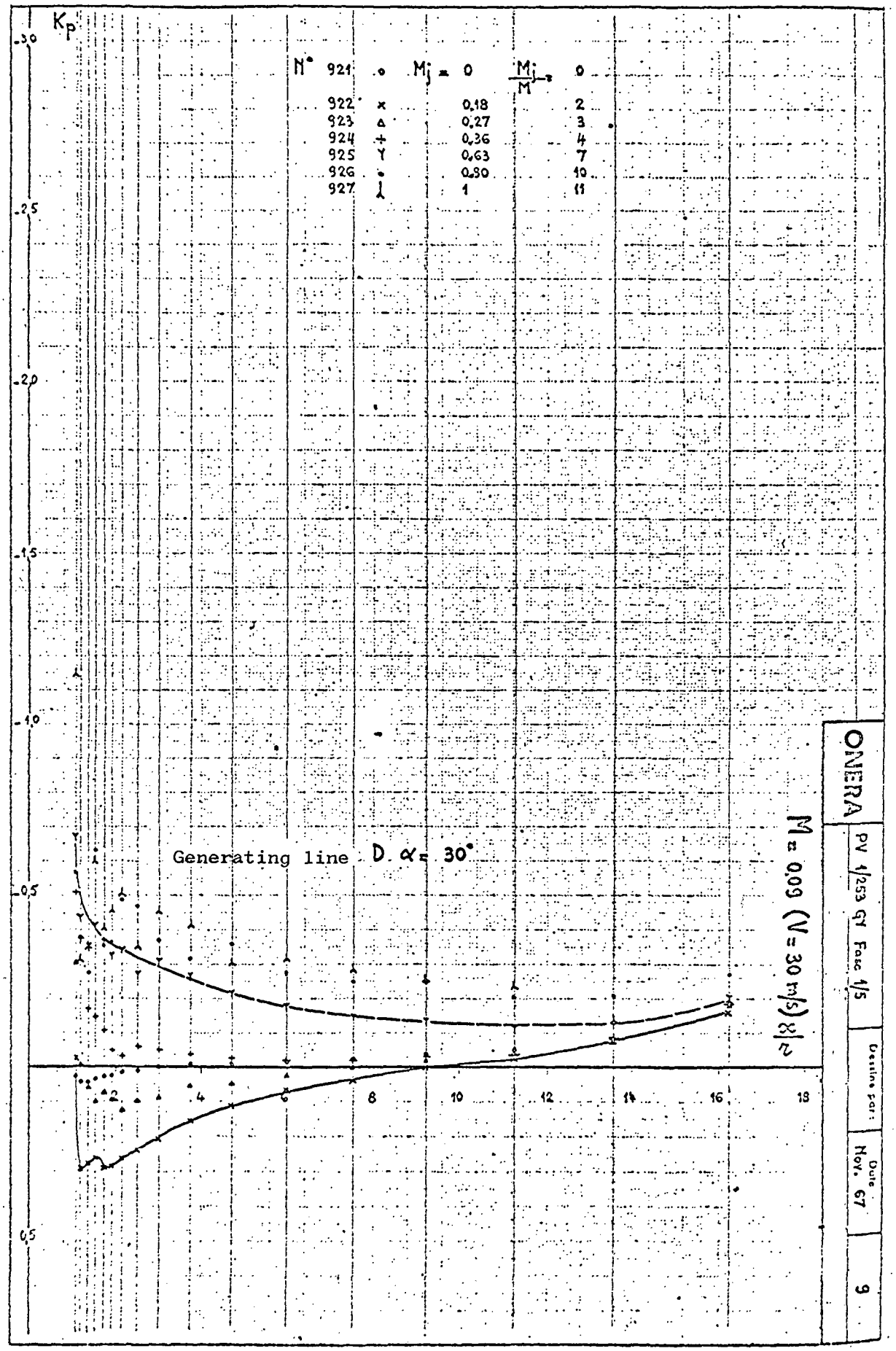

Figure 9. Jet interaction. Test in unheated state.

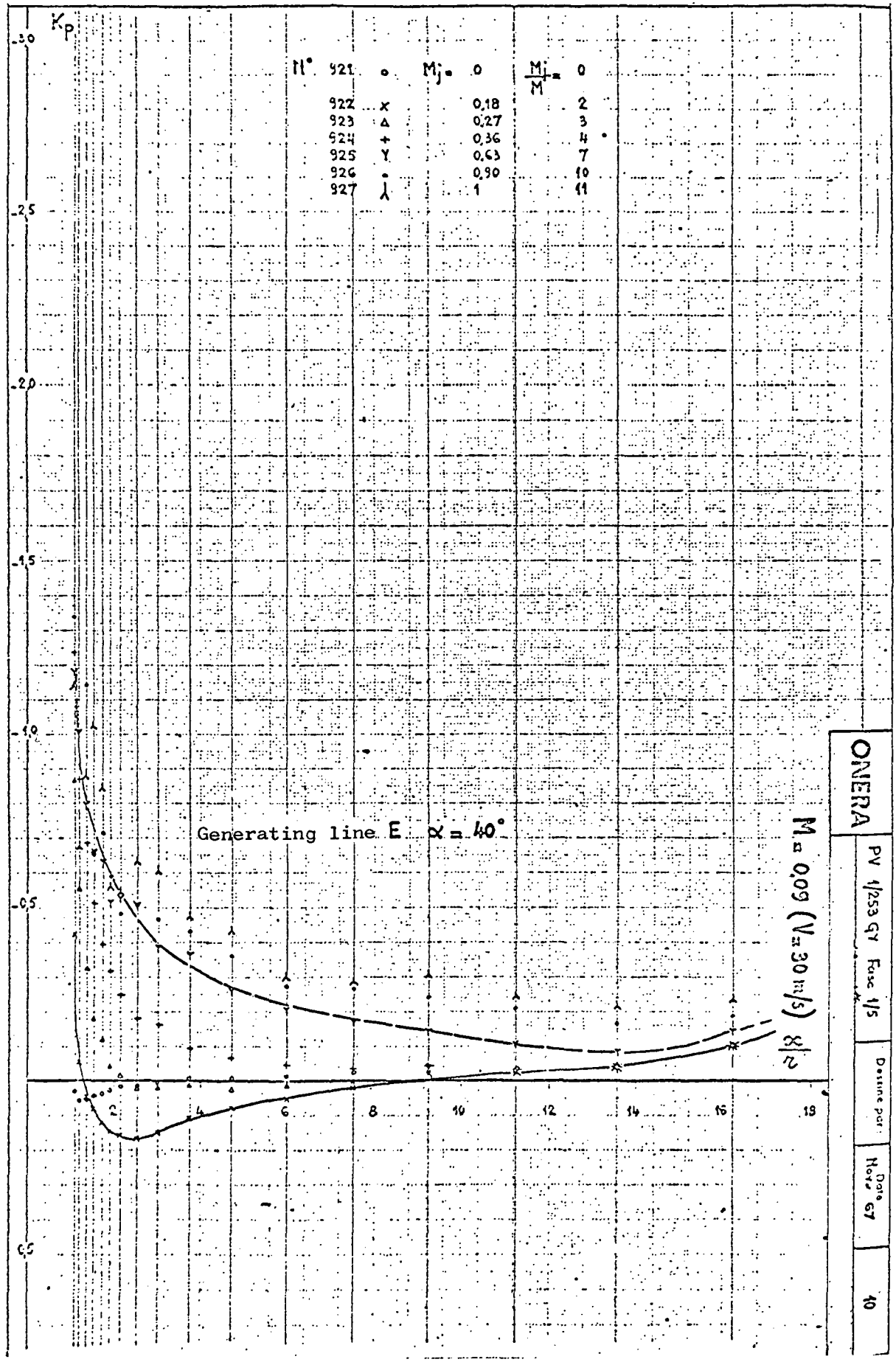

Figure 10. Jet interaction. Test in unheated state.

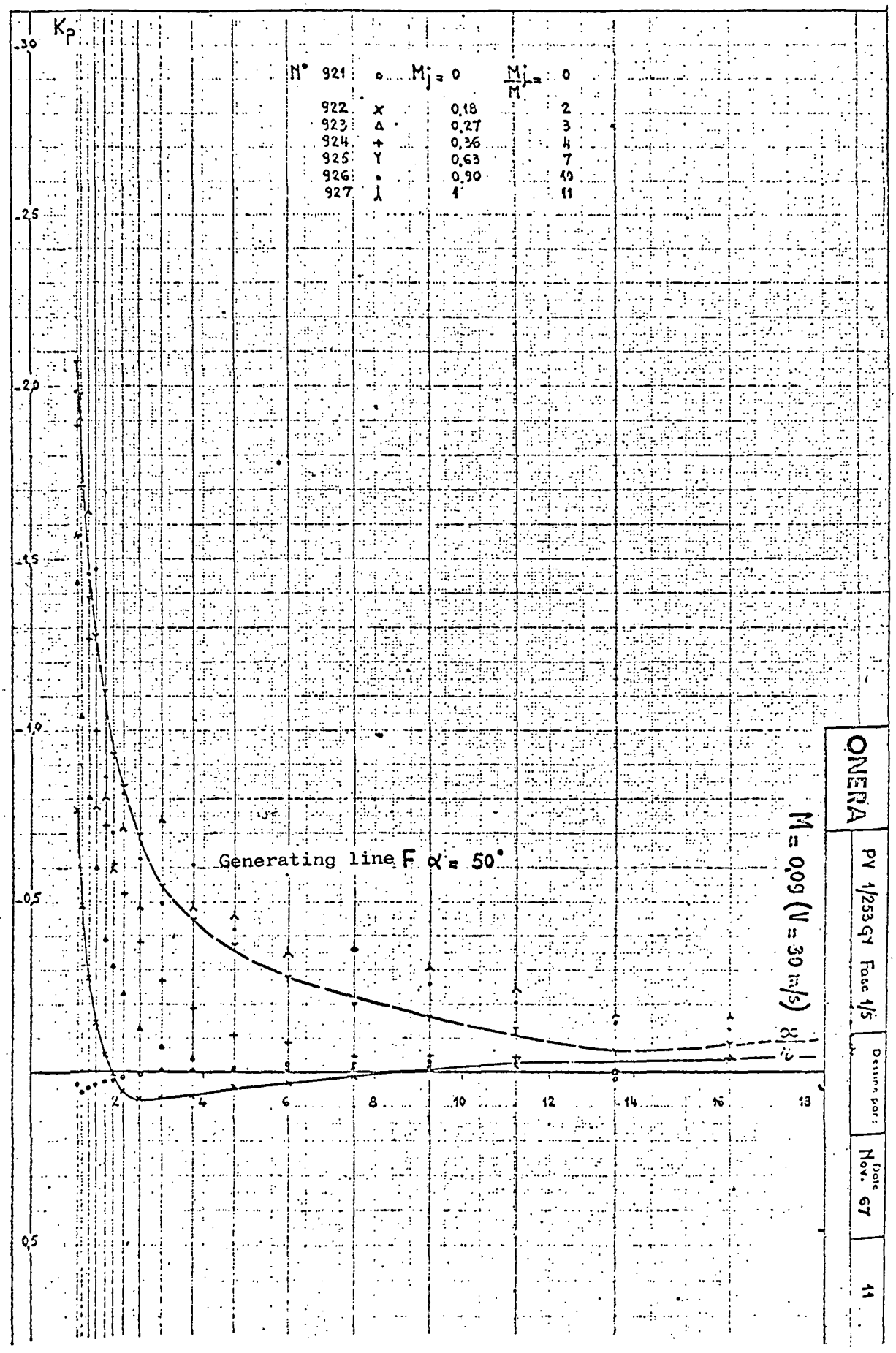

Figure 11. Jet interaction. Test in unheated state.

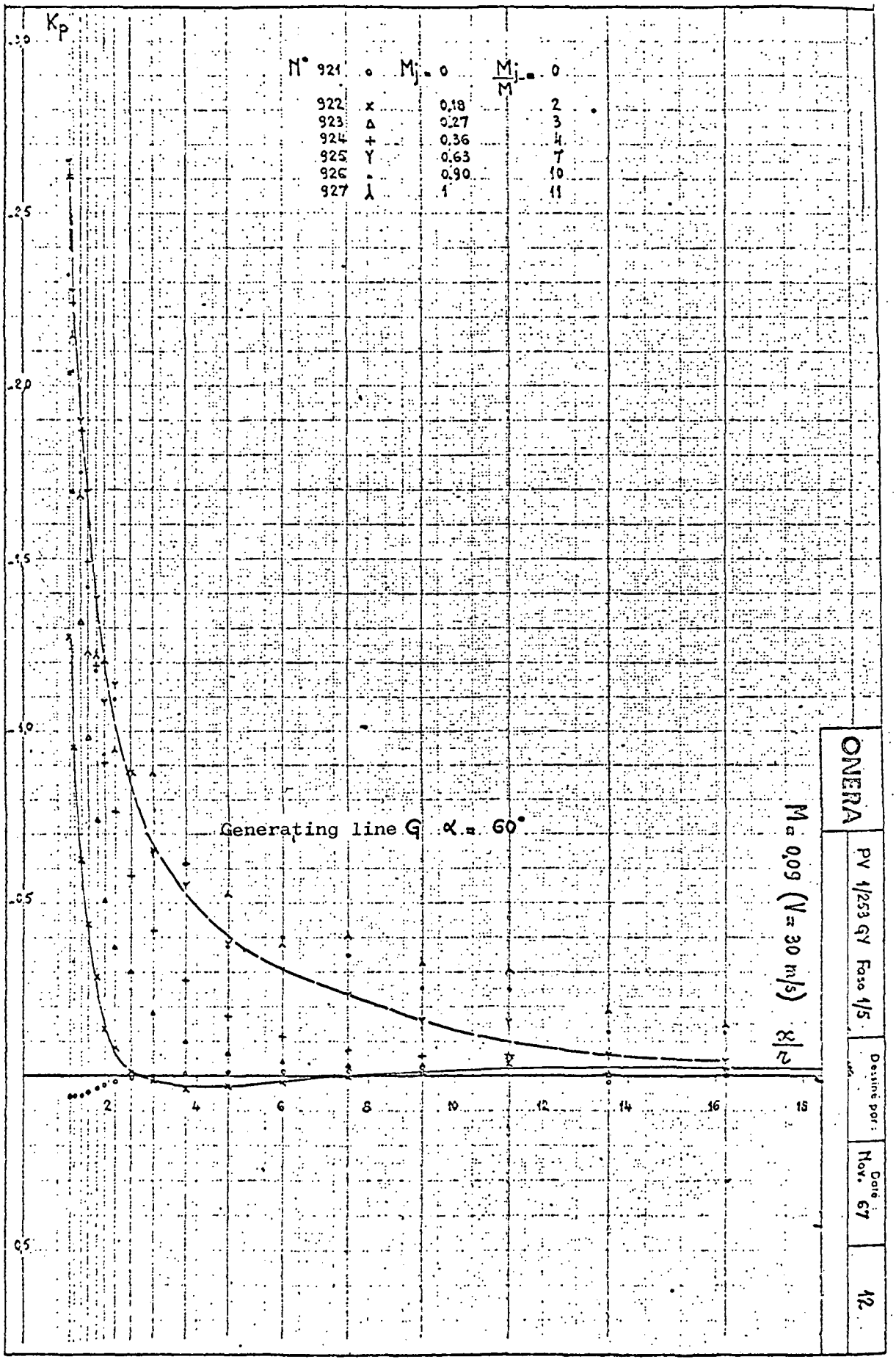

Figure 12. Jet interaction. Test in unheated state.

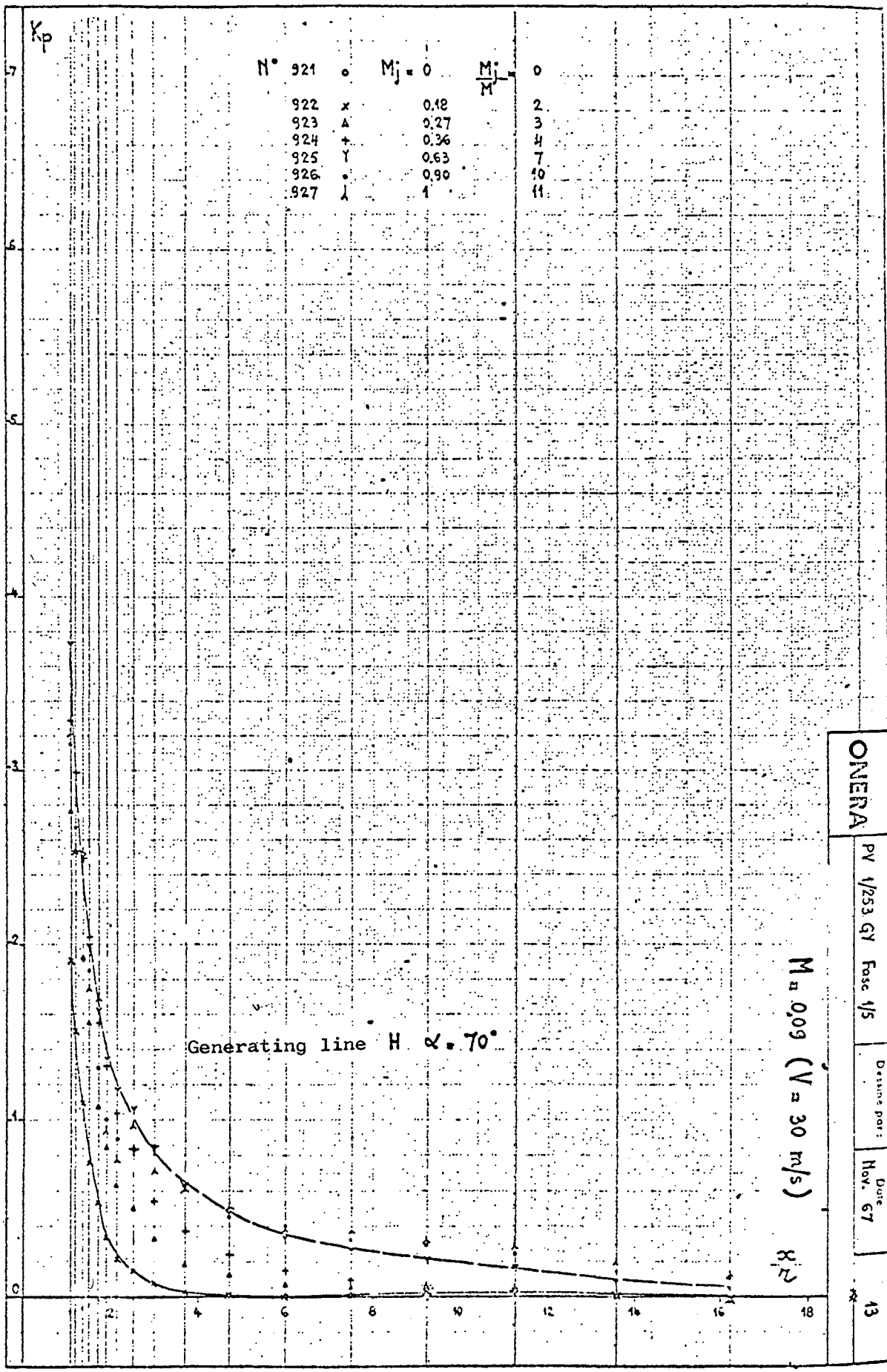

Figure 13. Jet interaction. Test in unheated state.

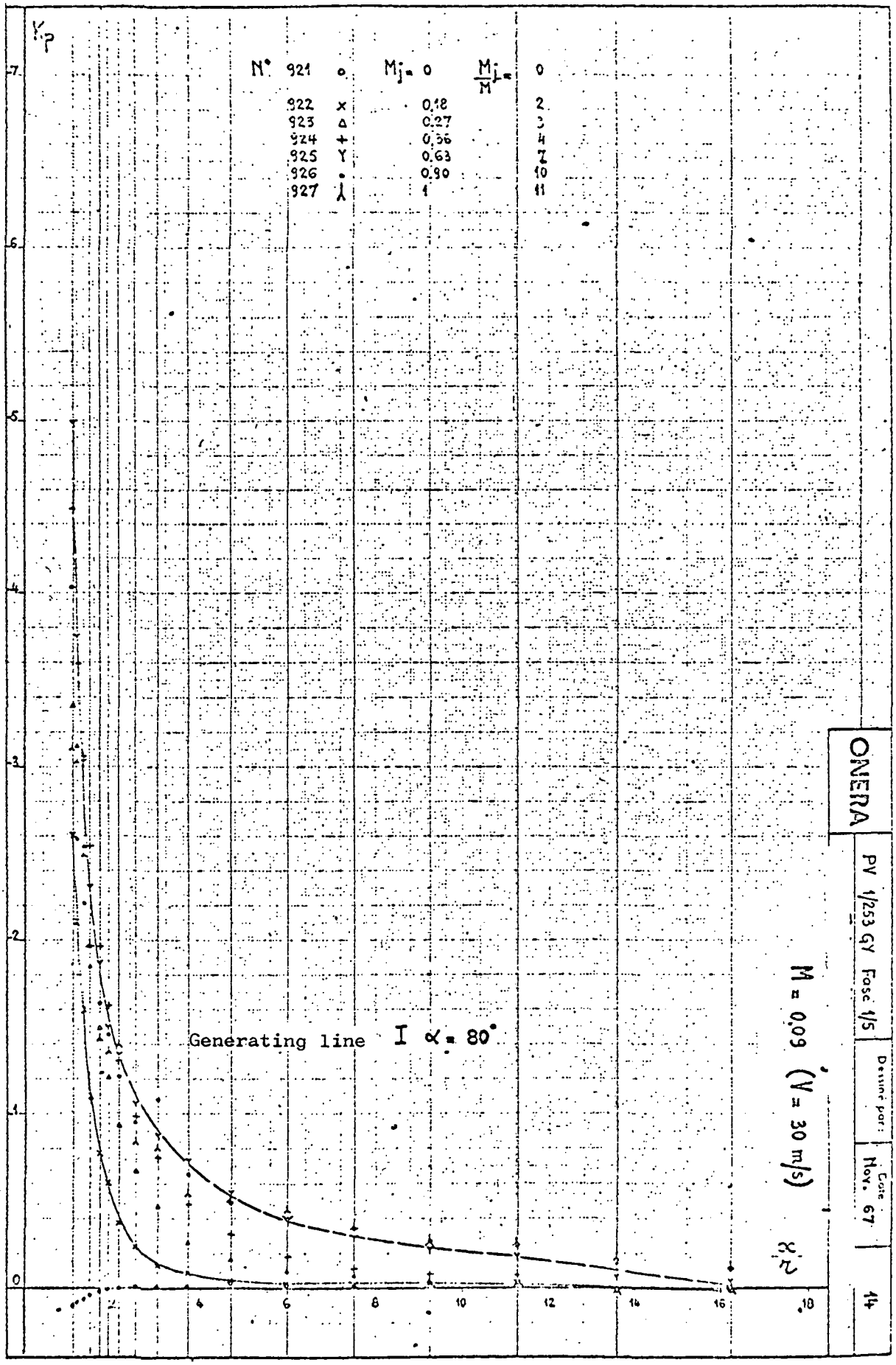

Figure 14. Jet interaction. Test in unheated state.

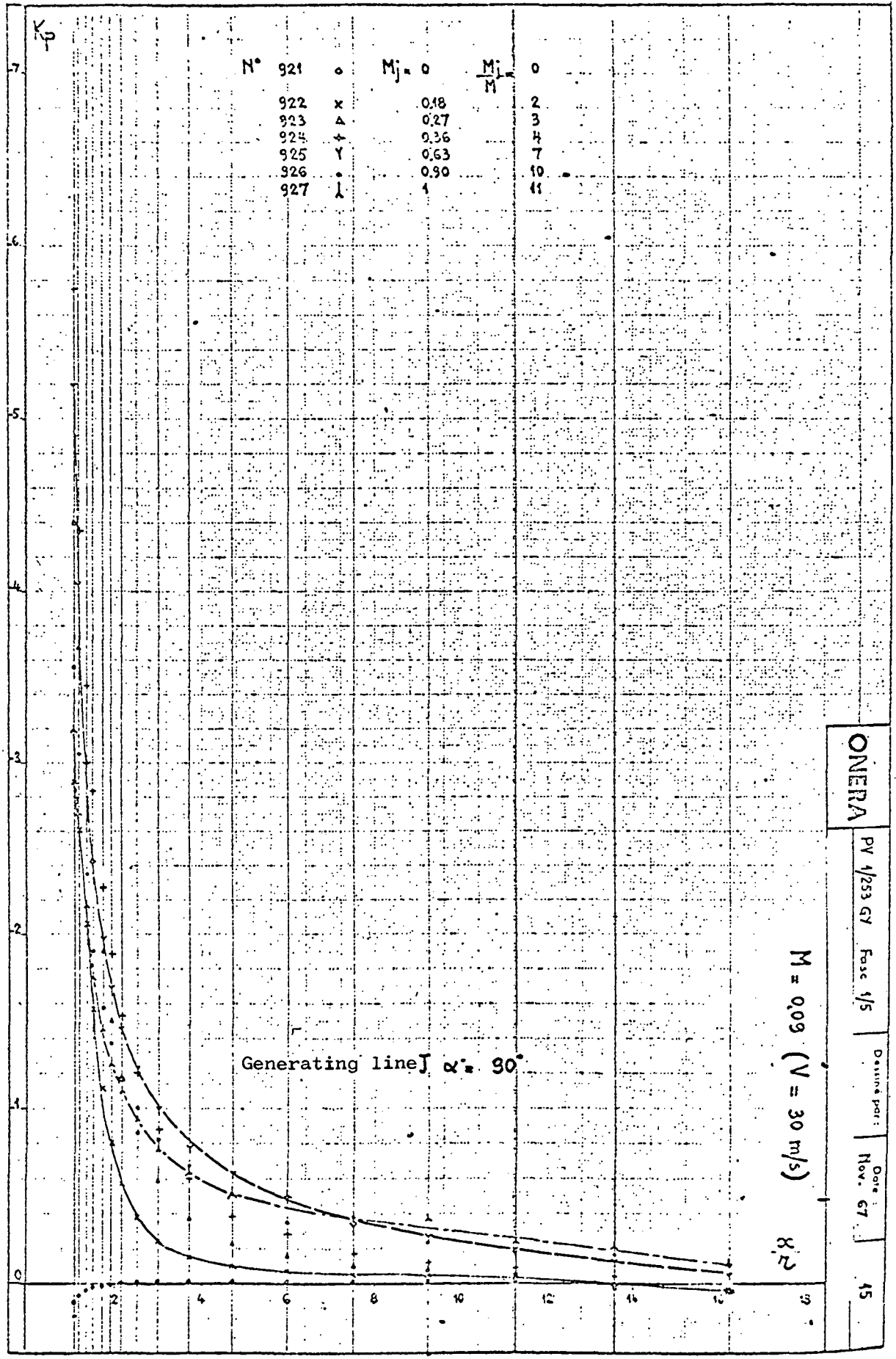

Figure 15. Jet interaction. Test in unheated state.

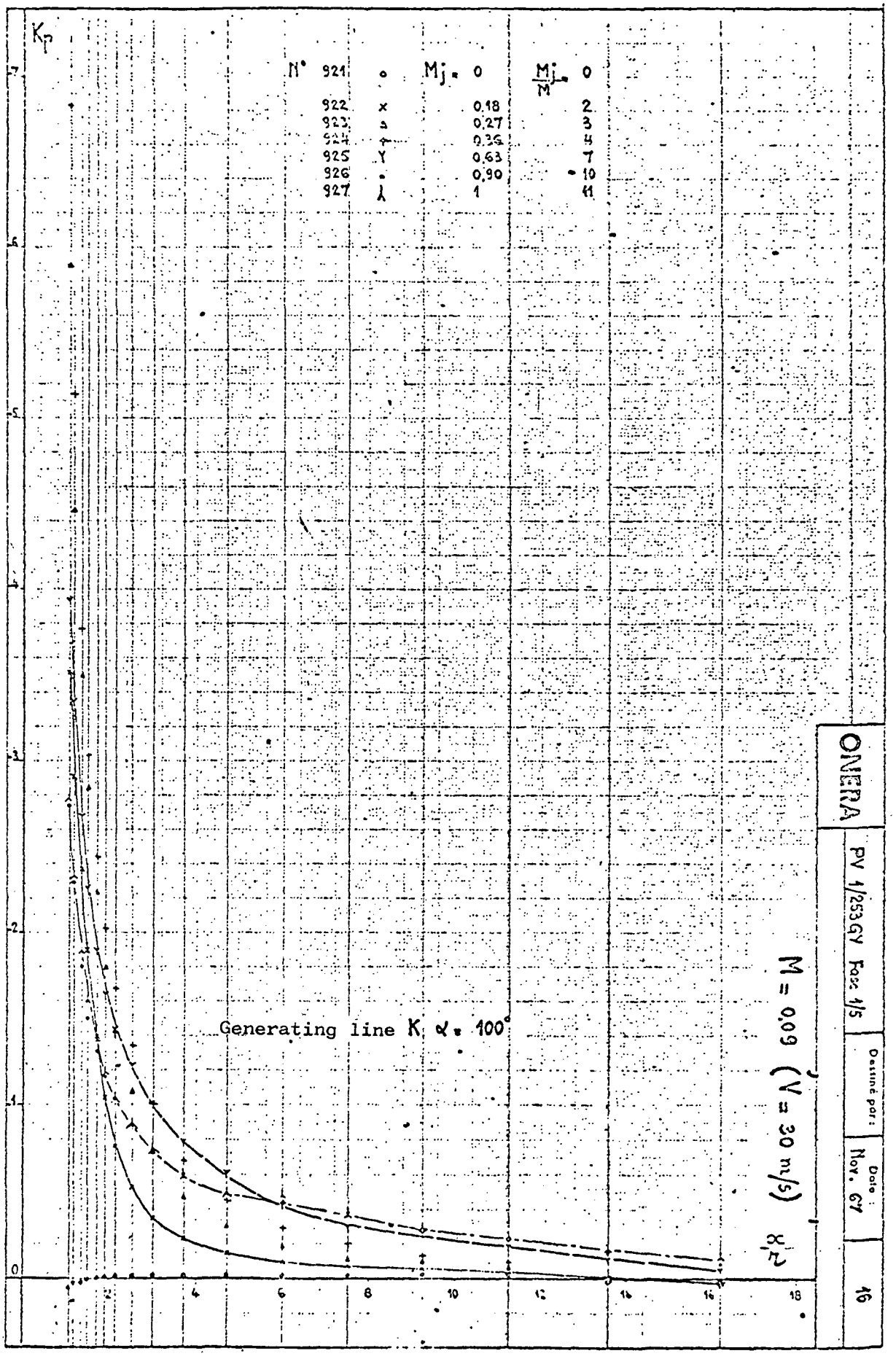

Figure 16. Jet interaction. Test in unheated state.

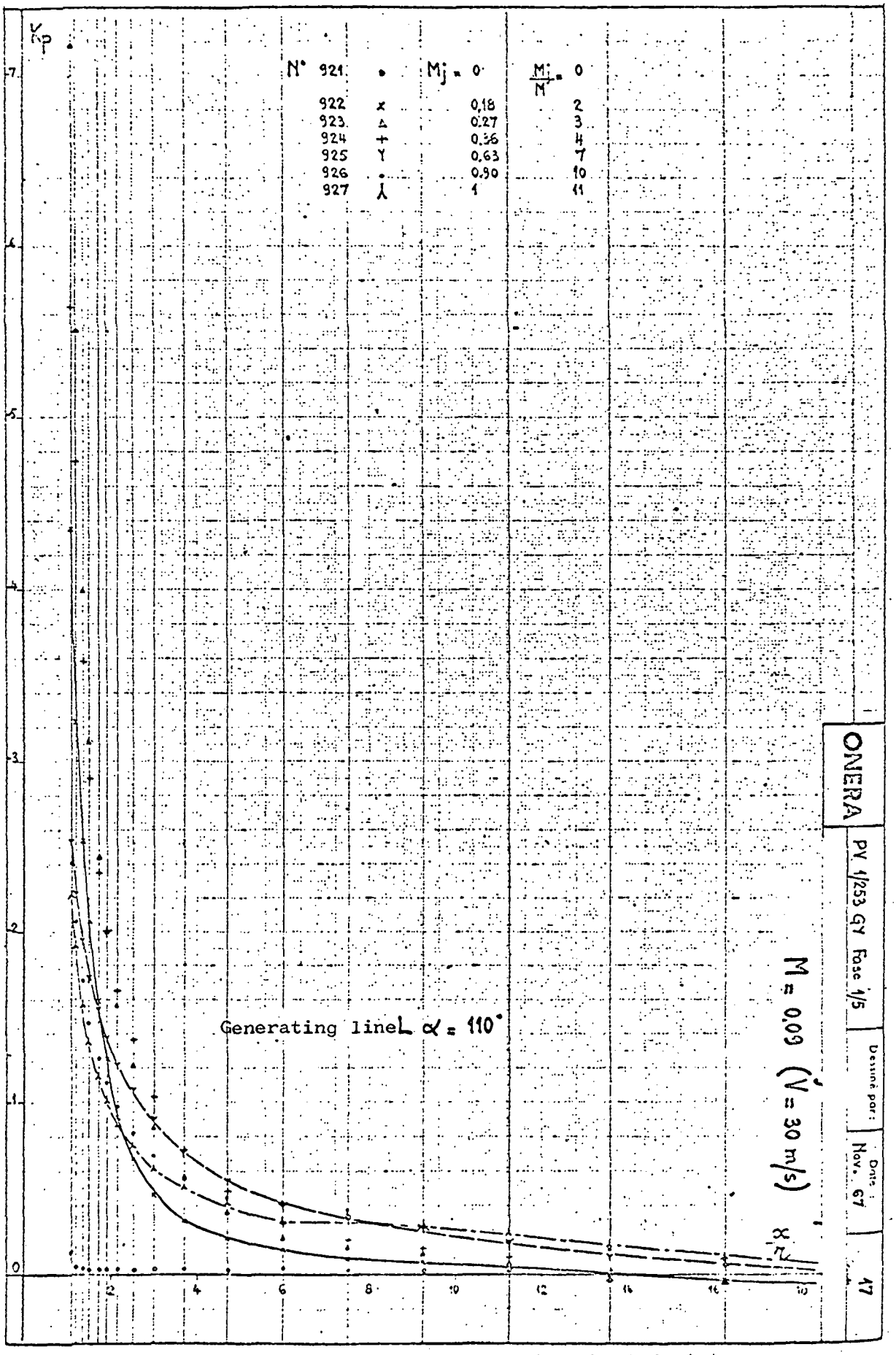

Figure 17. Jet interaction. Test in unheated state.

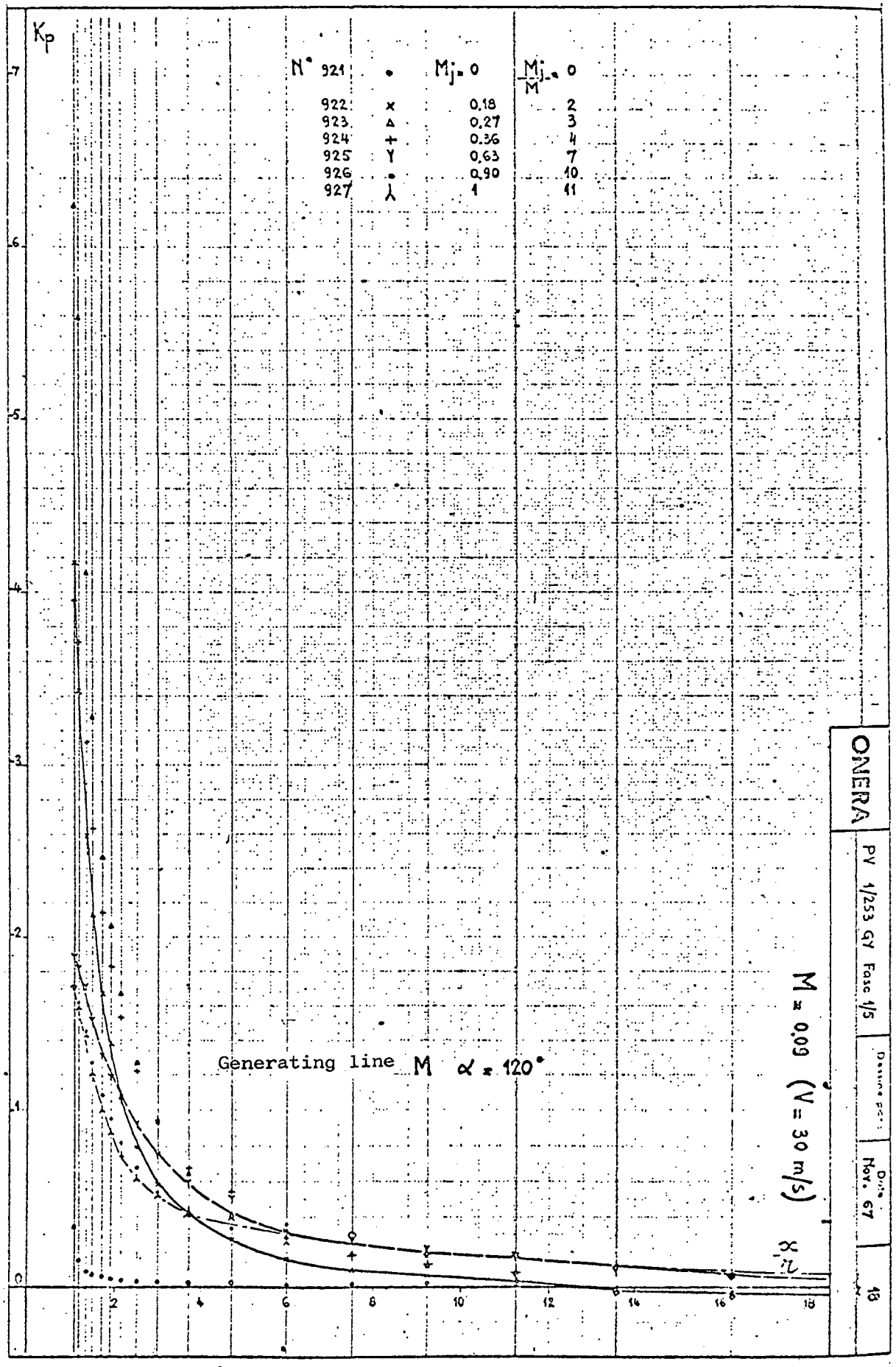

Figure 18. Jet interaction. Test in unheated state.

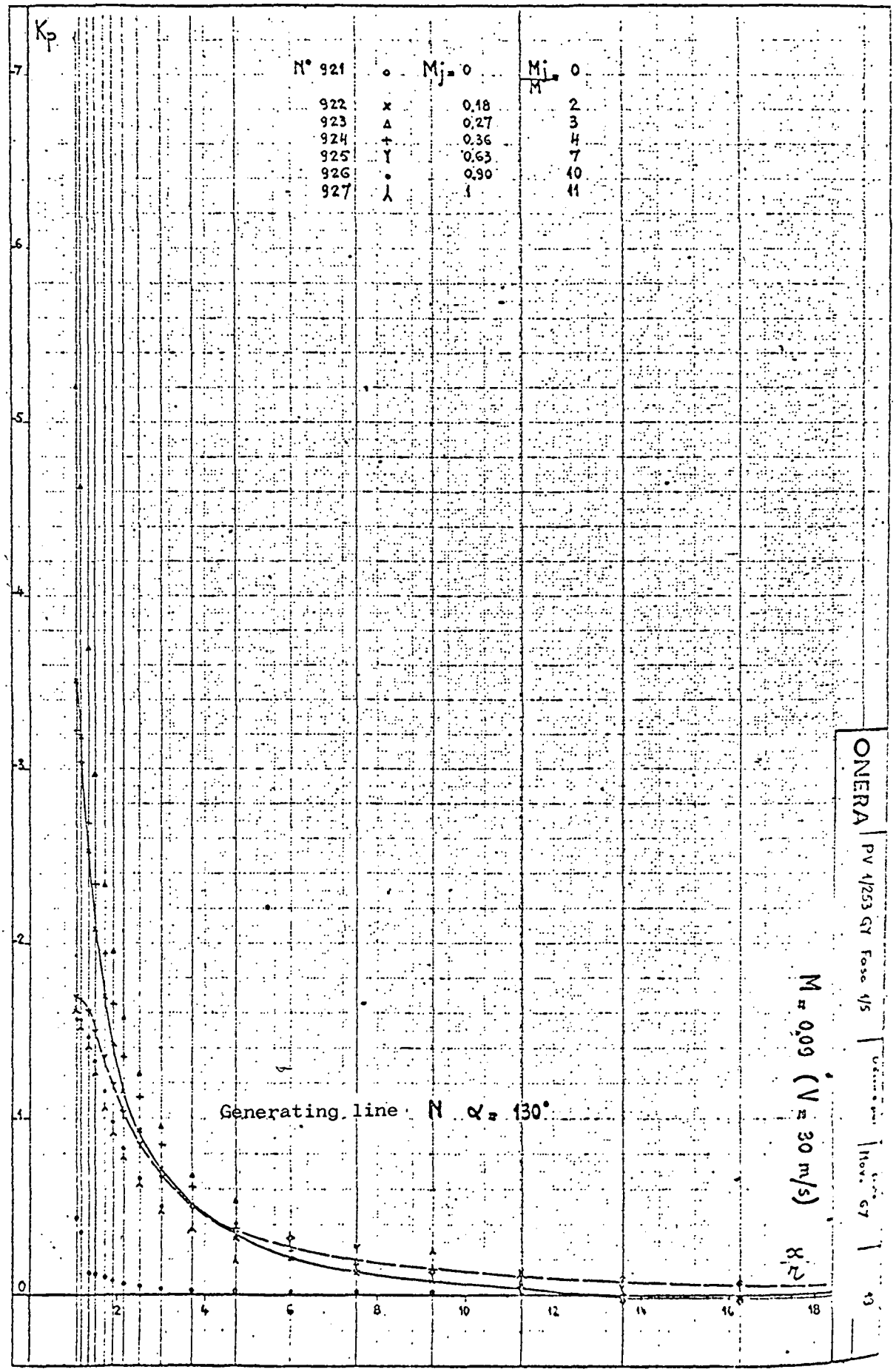

Figure 19. Jet interaction. Test in unheated state.

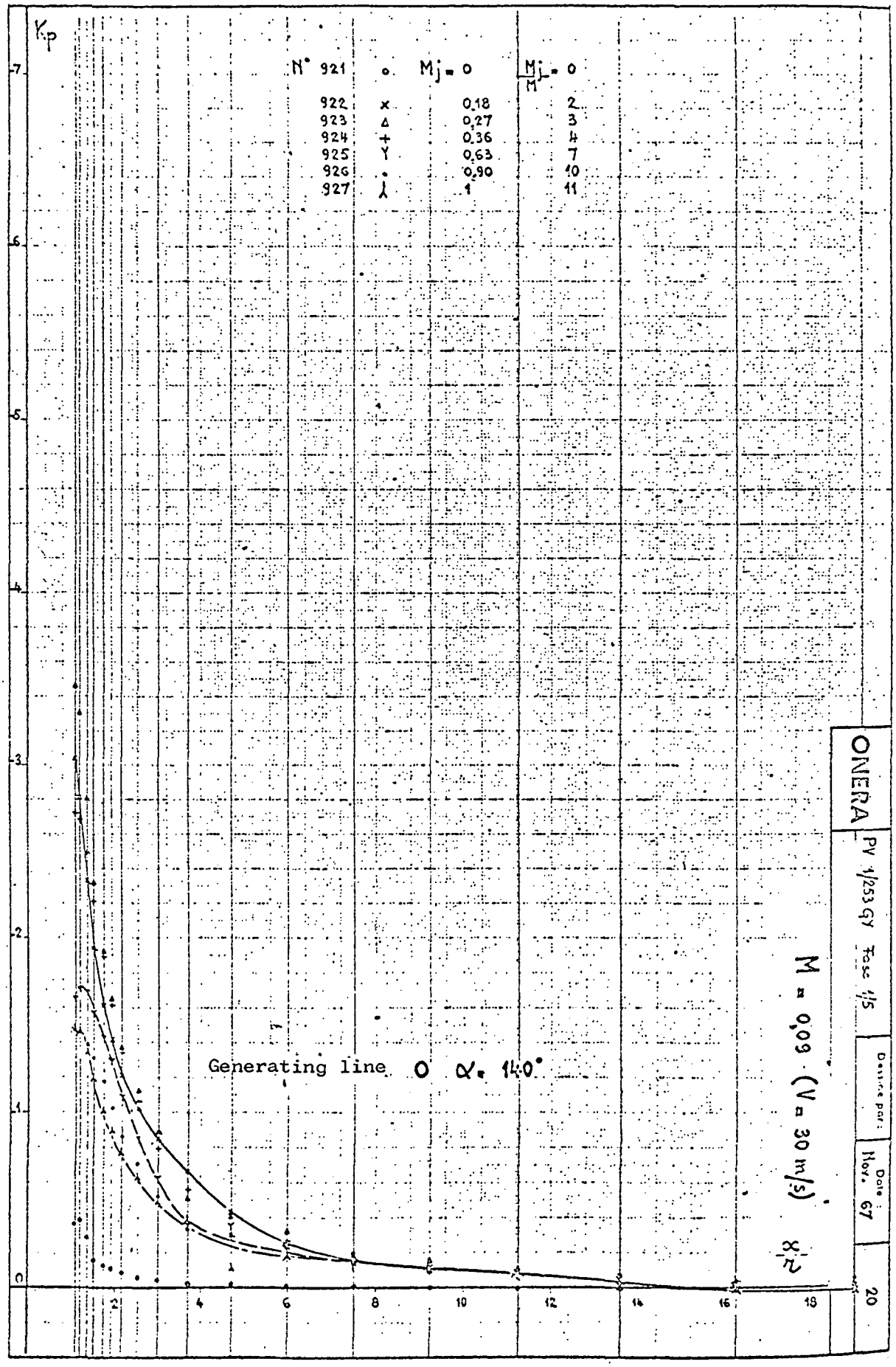

Figure 20. Jet interaction. Test in unheated state.

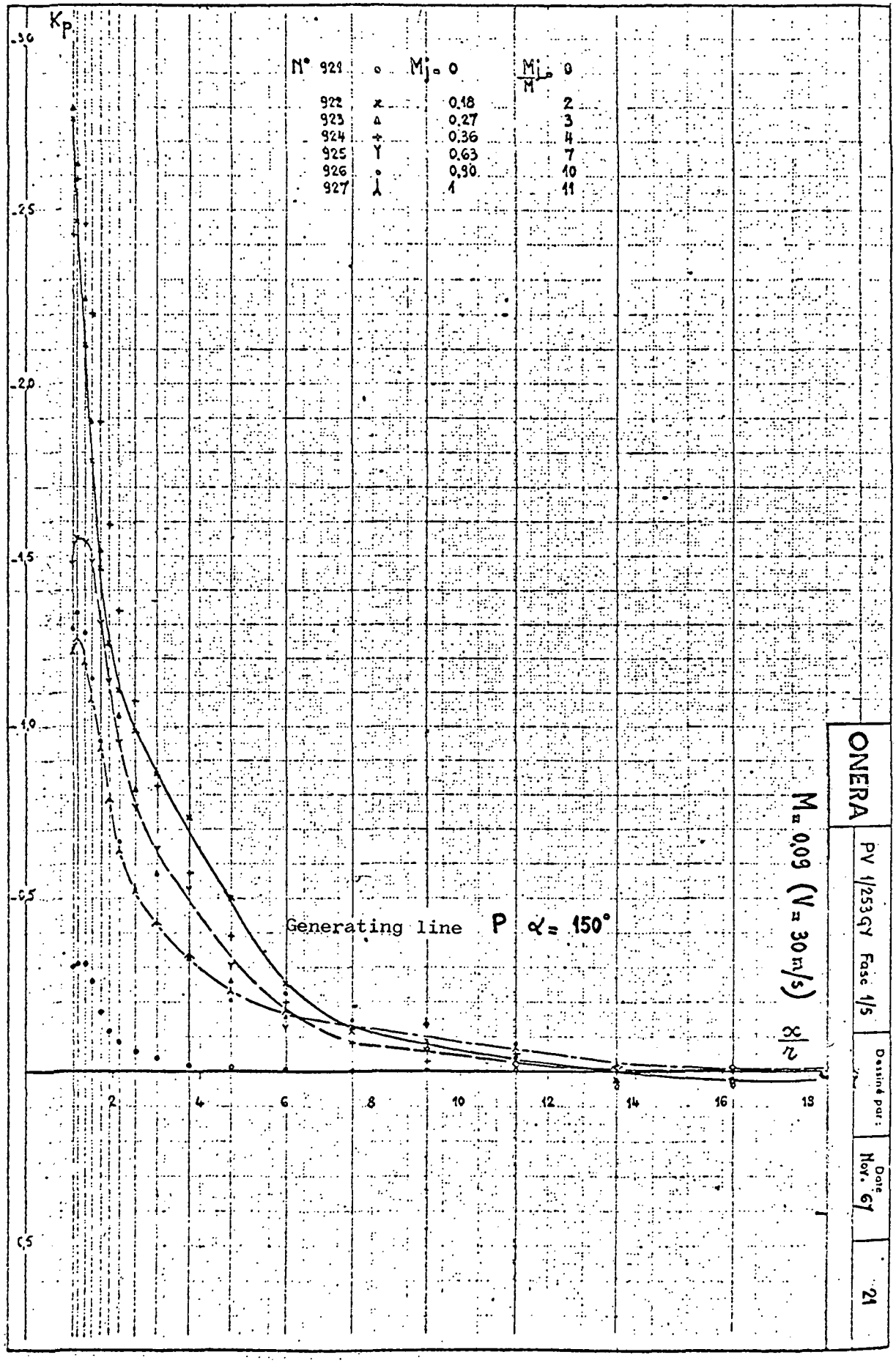

Figure 21. Jet interaction. Test in unheated state.

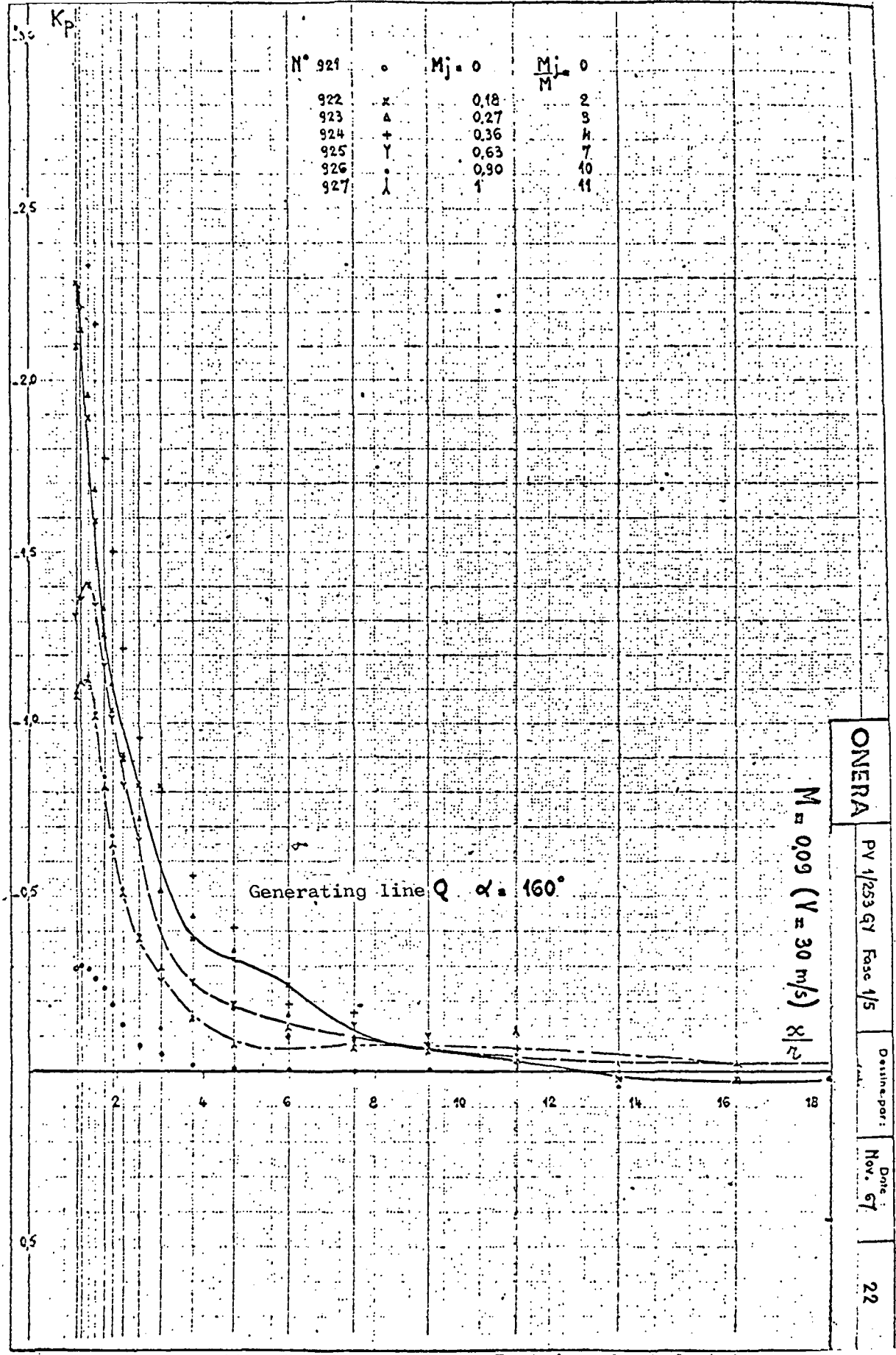

Figure 22. Jet interaction. Test in unheated state.

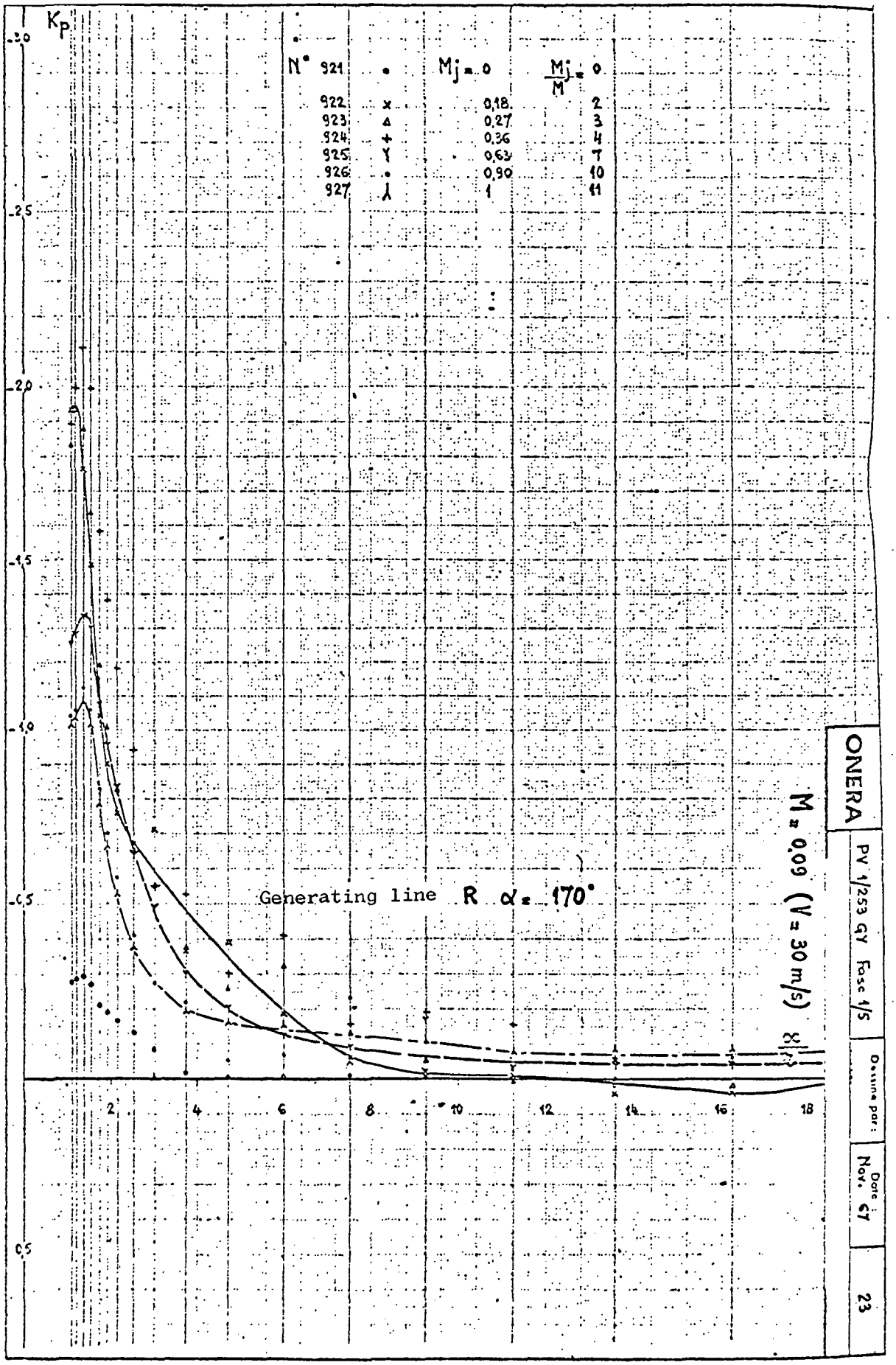

Figure 23. Jet interaction. Test in unheated state.

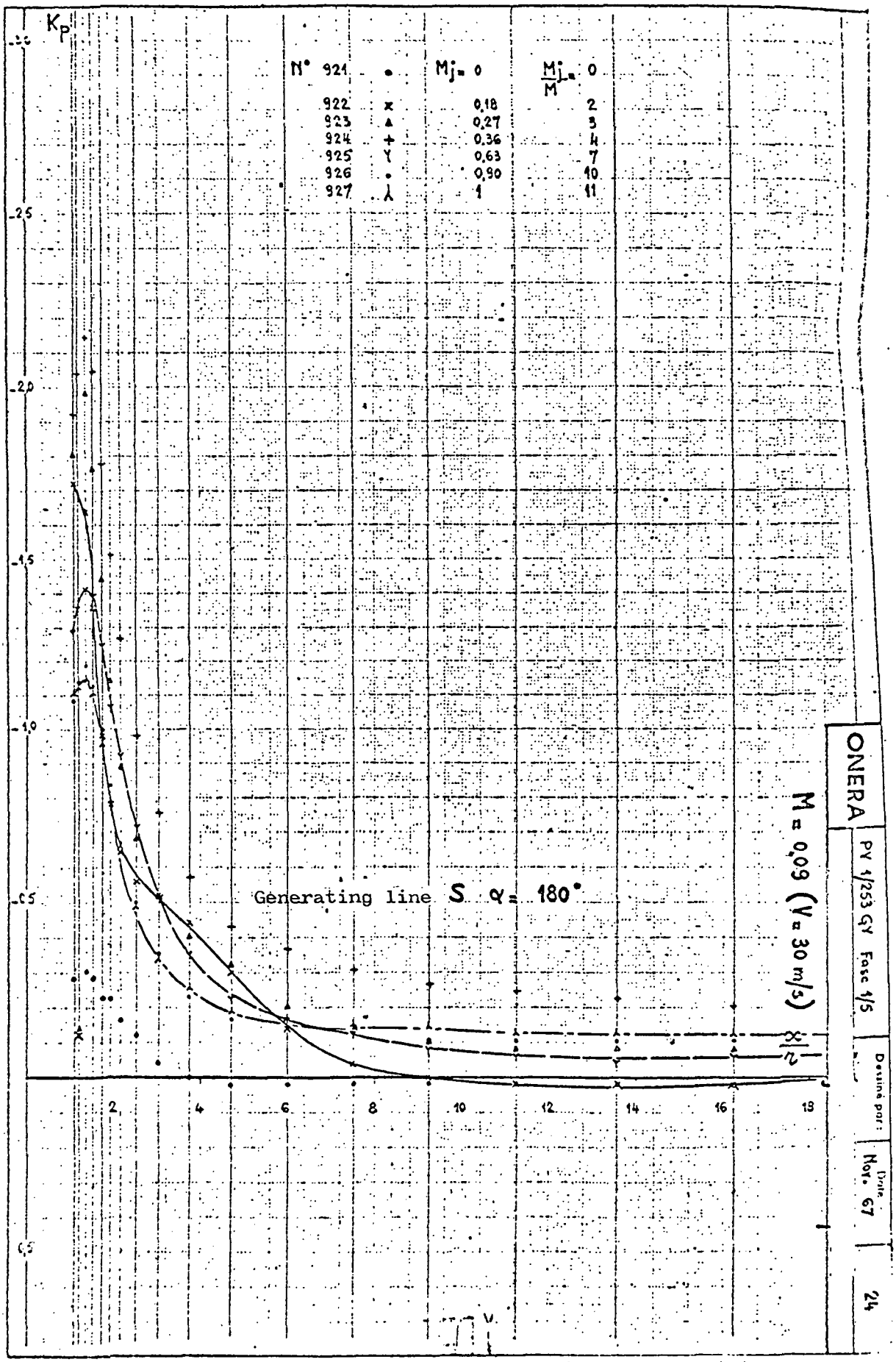

Figure 24. Jet interaction. Test in unheated state.

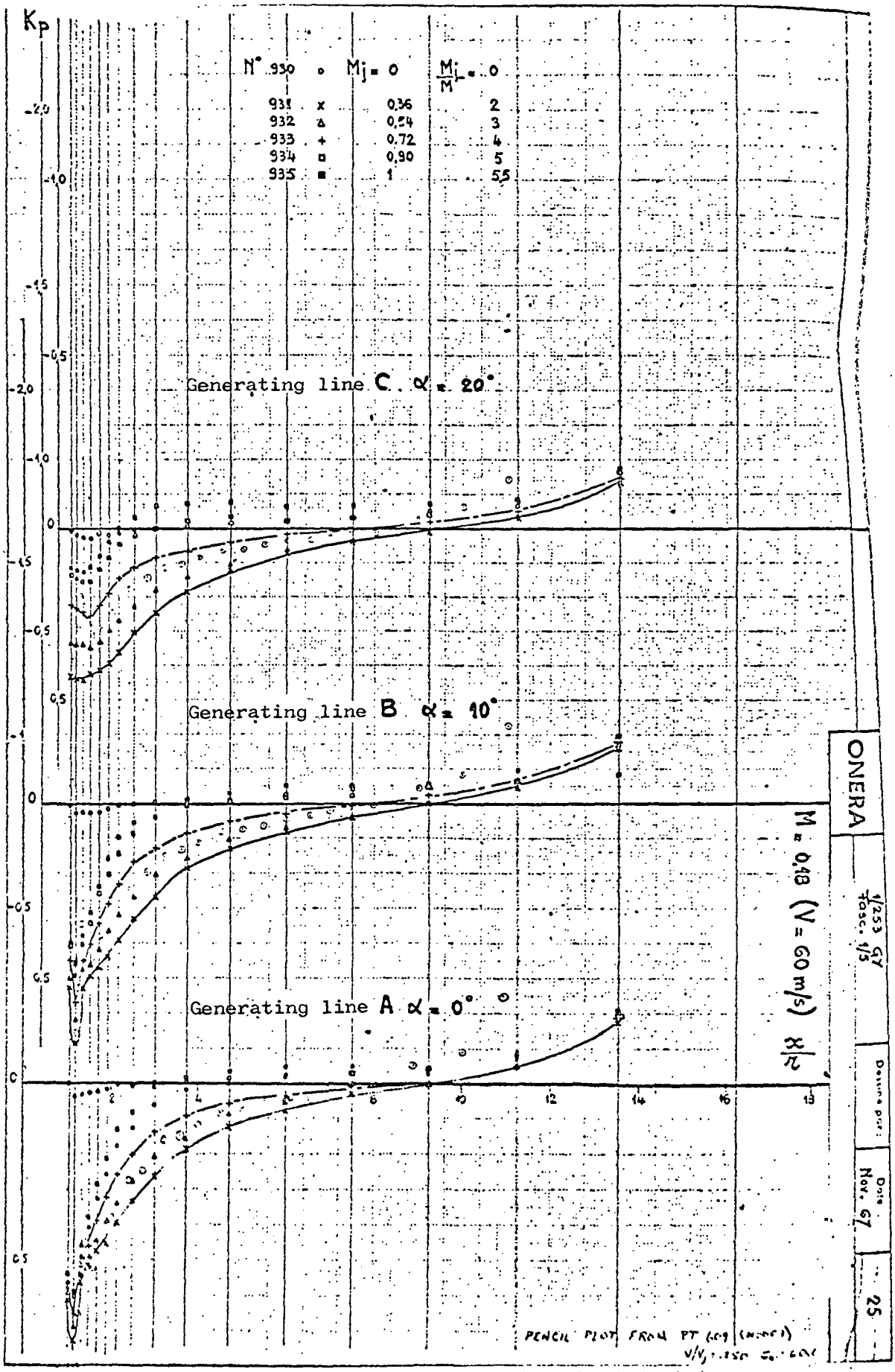
Kp
N° 930 ○ Mj = 0 Mj/M∞ = 0
931 × 0,36 2
932 △ 0,54 3
933 + 0,72 4
934 □ 0,90 5
935 ■ 1 5,5
Generating line C α = 20°
Generating line B α = 10°
Generating line A α = 0°
M = 0,48 (V = 60 m/s) x/l
ONERA
1/253 GY
Tosc. 1/3
Nov. 67
25
PENCIL PLOT FROM PT 609 (INDOOR)

Figure 25. Jet interaction. Test in unheated state.

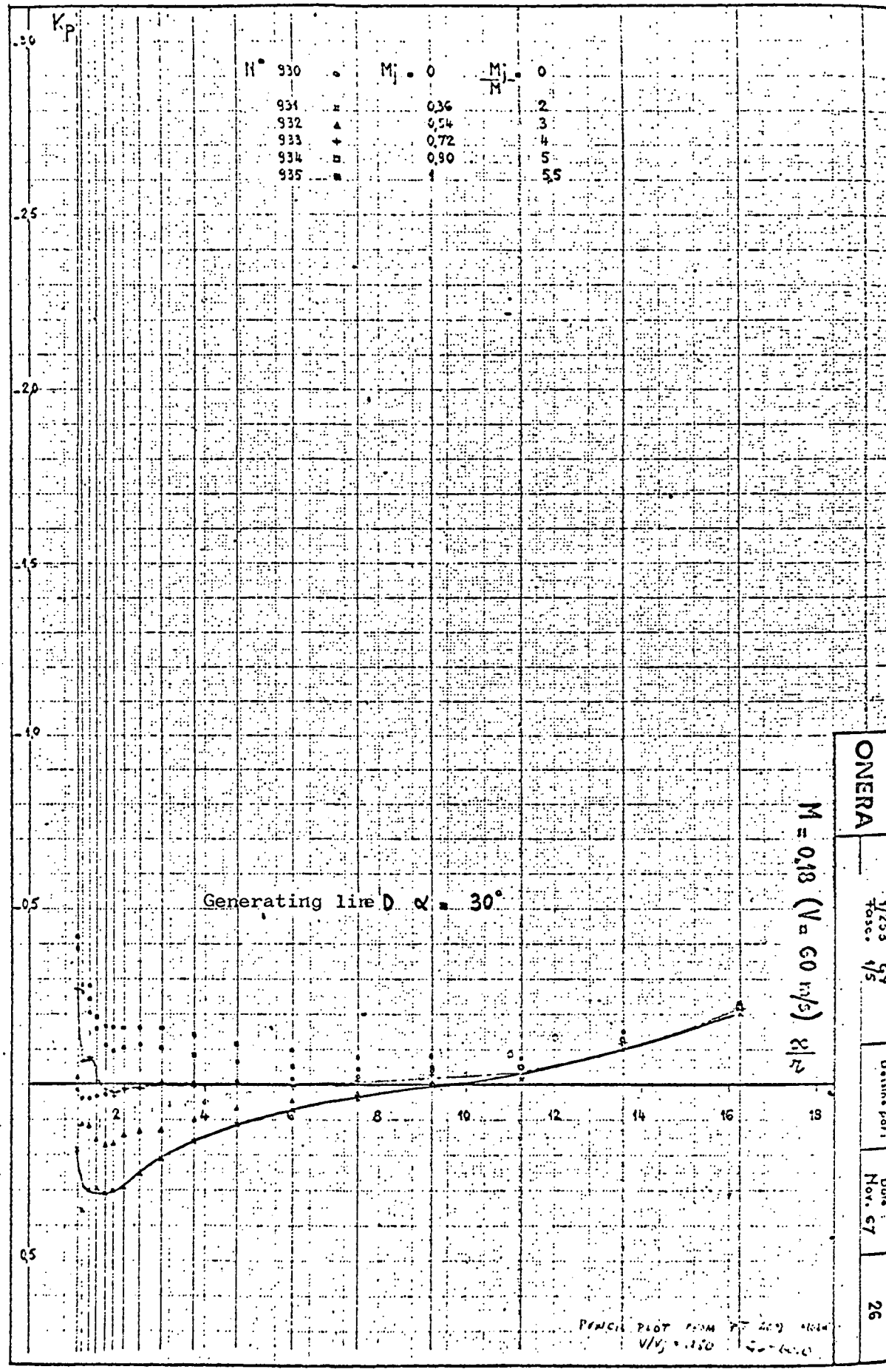

Figure 26. Jet interaction. Test in unheated state.

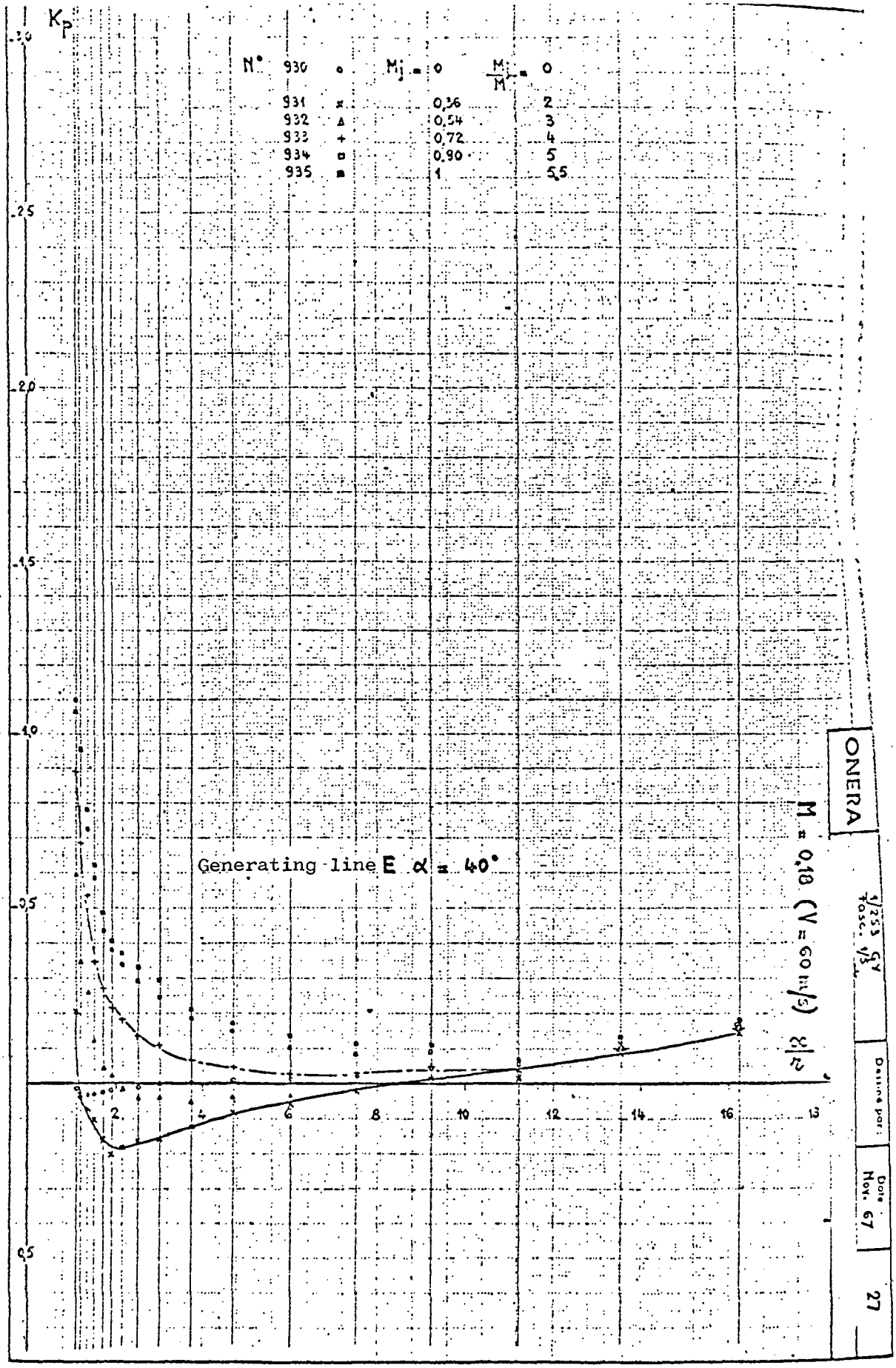

Figure 27. Jet interaction. Test in unheated state.

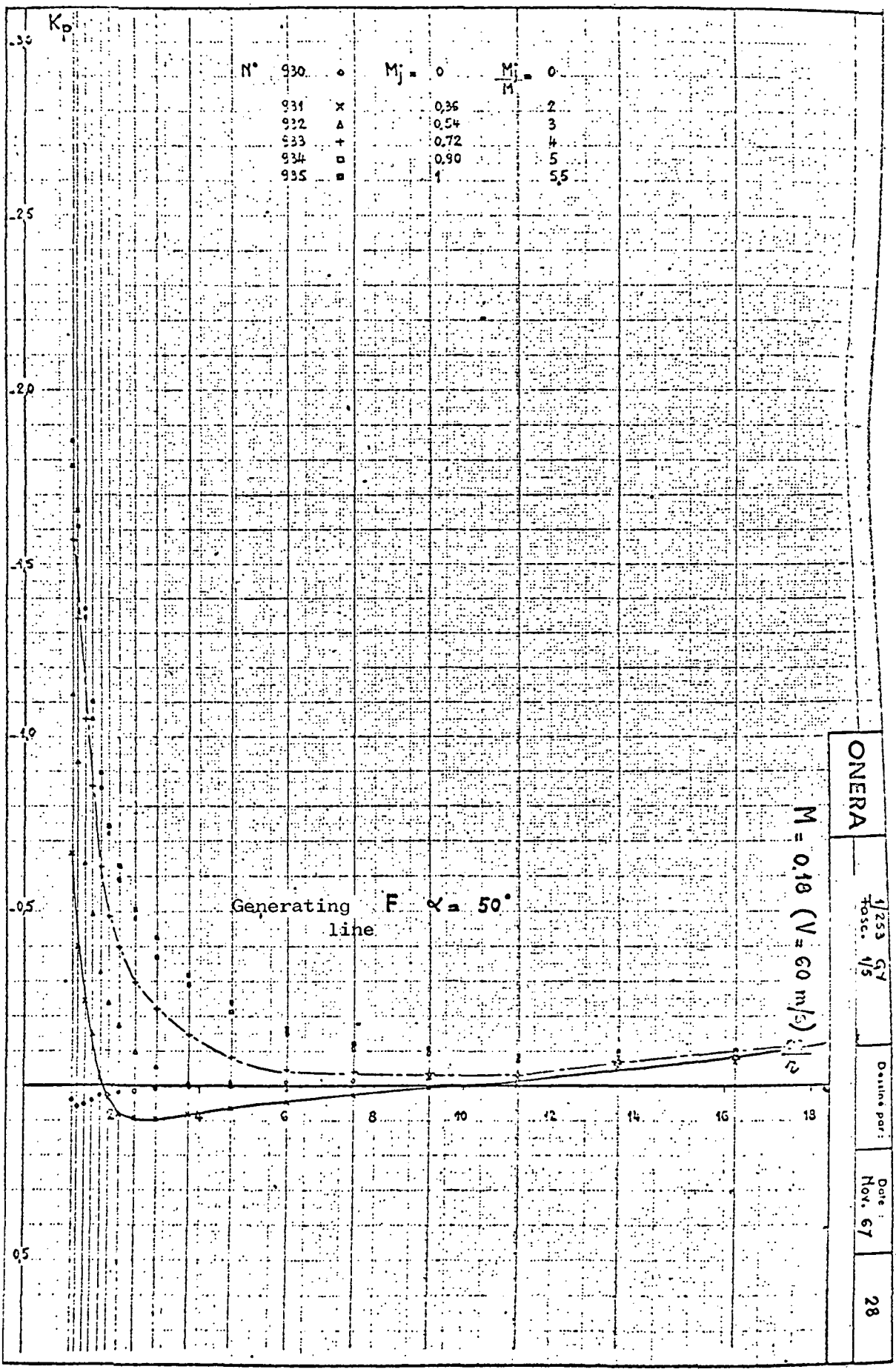

Figure 28. Jet interaction. Test in unheated state.

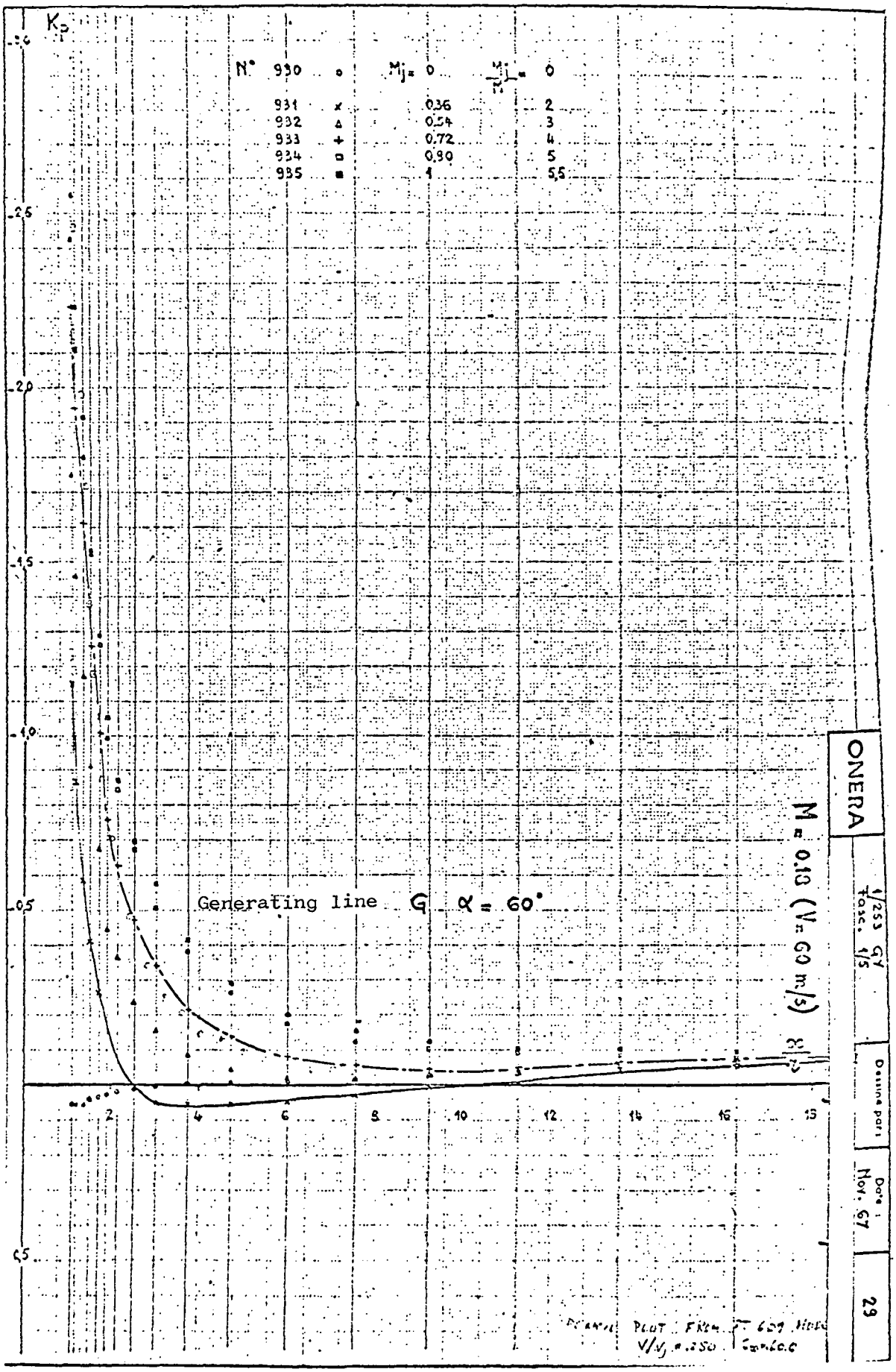

Figure 29. Jet interaction. Test in unheated state.

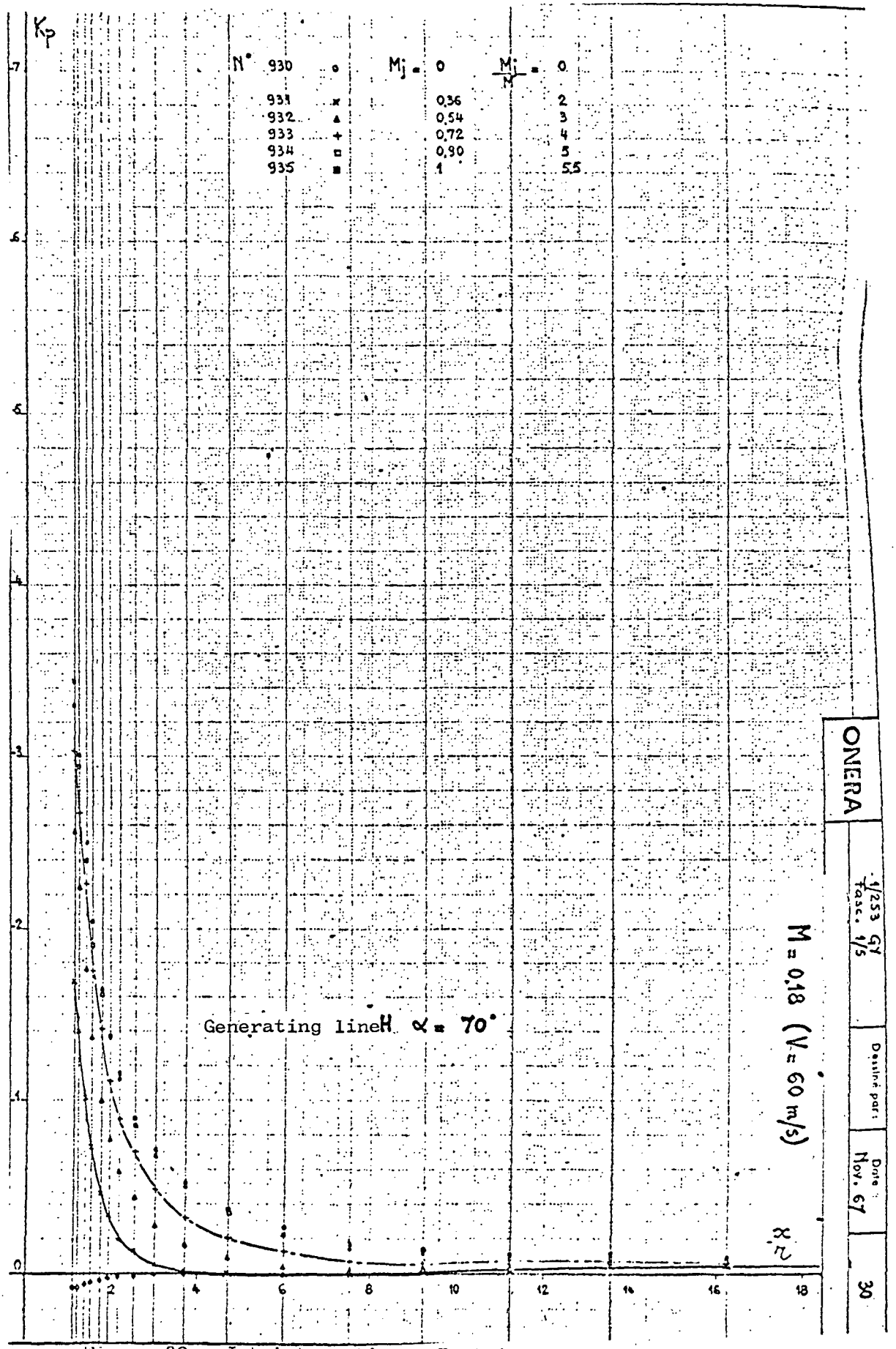

Figure 30. Jet interaction. Test in unheated state.

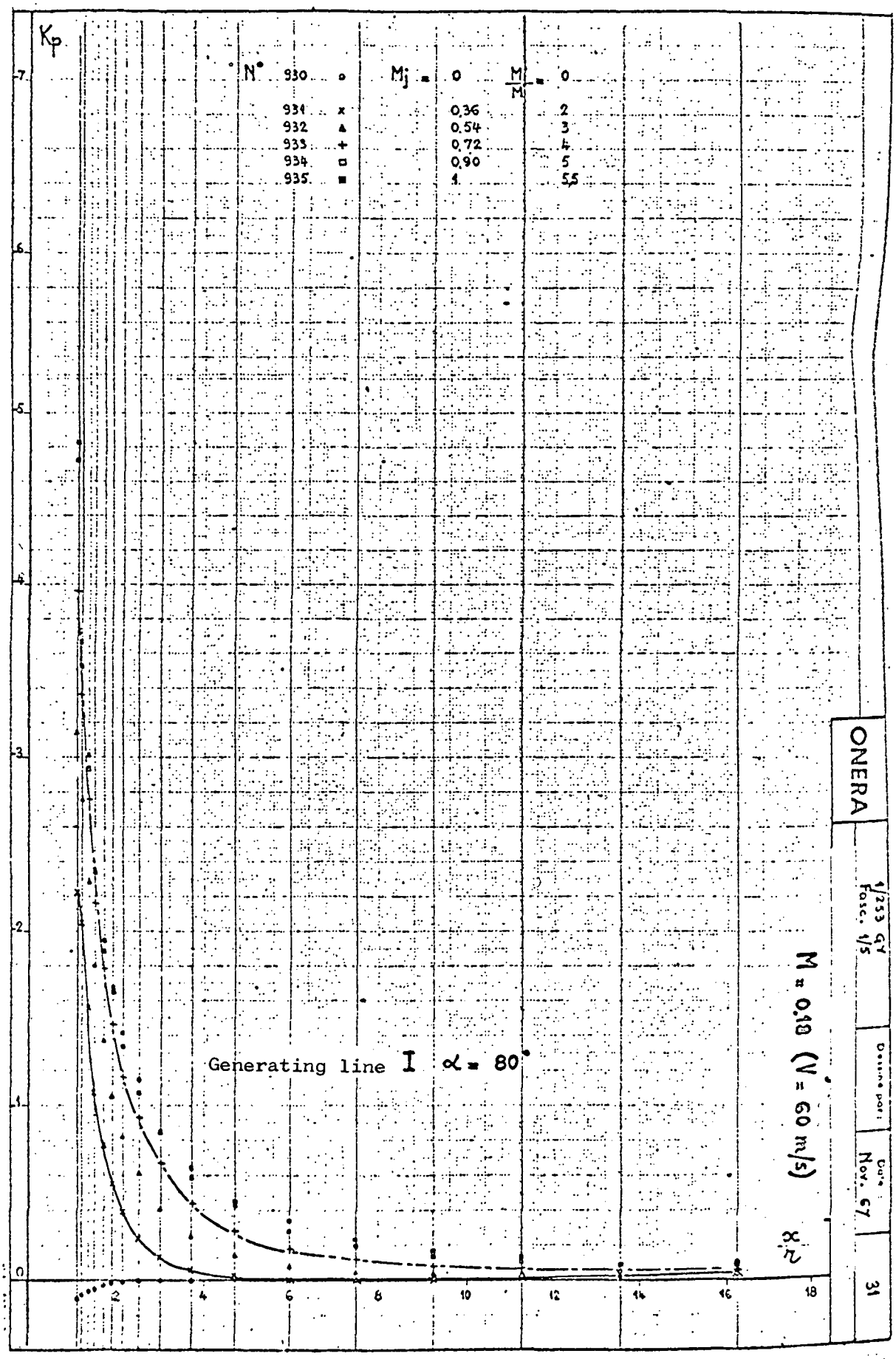

Figure 31. Jet interaction. Test in unheated state.

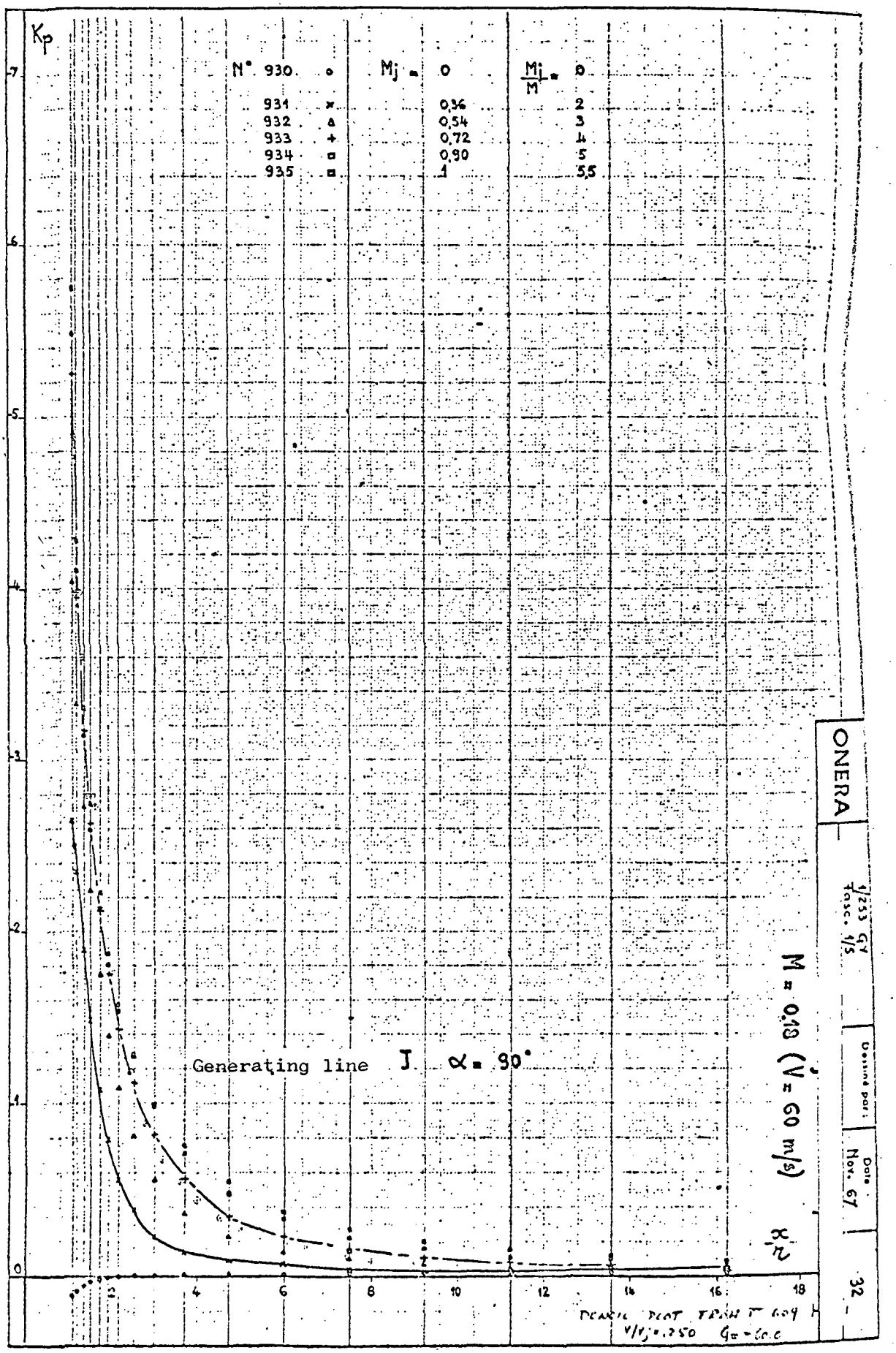

Figure 32. Jet interaction. Test in unheated state.

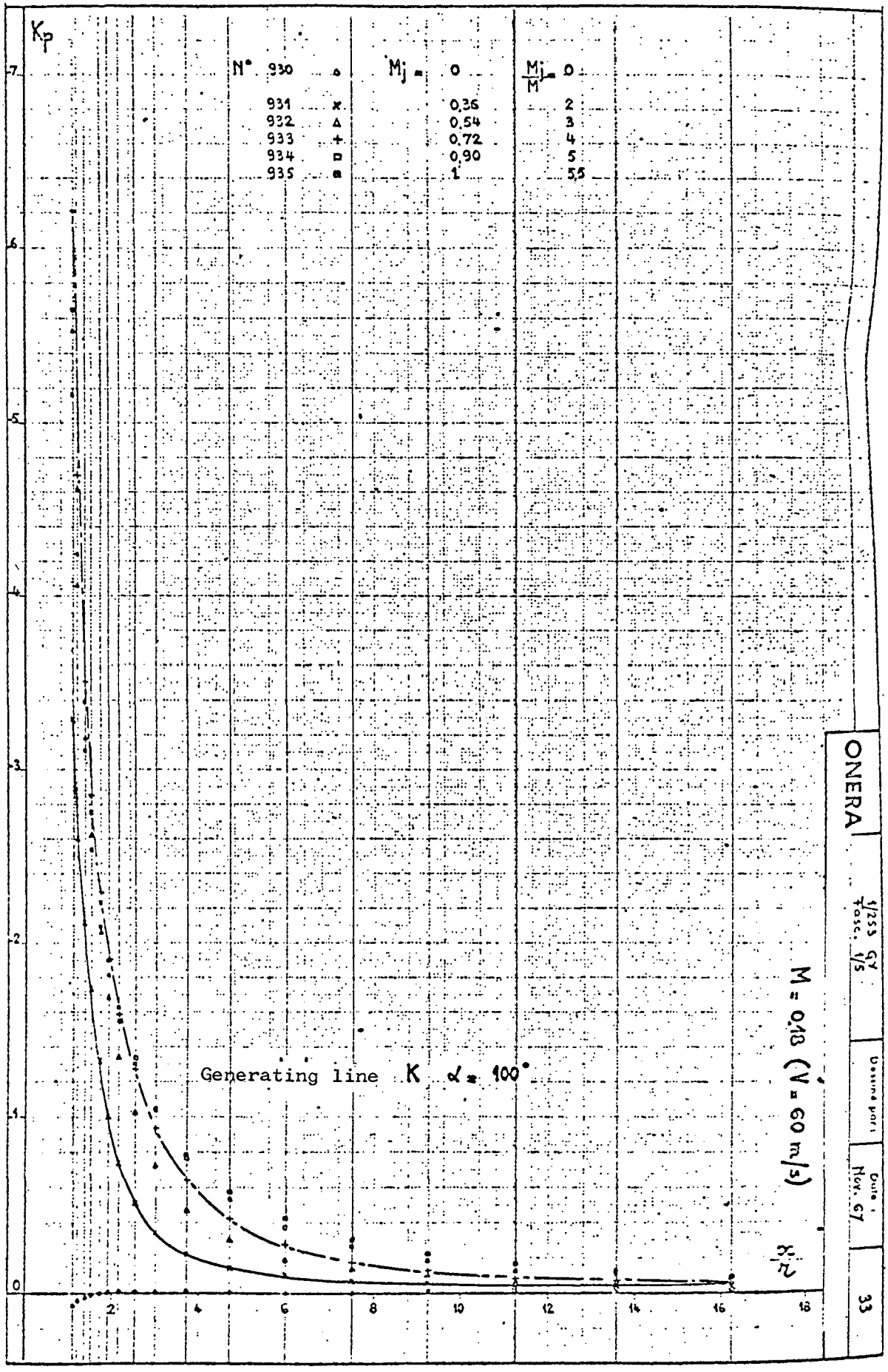

Figure 33. Jet interaction. Test in unheated state.

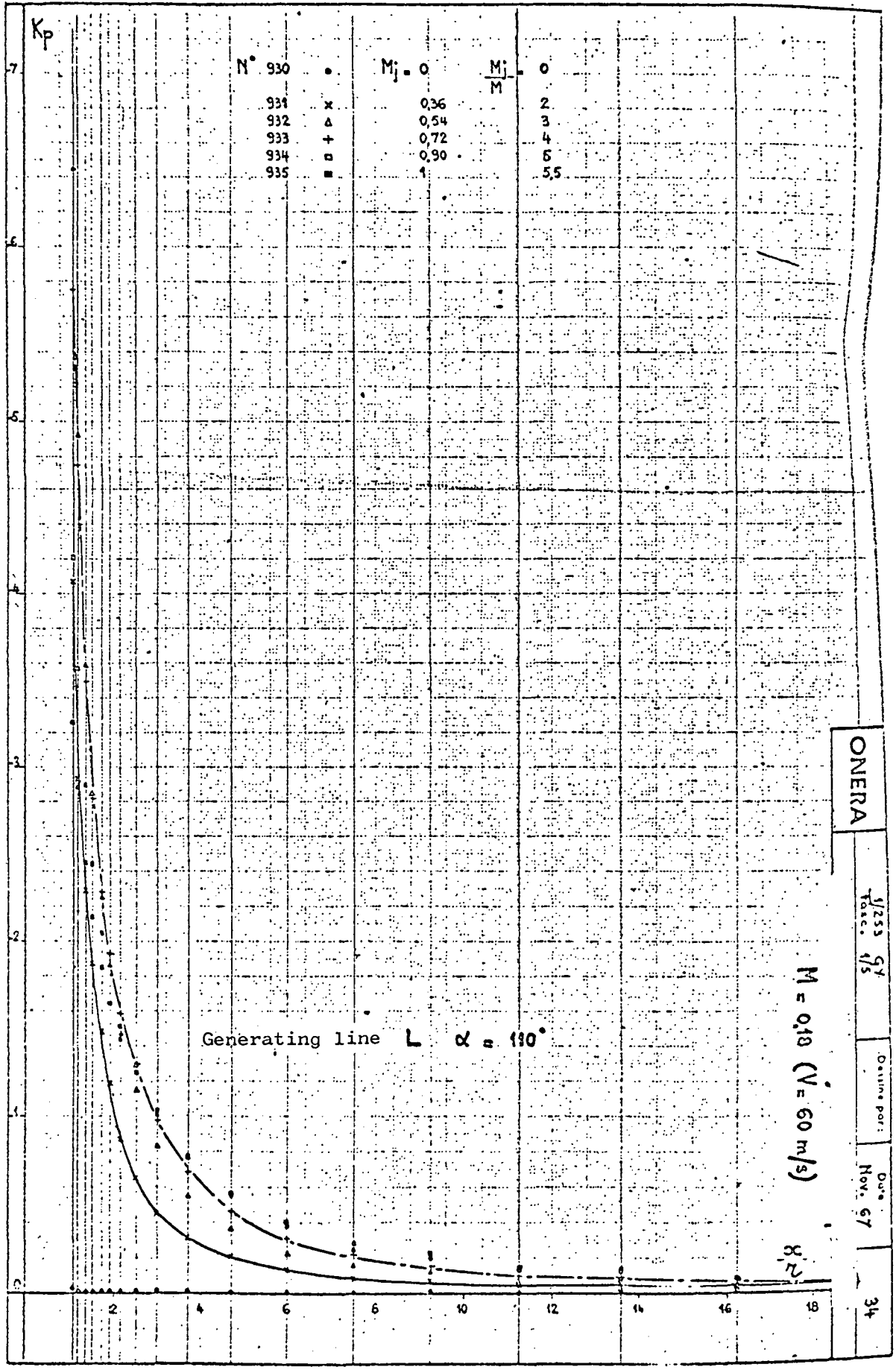

Figure 34. Jet interaction. Test in unheated state.

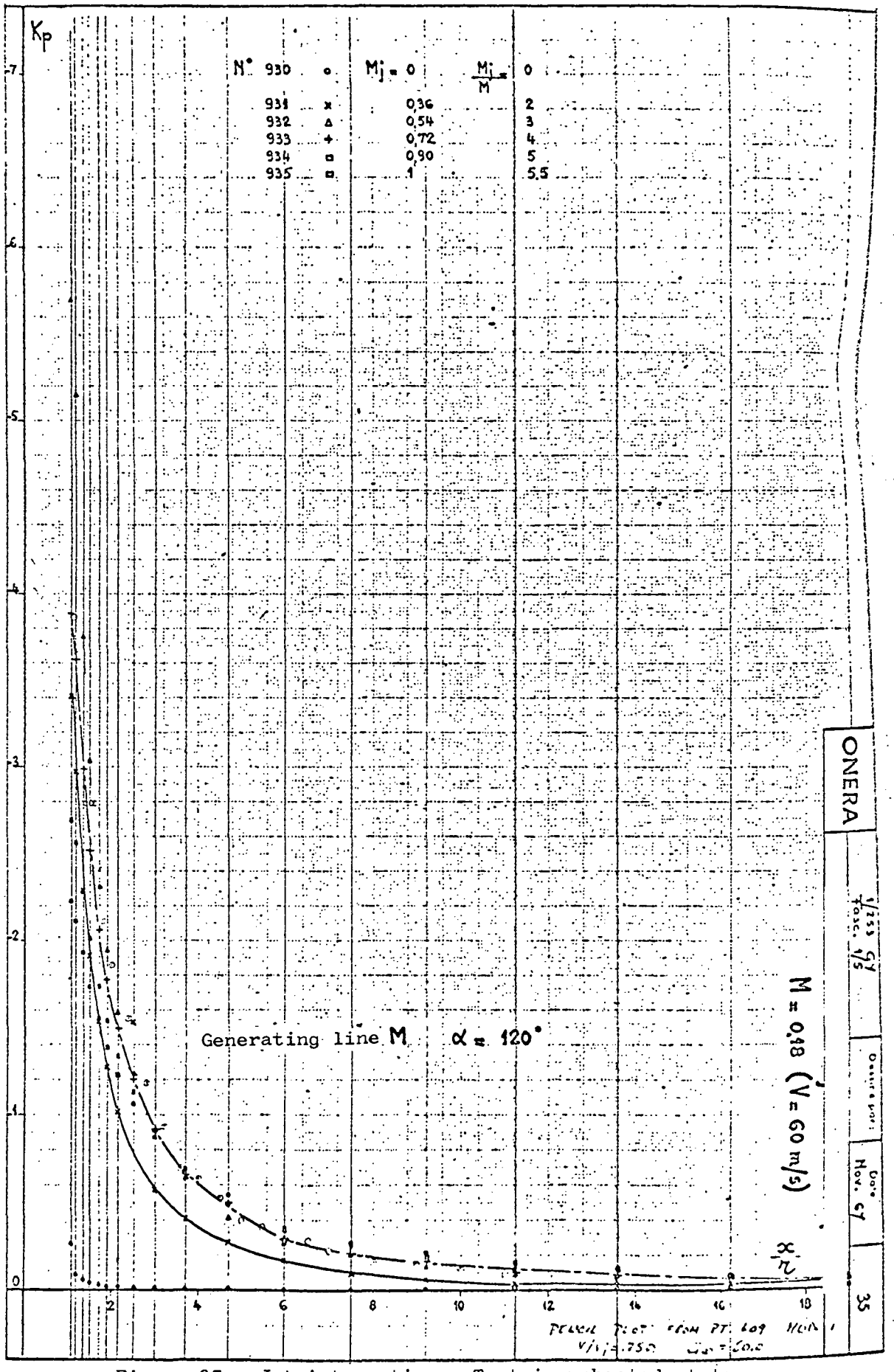

Figure 35. Jet interaction. Test in unheated state.

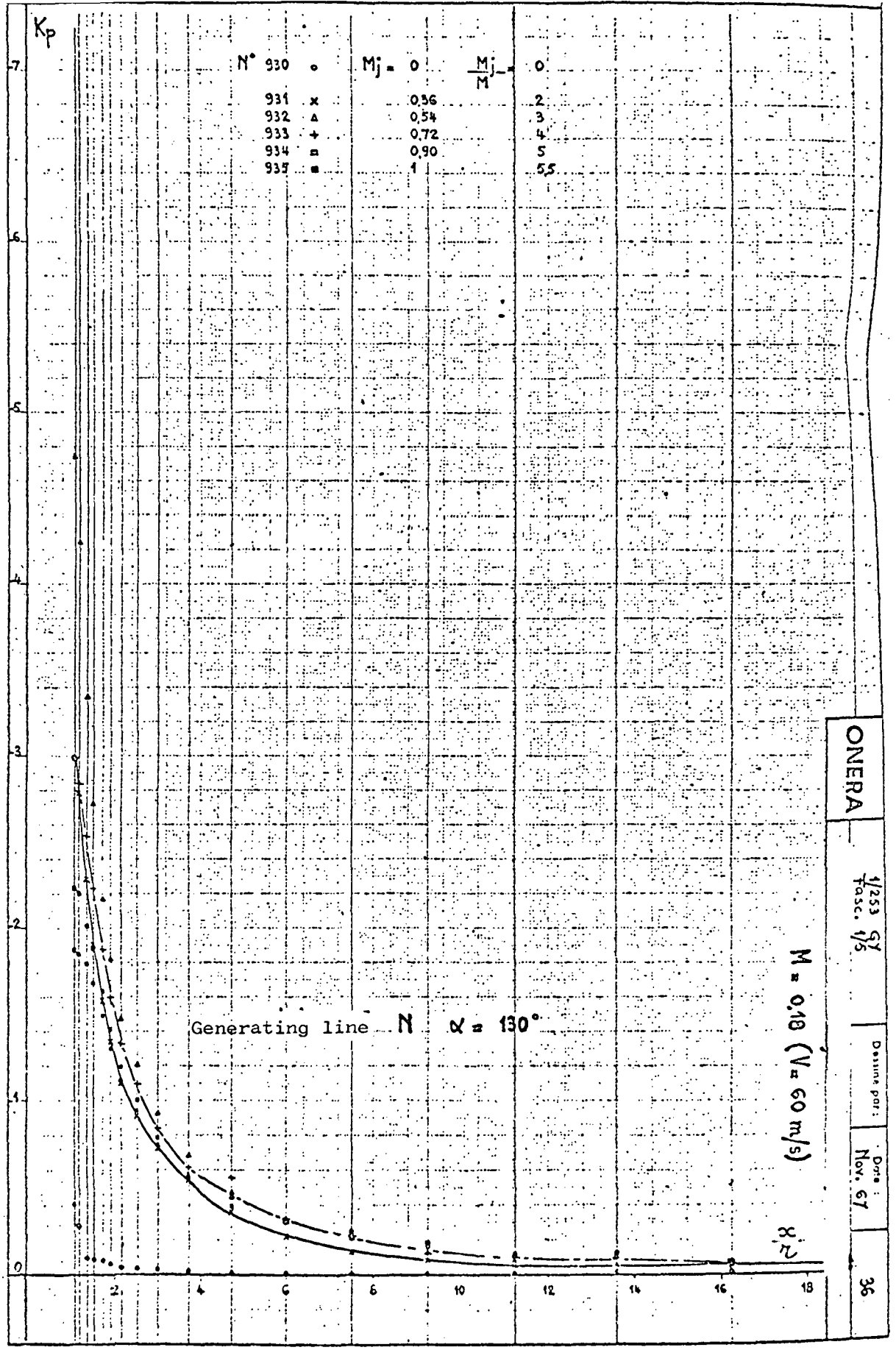

Figure 36. Jet interaction. Test in unheated state.

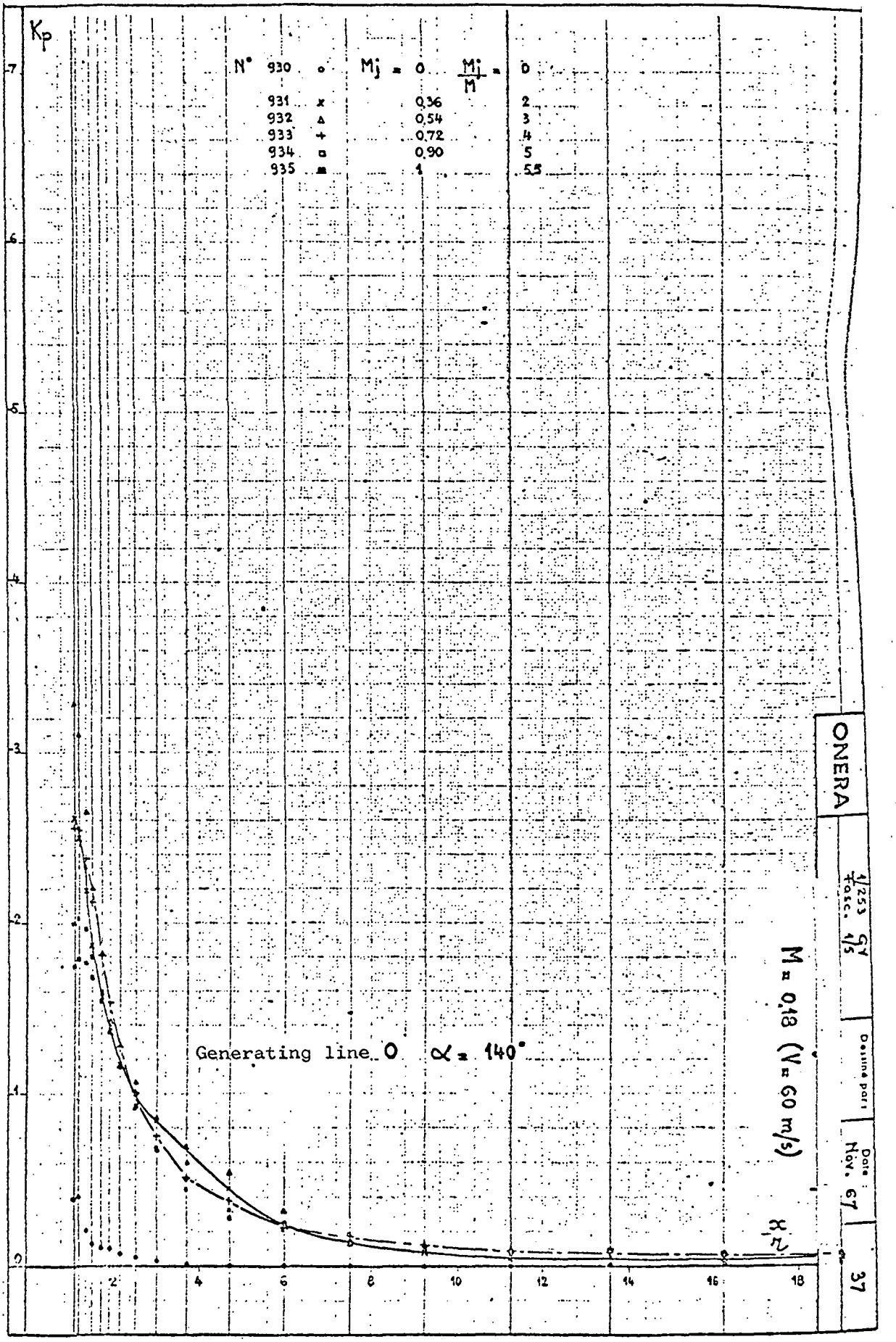

Figure 37. Jet interaction. Test in unheated state.

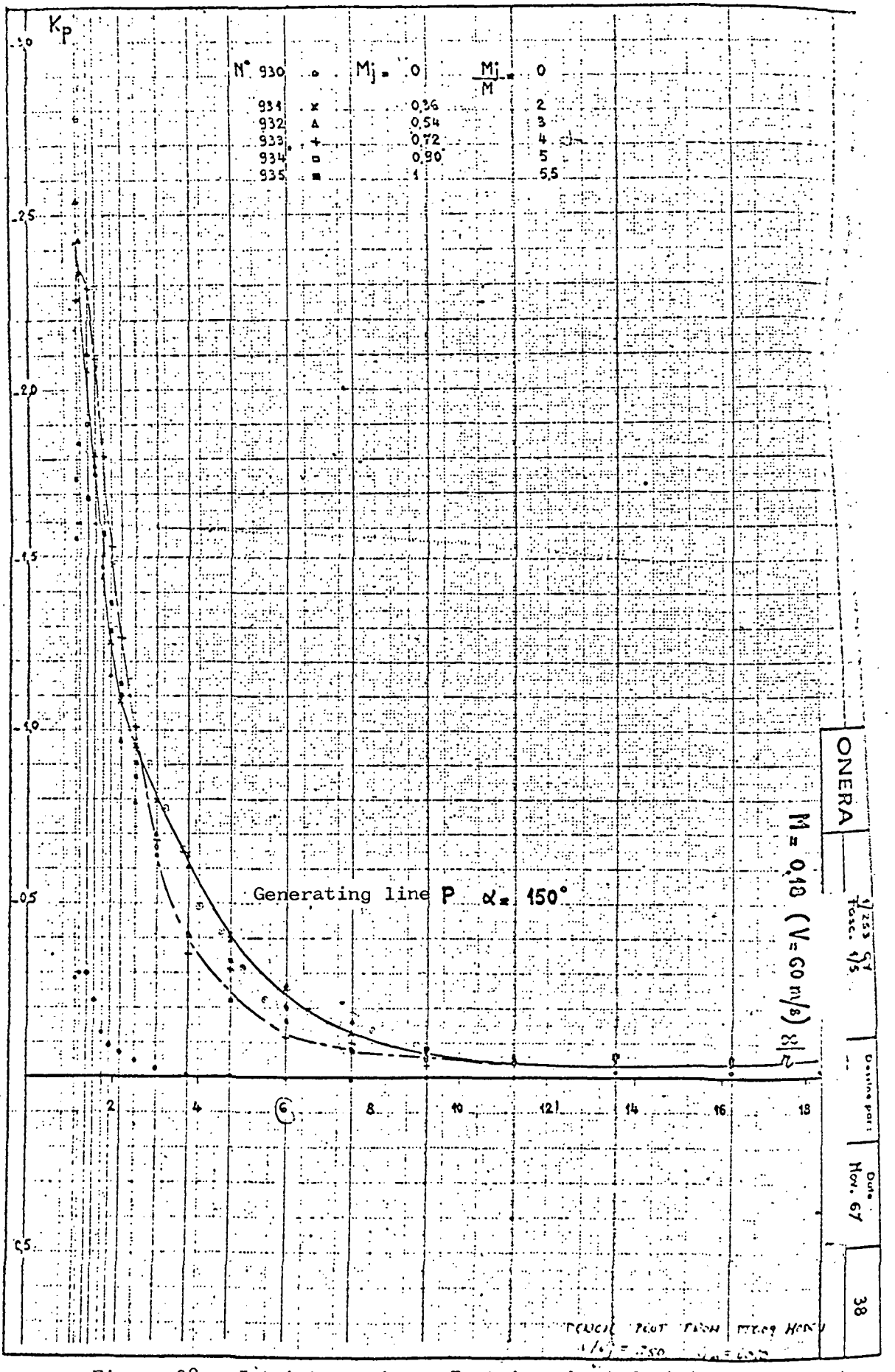

Figure 38. Jet interaction. Test in unheated state.

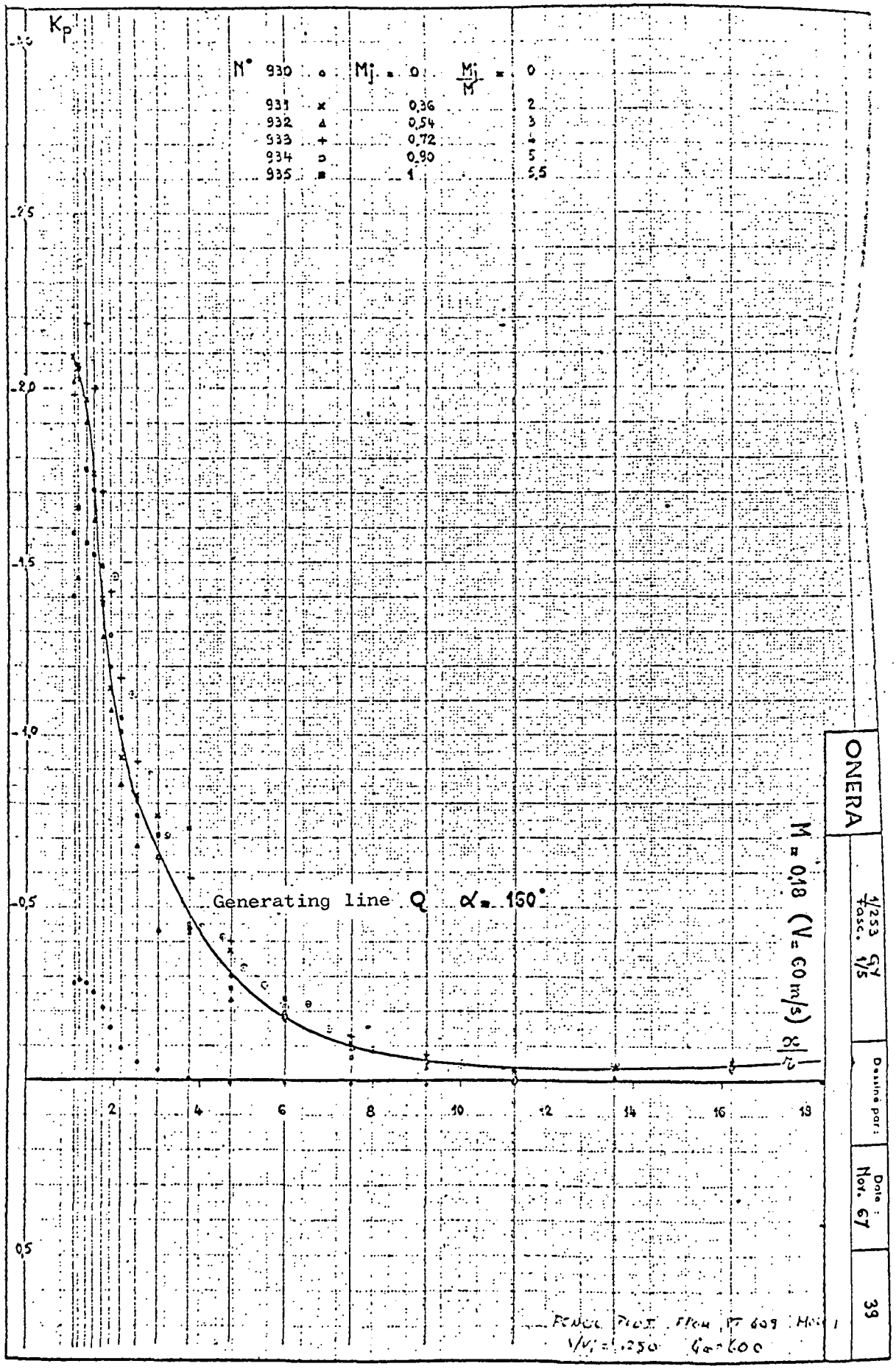

Figure 39. Jet interaction. Test in unheated state.

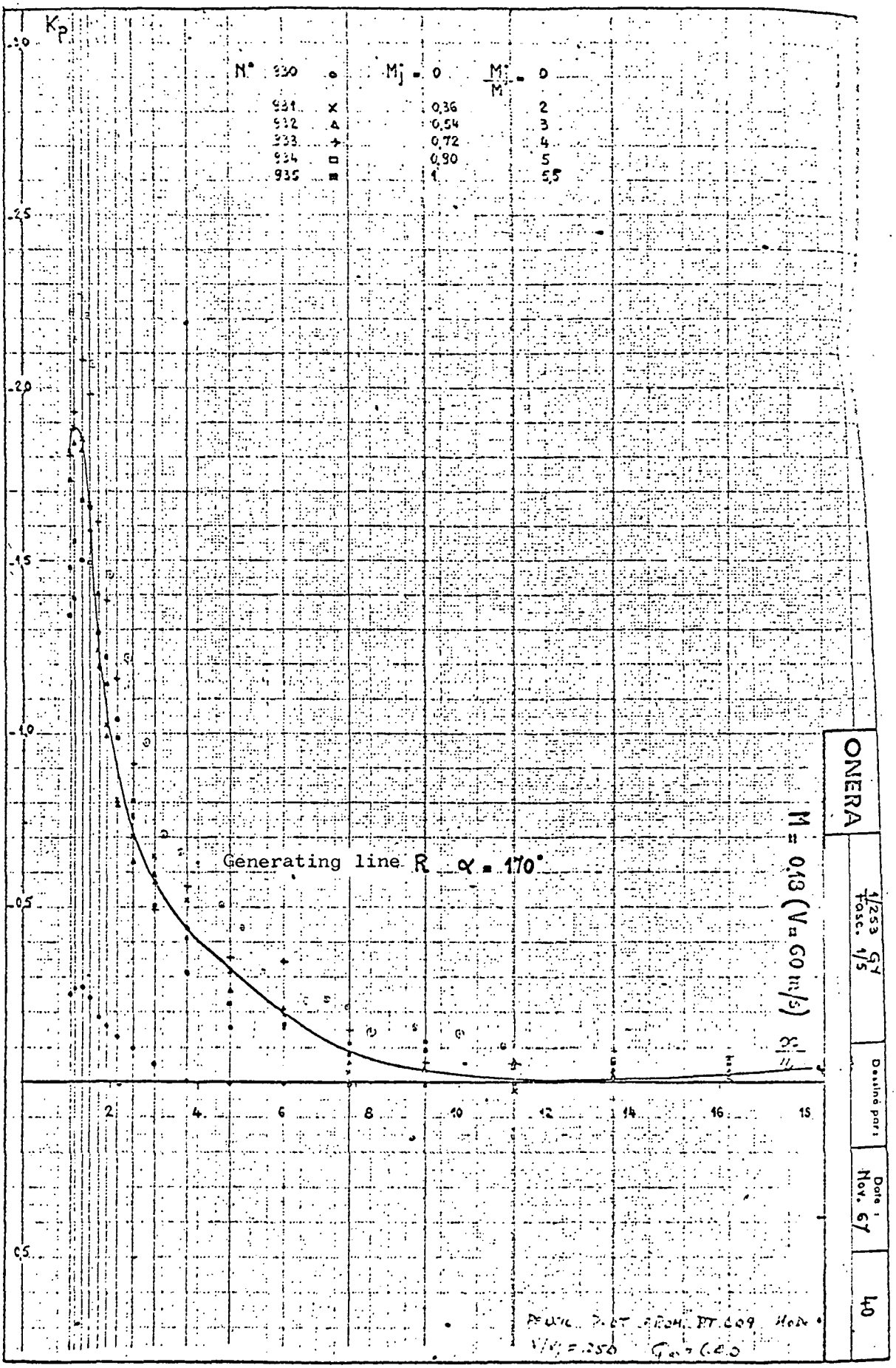

Figure 40. Jet interaction. Test in unheated state.

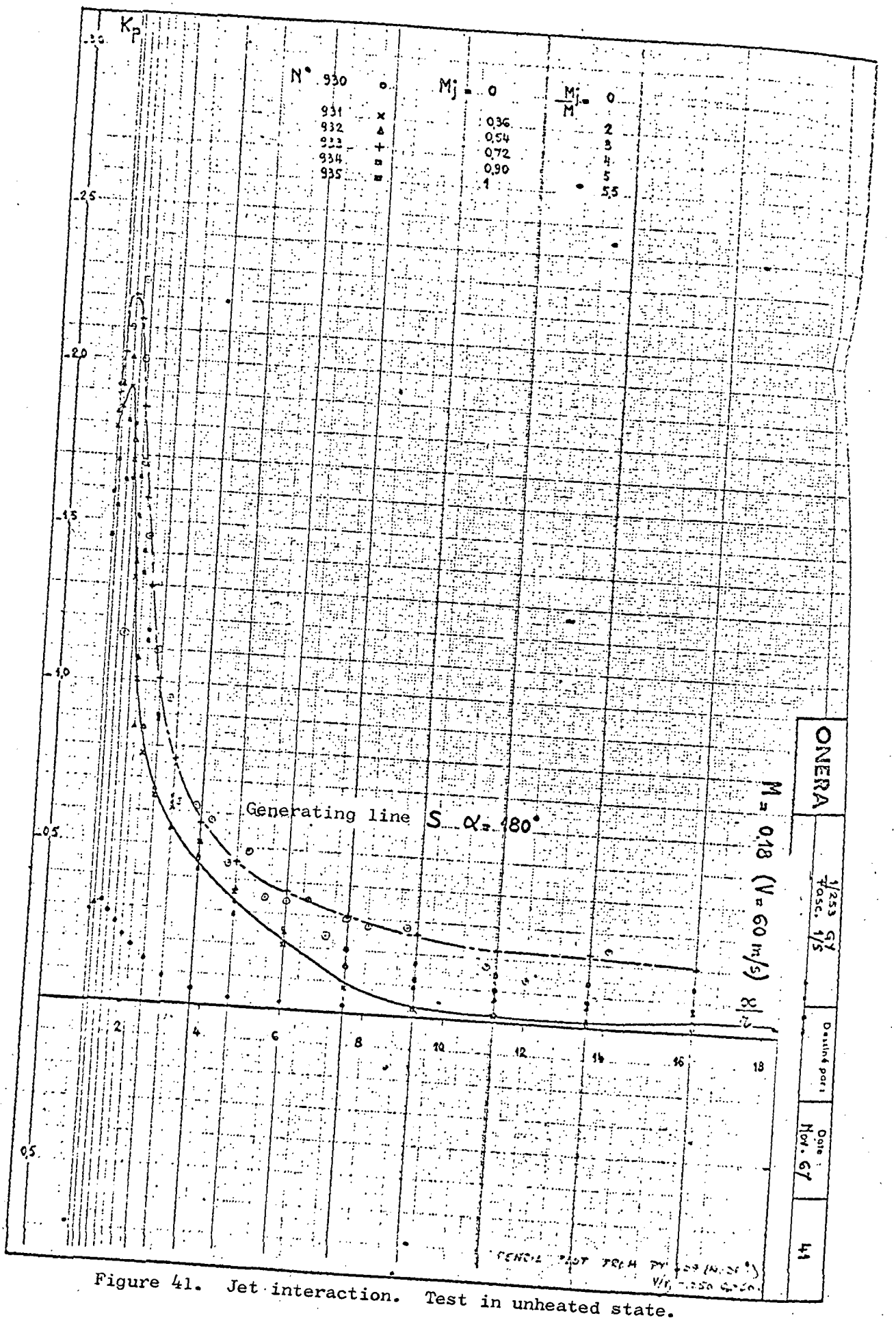

Figure 41. Jet interaction. Test in unheated state.

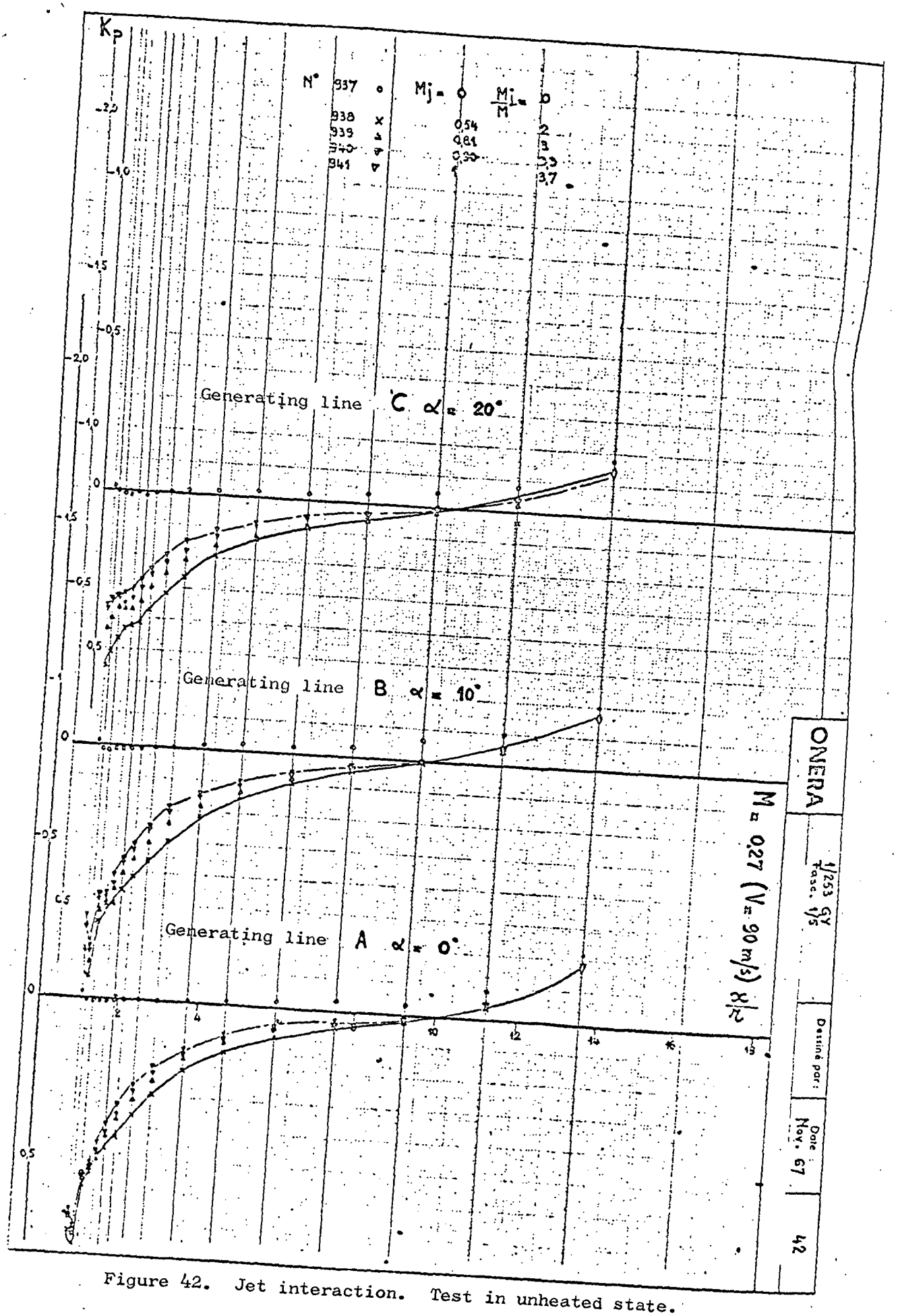

Figure 42. Jet interaction. Test in unheated state.

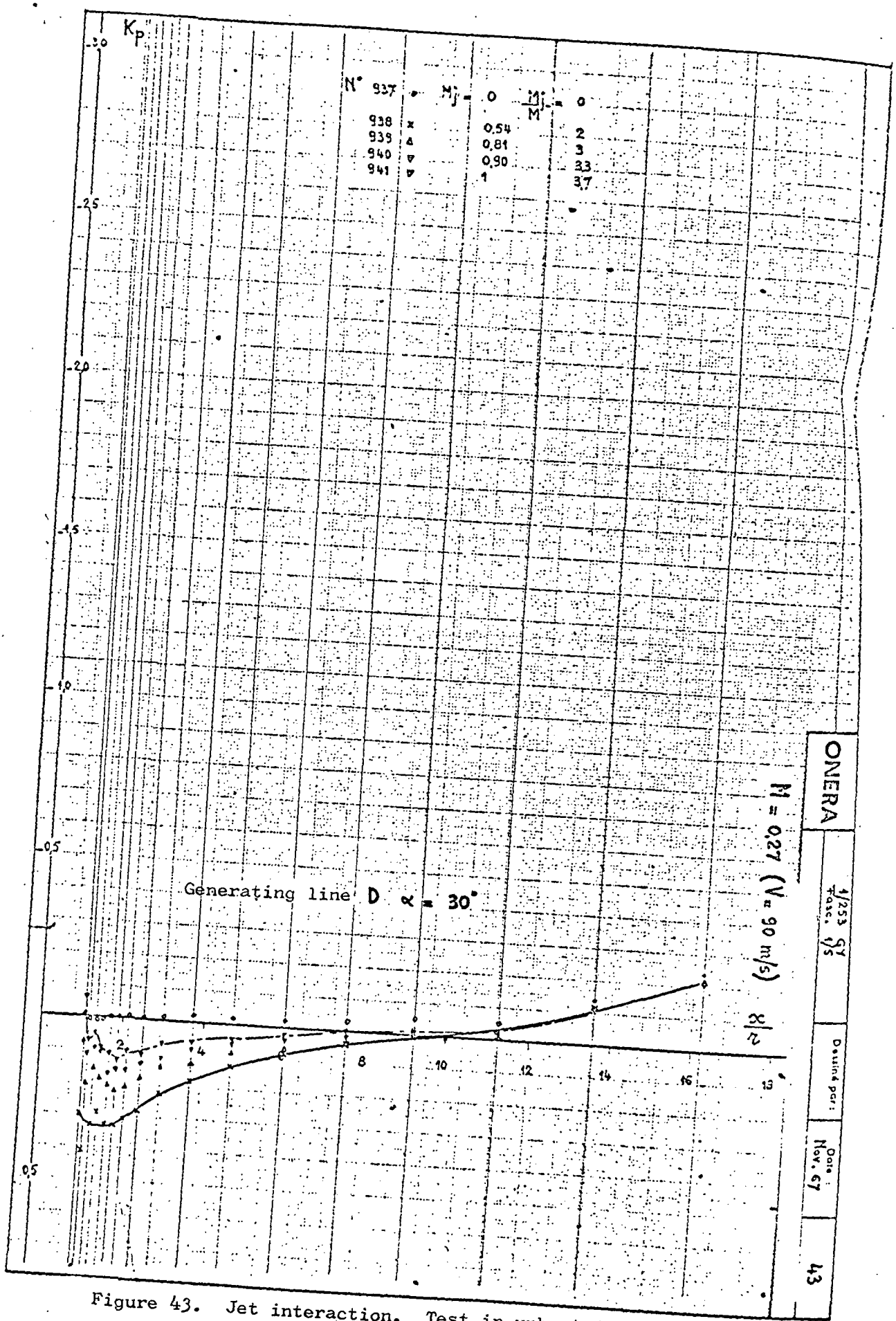

Figure 43. Jet interaction. Test in unheated state.

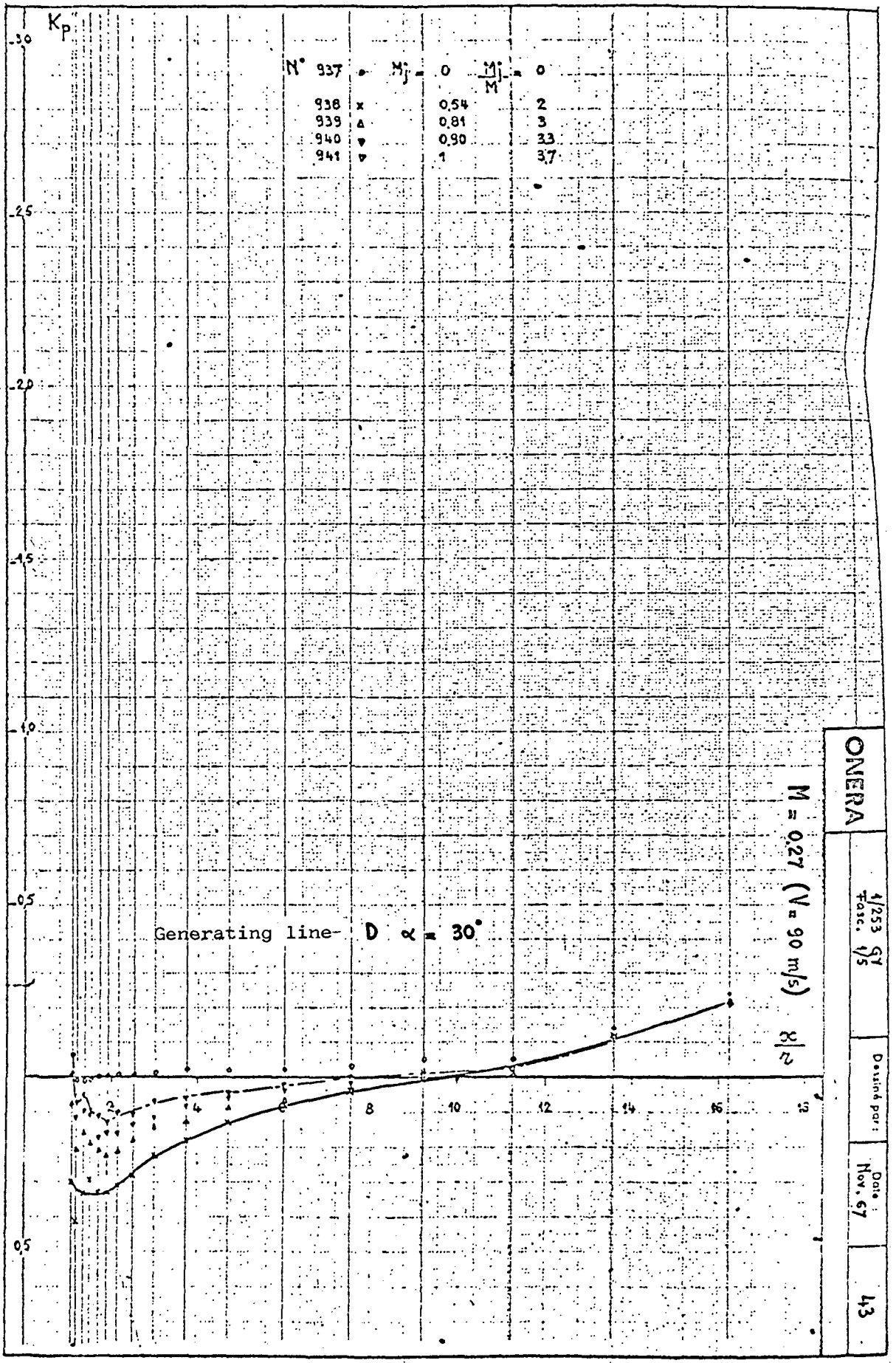

Figure 43. Jet interaction. Test in unheated state.

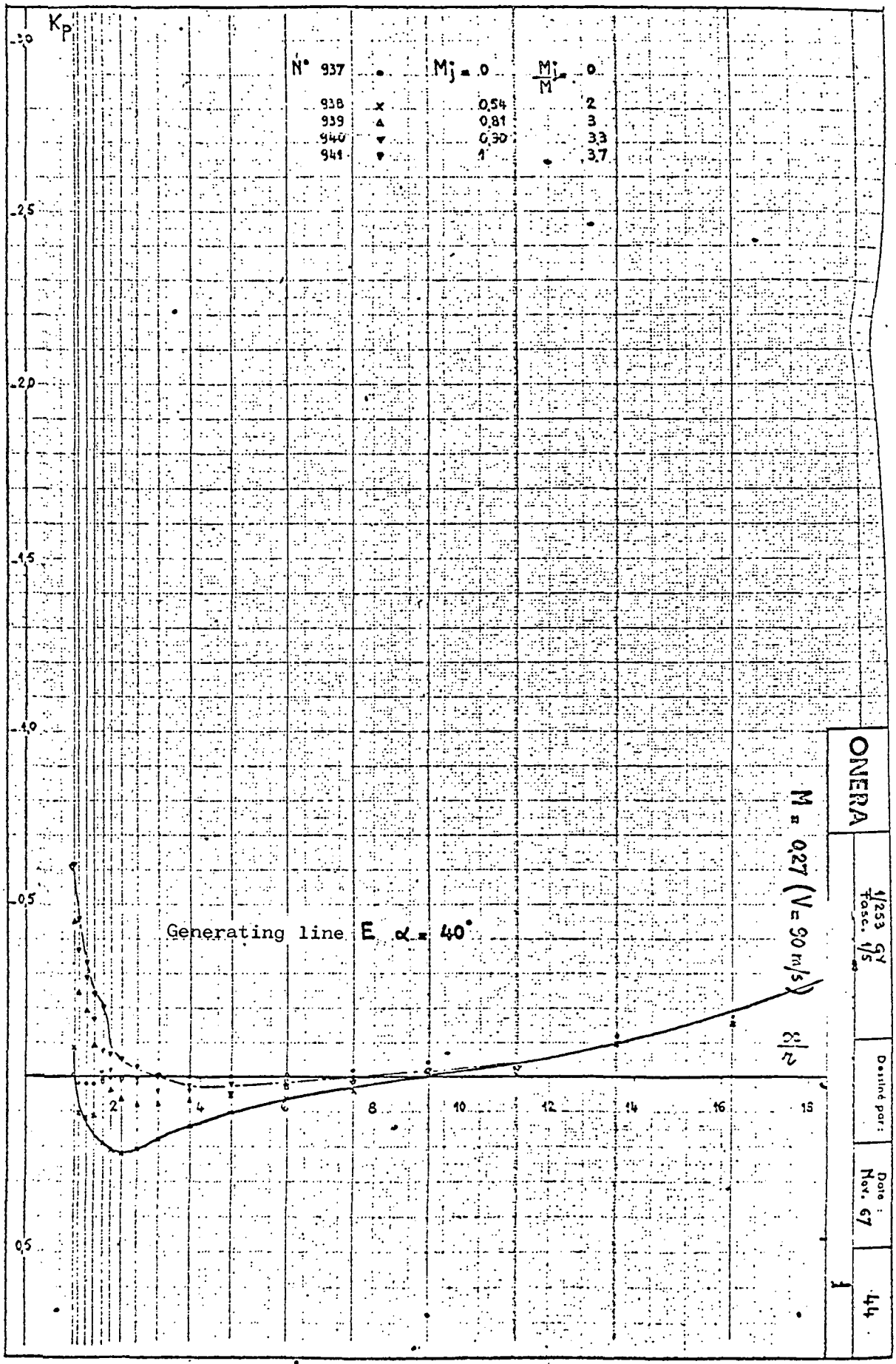

Figure 44. Jet interaction. Test in unheated state.

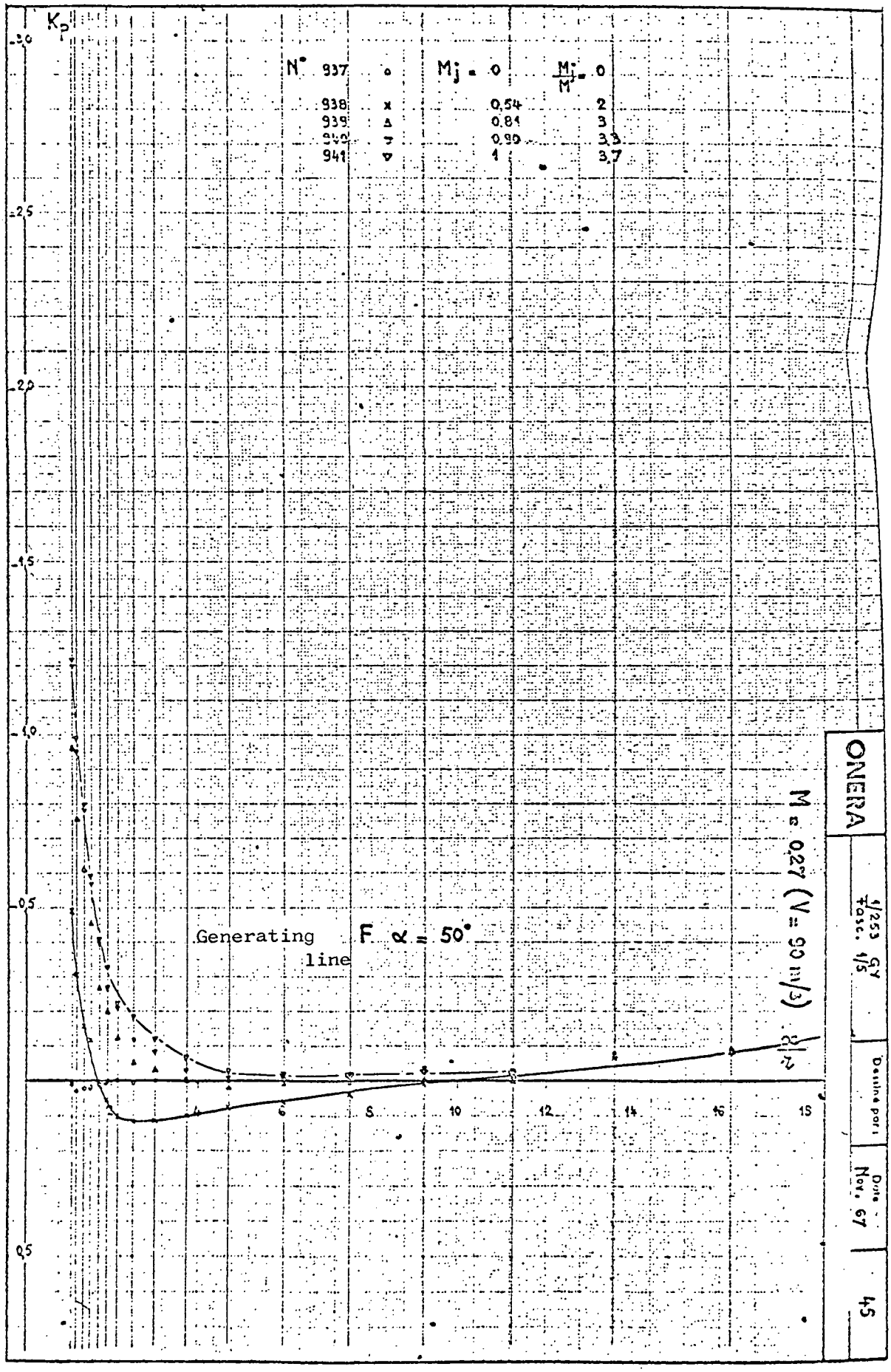

Figure 45. Jet interaction. Test in unheated state.

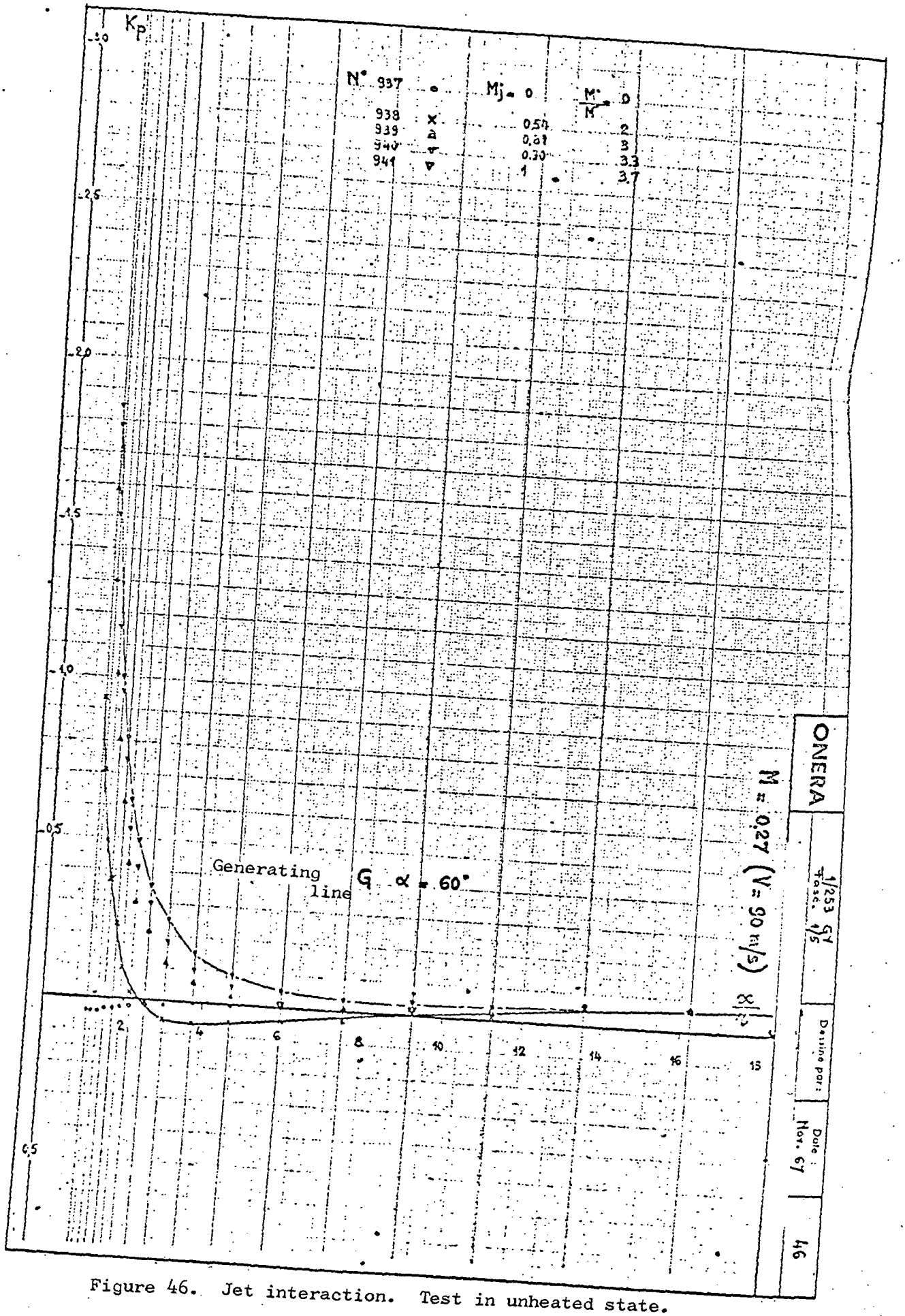

Figure 46. Jet interaction. Test in unheated state.

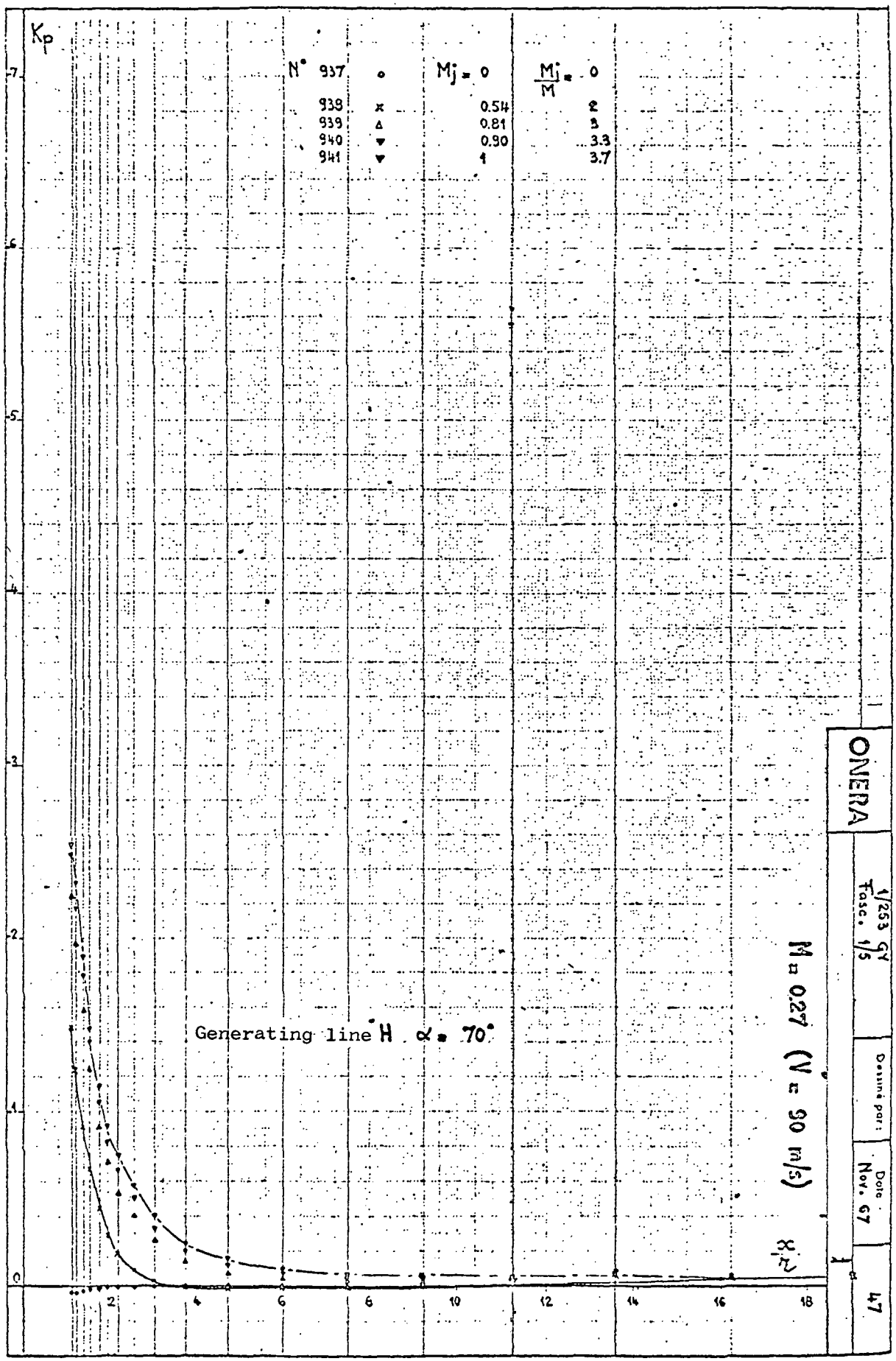

Figure 47. Jet interaction. Test in unheated state.

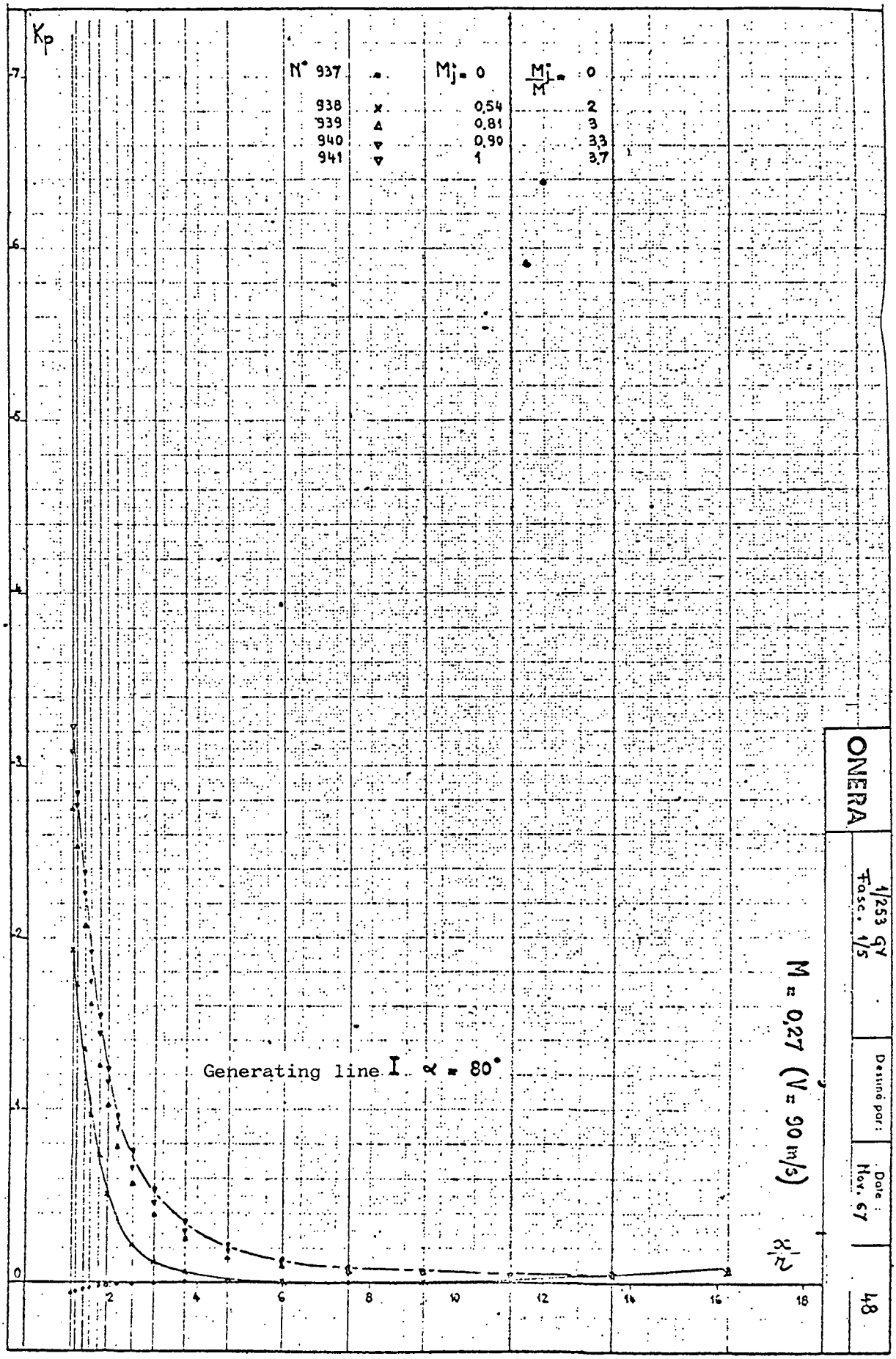

Figure 48. Jet interaction. Test in unheated state.

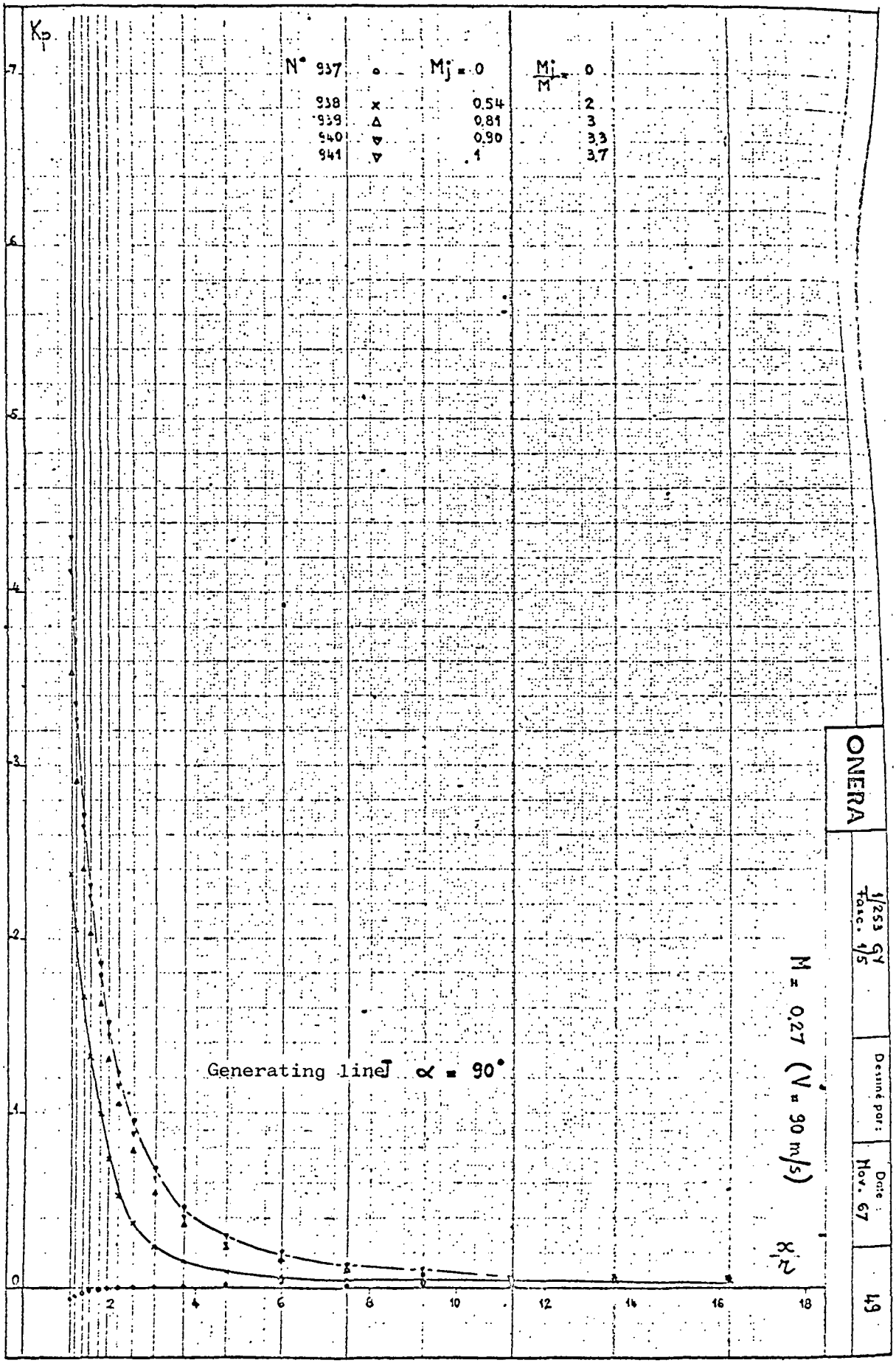

Figure 49. Jet interaction. Test in unheated state.

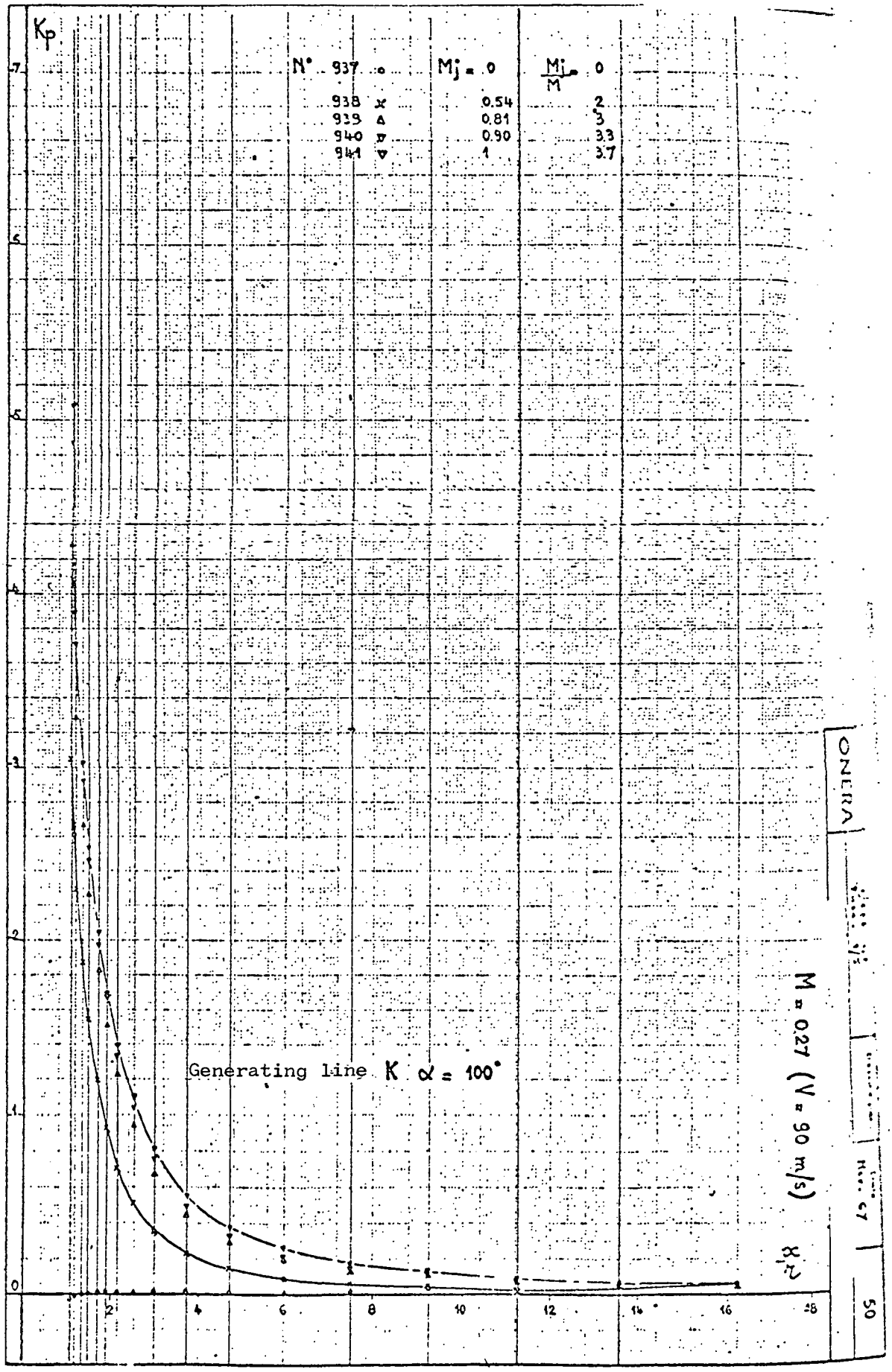

Figure 50. Jet interaction. Test in unheated state.

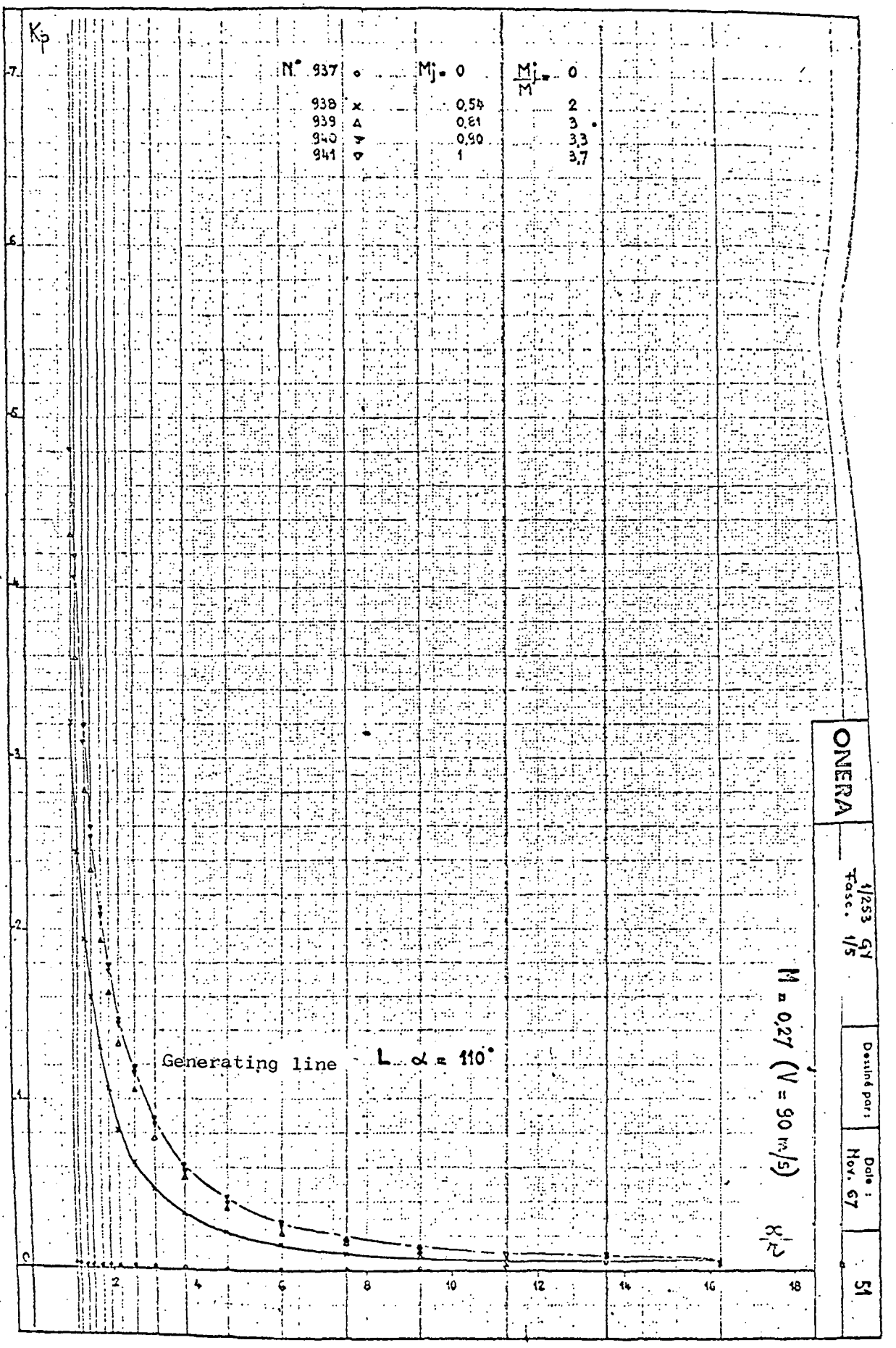

Figure 51. Jet interaction. Test in unheated state.

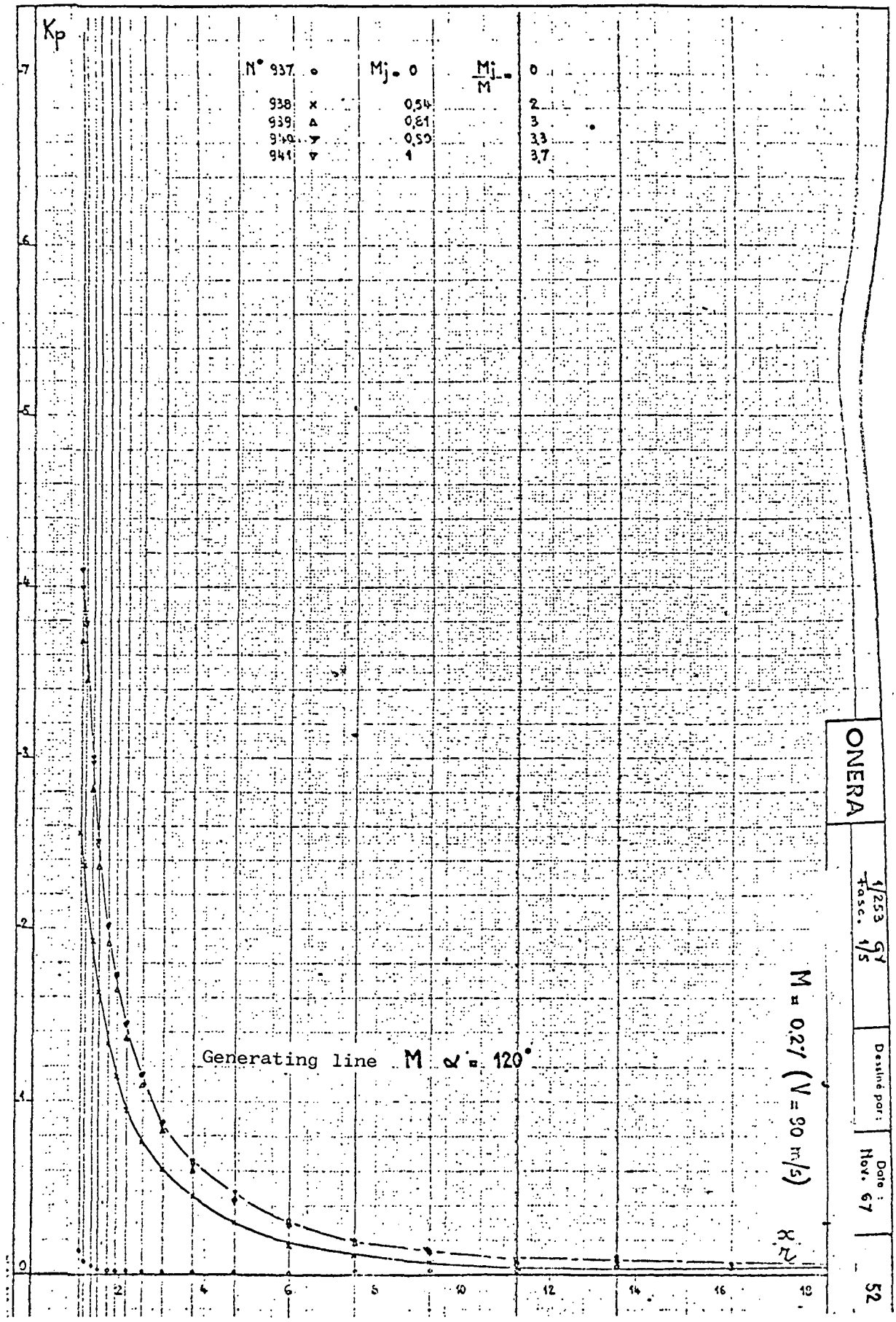

Figure 52. Jet interaction. Test in unheated state.

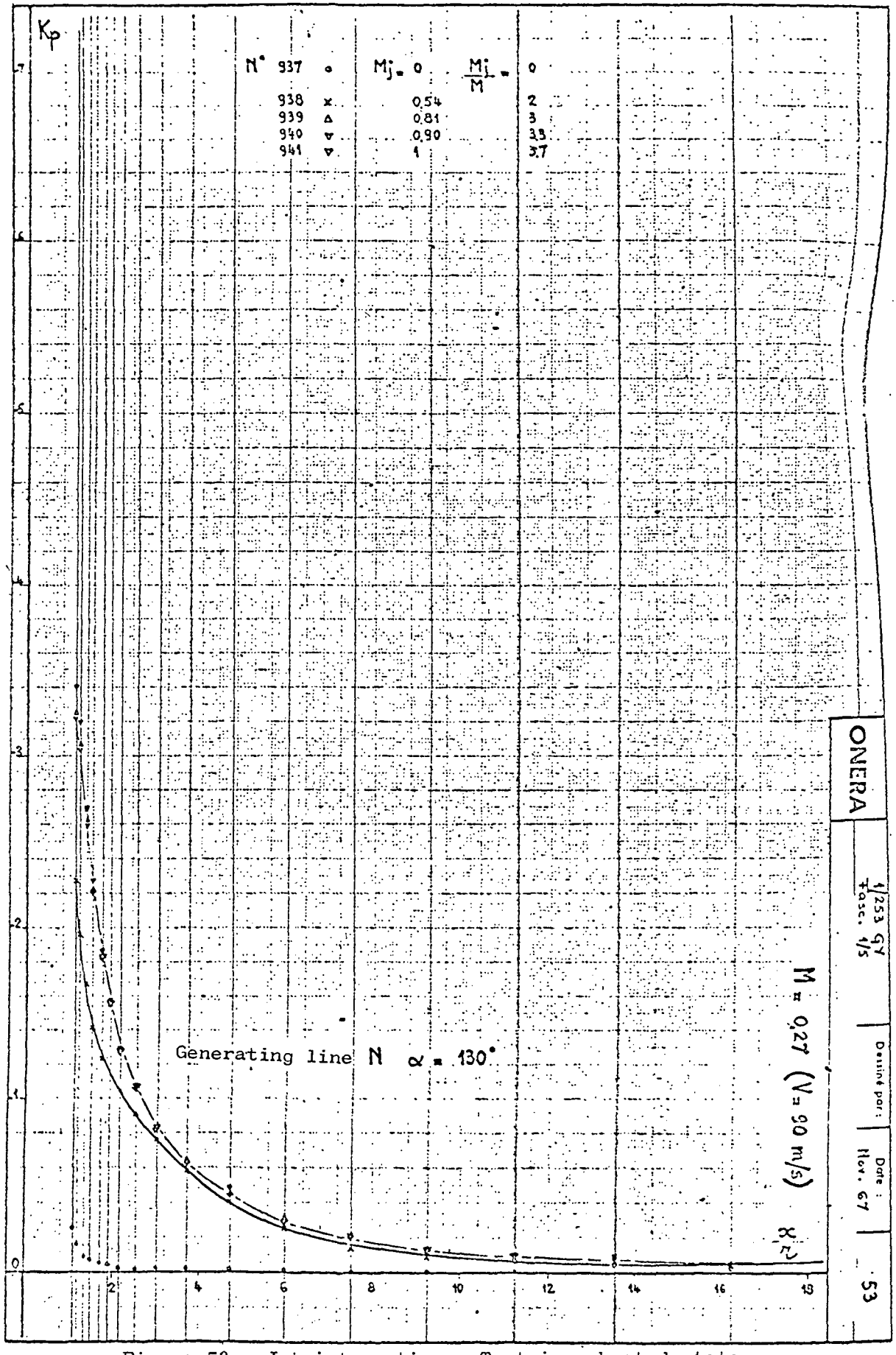

Figure 53. Jet interaction. Test in unheated state.

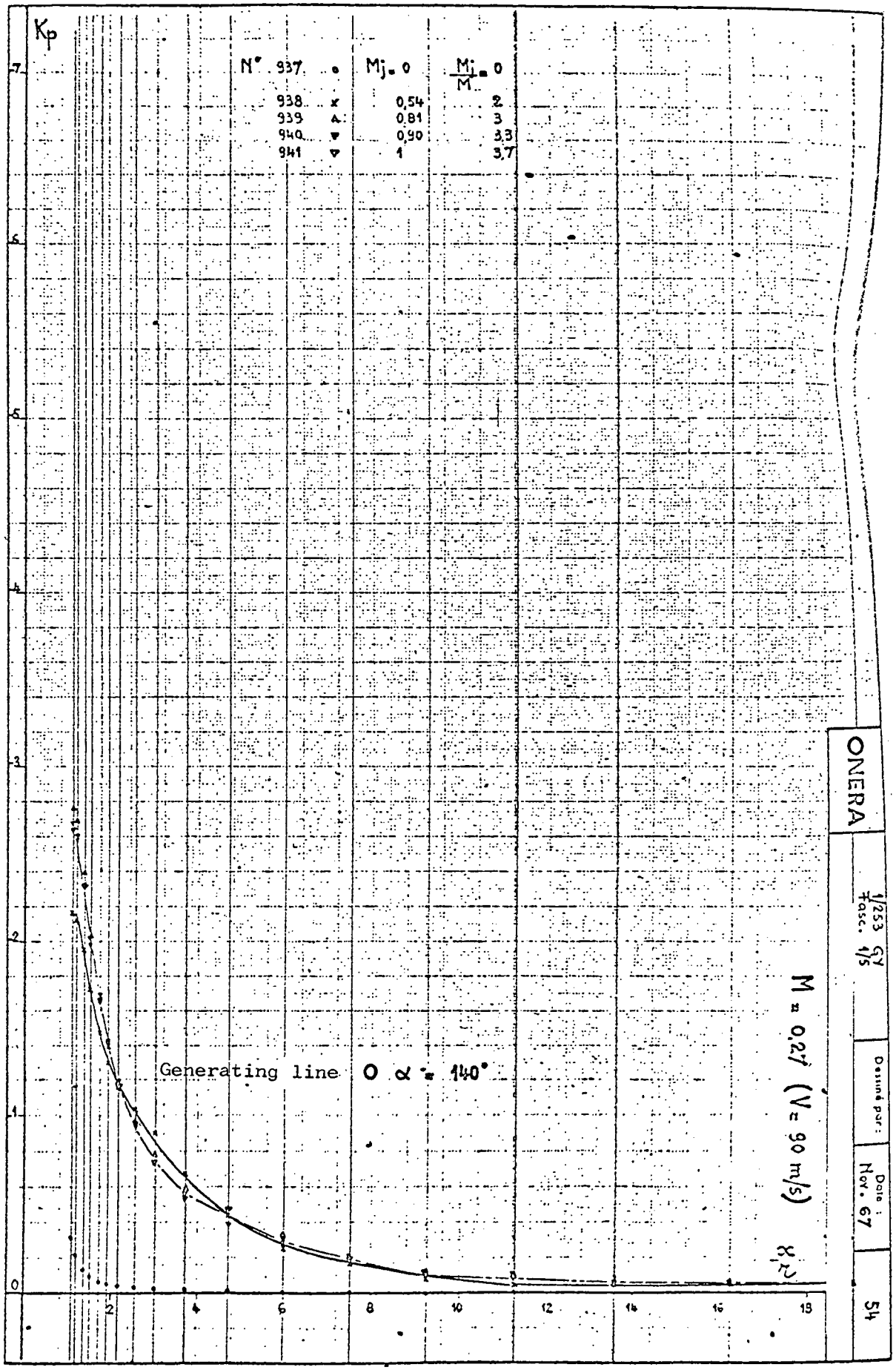

Figure 54. Jet interaction. Test in unheated state.

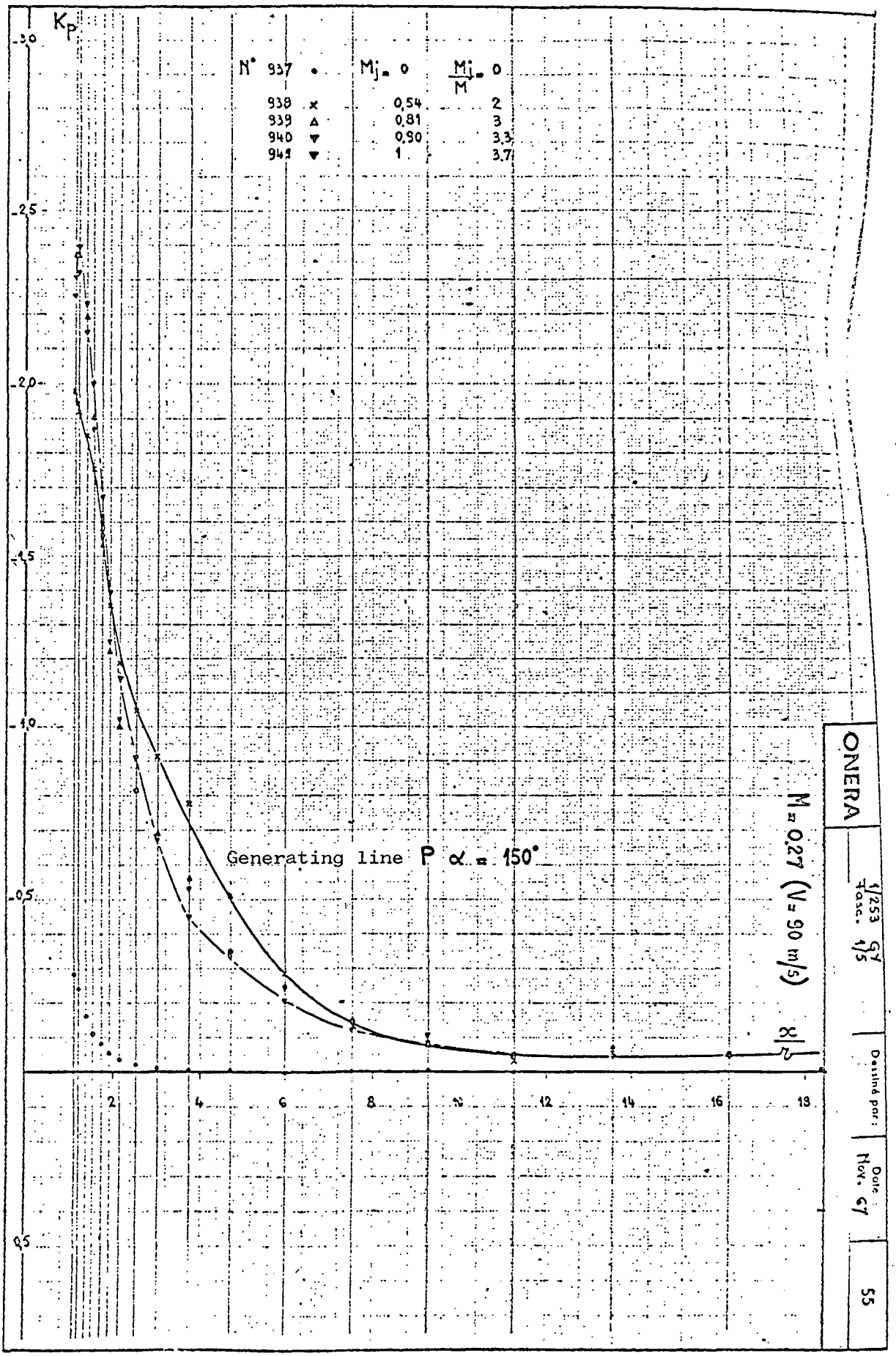

Figure 55. Jet interaction. Test in unheated state.

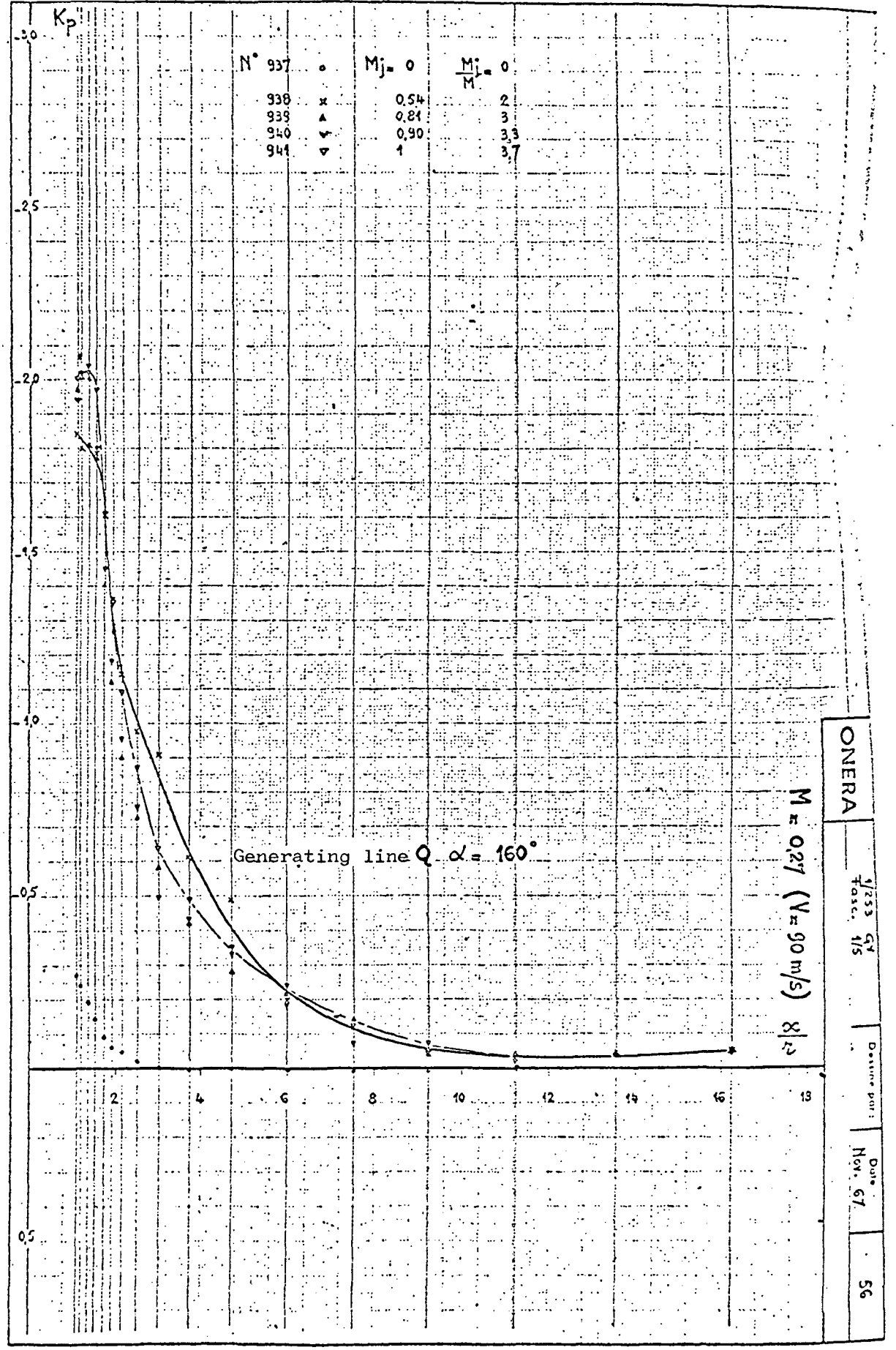

Figure 56. Jet interaction. Test in unheated state.

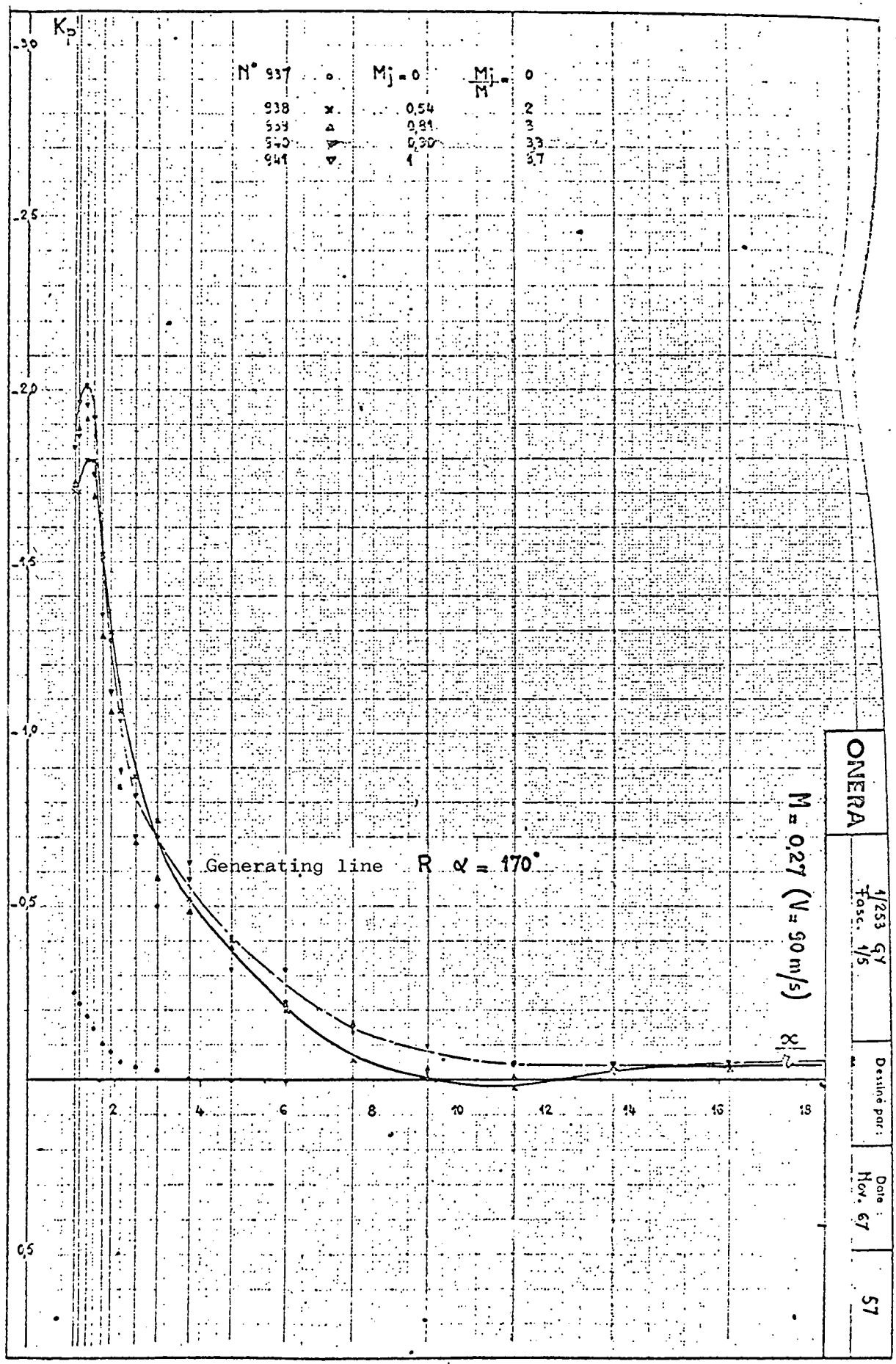

Figure 57. Jet interaction. Test in unheated state.

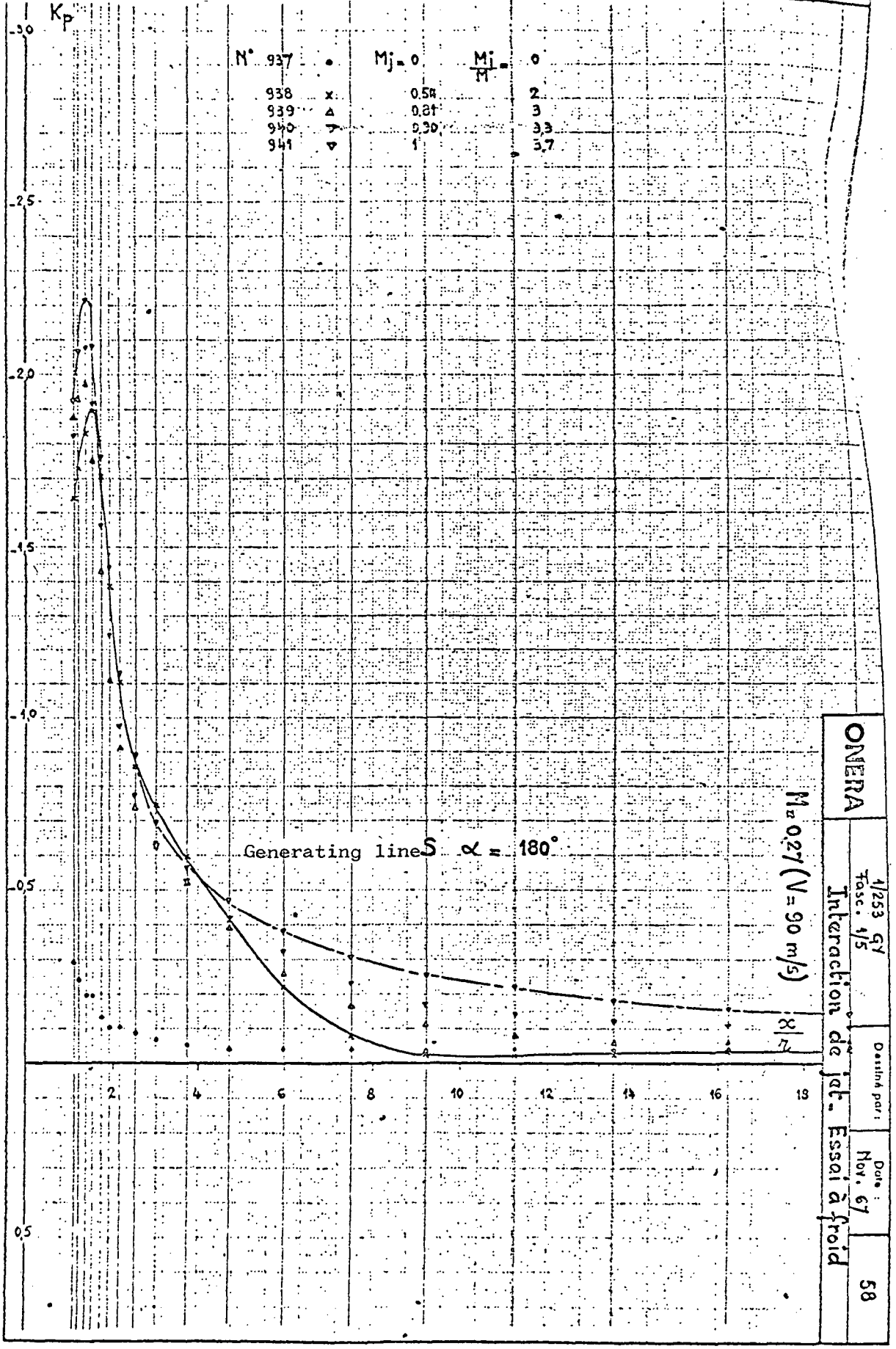

Figure 58. Jet interaction. Test in unheated state.

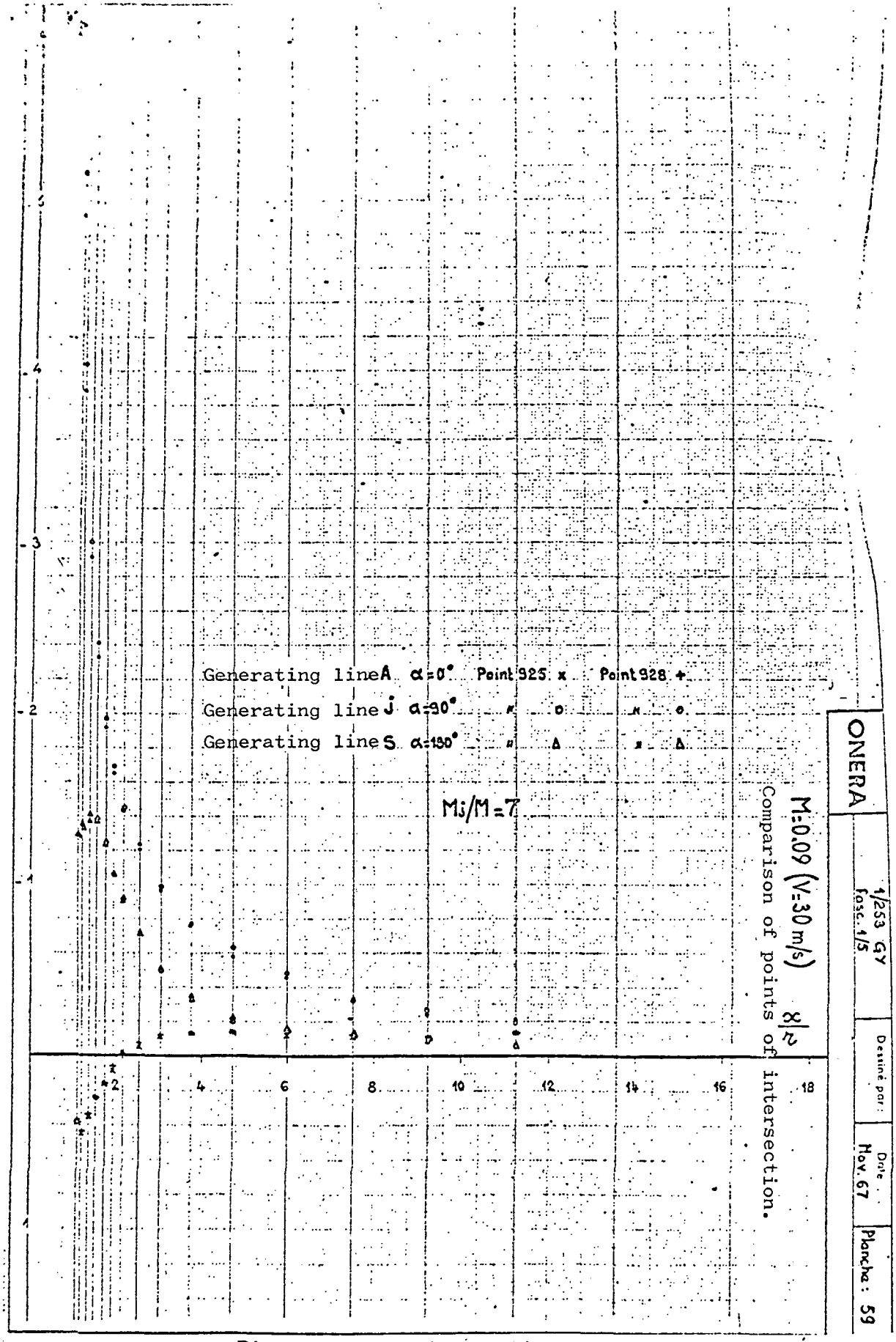
Generating line A α=0° Point 925 x Point 928 +
Generating line J α=90° " o " o
Generating line S α=180° " Δ " Δ
Mj/M=7
M=0.09 (V=30 m/s)
Comparison of points of intersection.
ONERA
1/253 GY
fasc. 1/5
Dessiné par :
Date : Nov. 67
Planche : 59

Figure 59. Jet interaction.

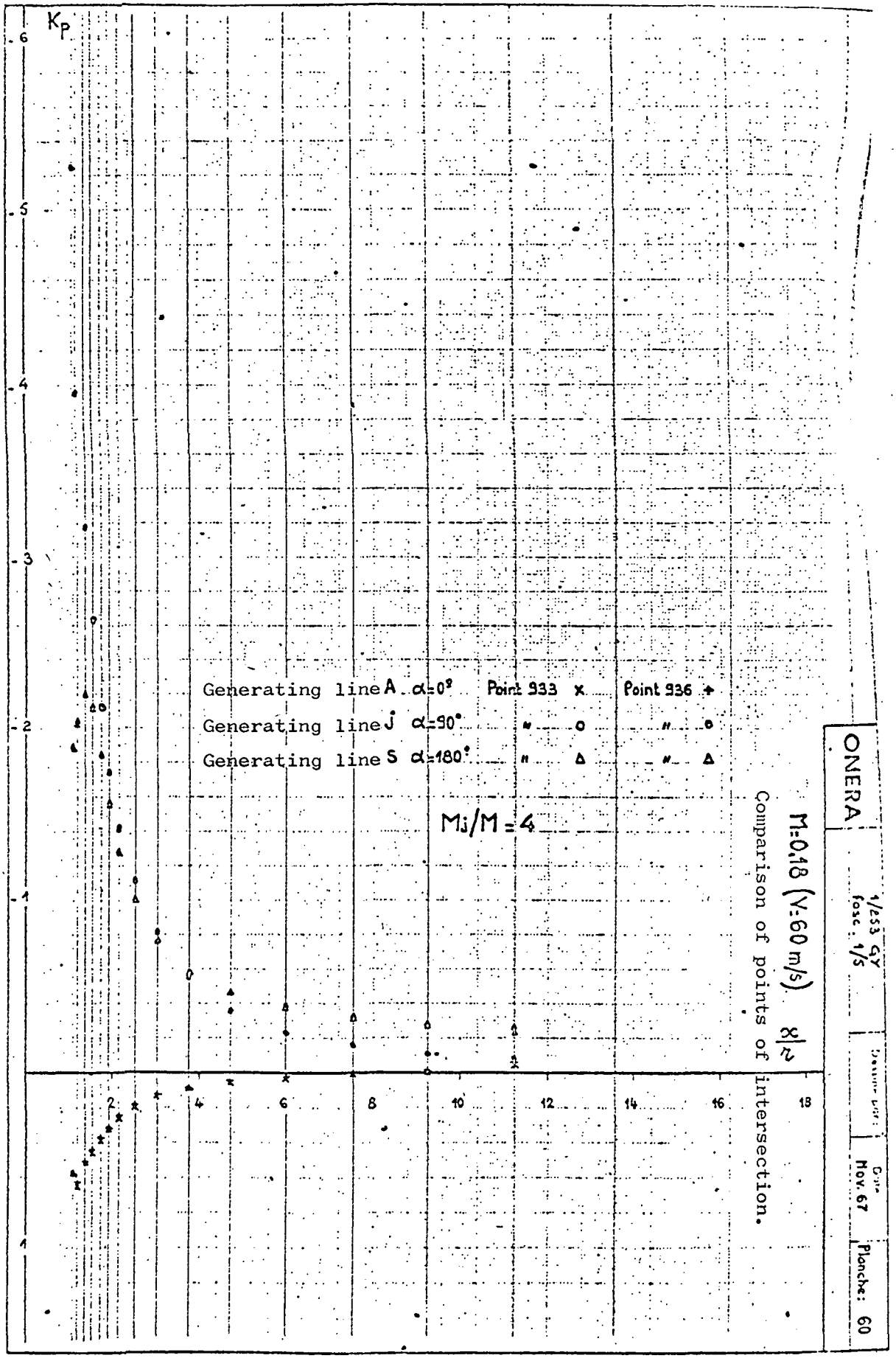
K_P
Generating line A α=0° Point 933 × Point 936 +
Generating line J α=90° " o " o
Generating line S α=180° " Δ " Δ
Mj/M = 4
M=0.18 (V=60 m/s)
Comparison of points of intersection.
ONERA
Planche: 60

Figure 60. Jet interaction.

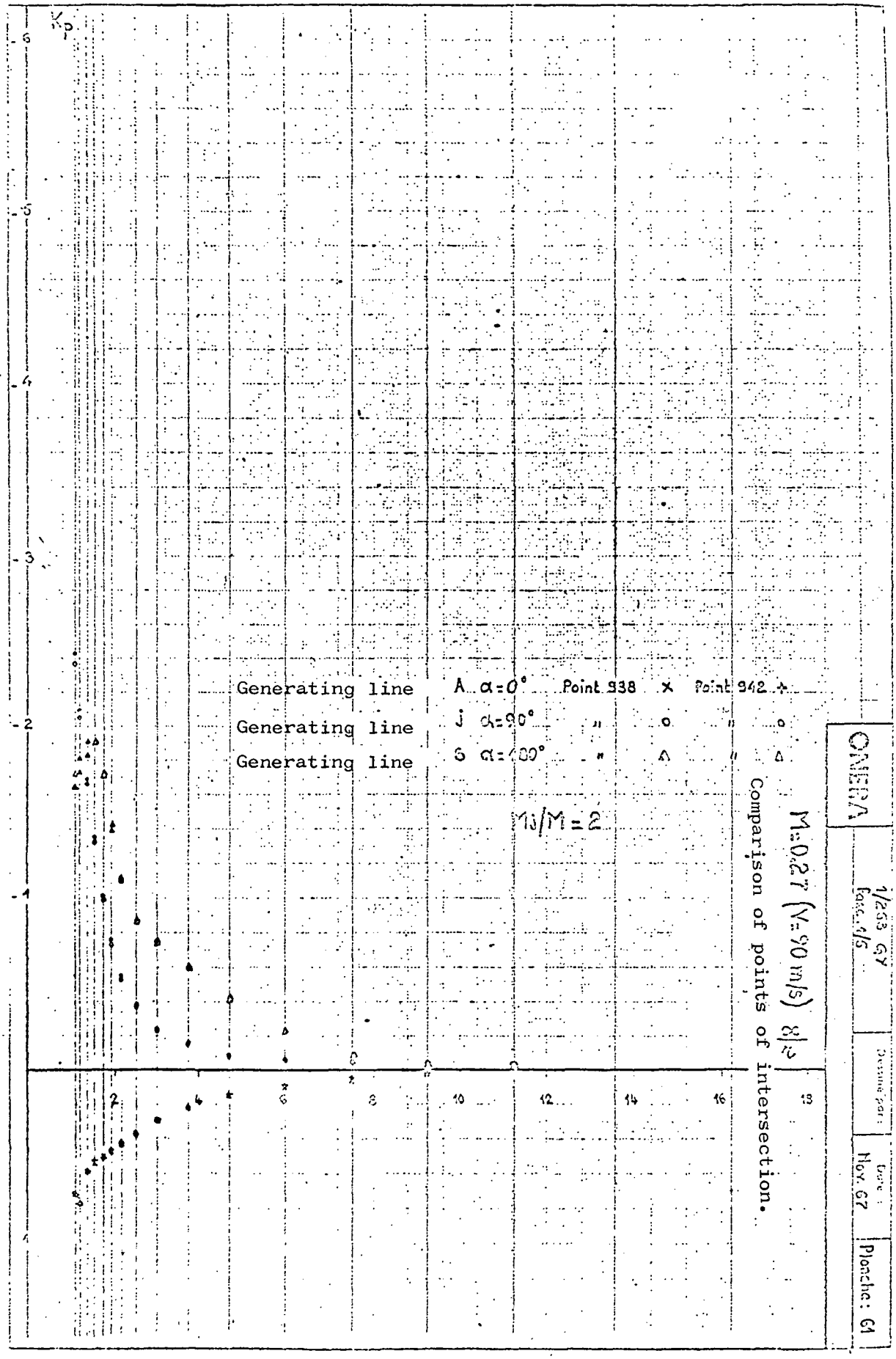
Generating line A α=0° Point 938 × Point 942 +
Generating line J α=90° " o " o
Generating line S α=180° " Δ " Δ
Mj/M = 2
M=0.27 (V=90 m/s) x/r
Comparison of points of intersection.
ONERA
1/253 GY
Planche: G1

Figure 61. Jet interaction.

ONERA | ONERA | P.V 4/2580 Fasc. 1/5 | DATE: 11.1967 | Planche: 62

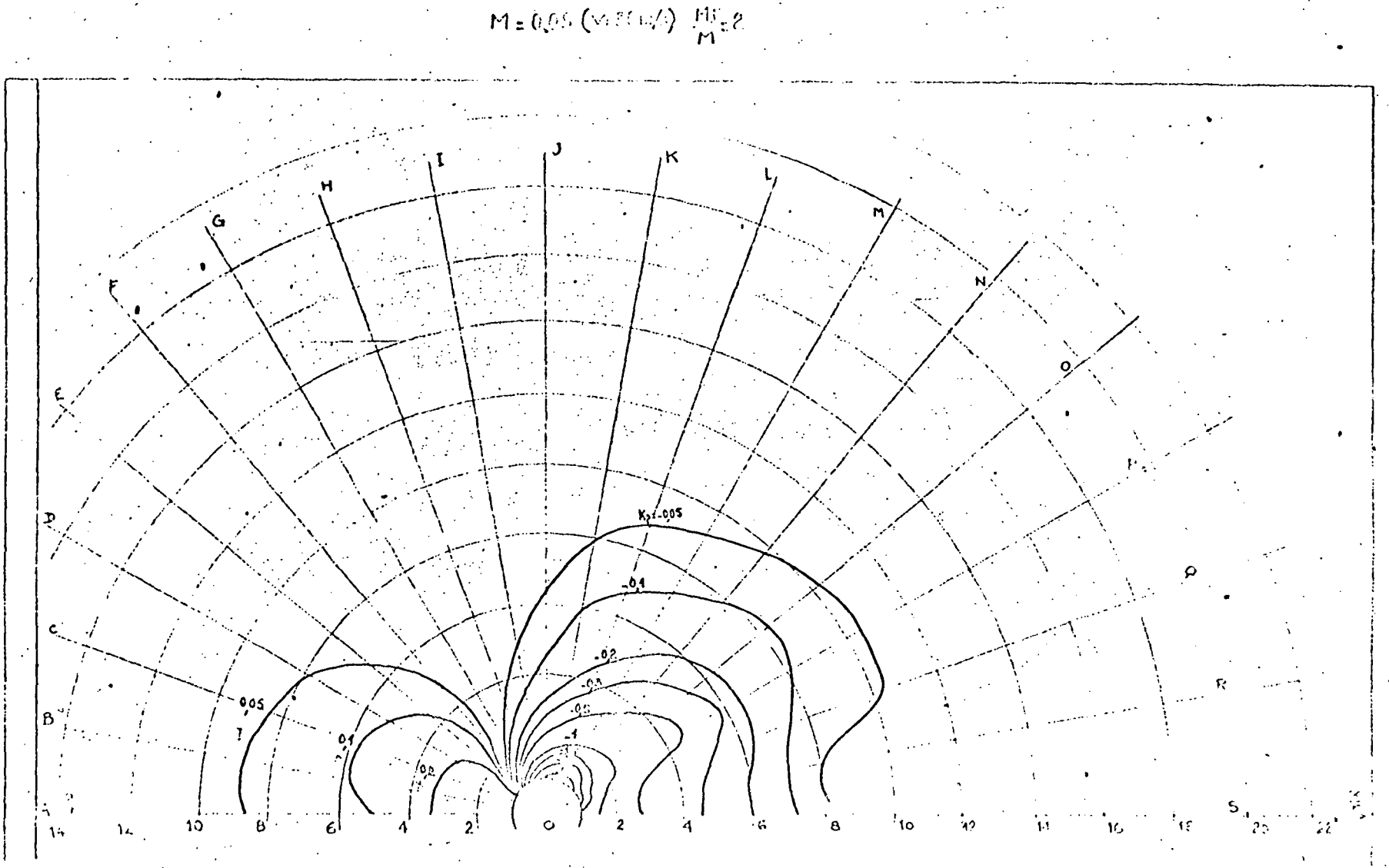

Figure 62. Jet interaction.

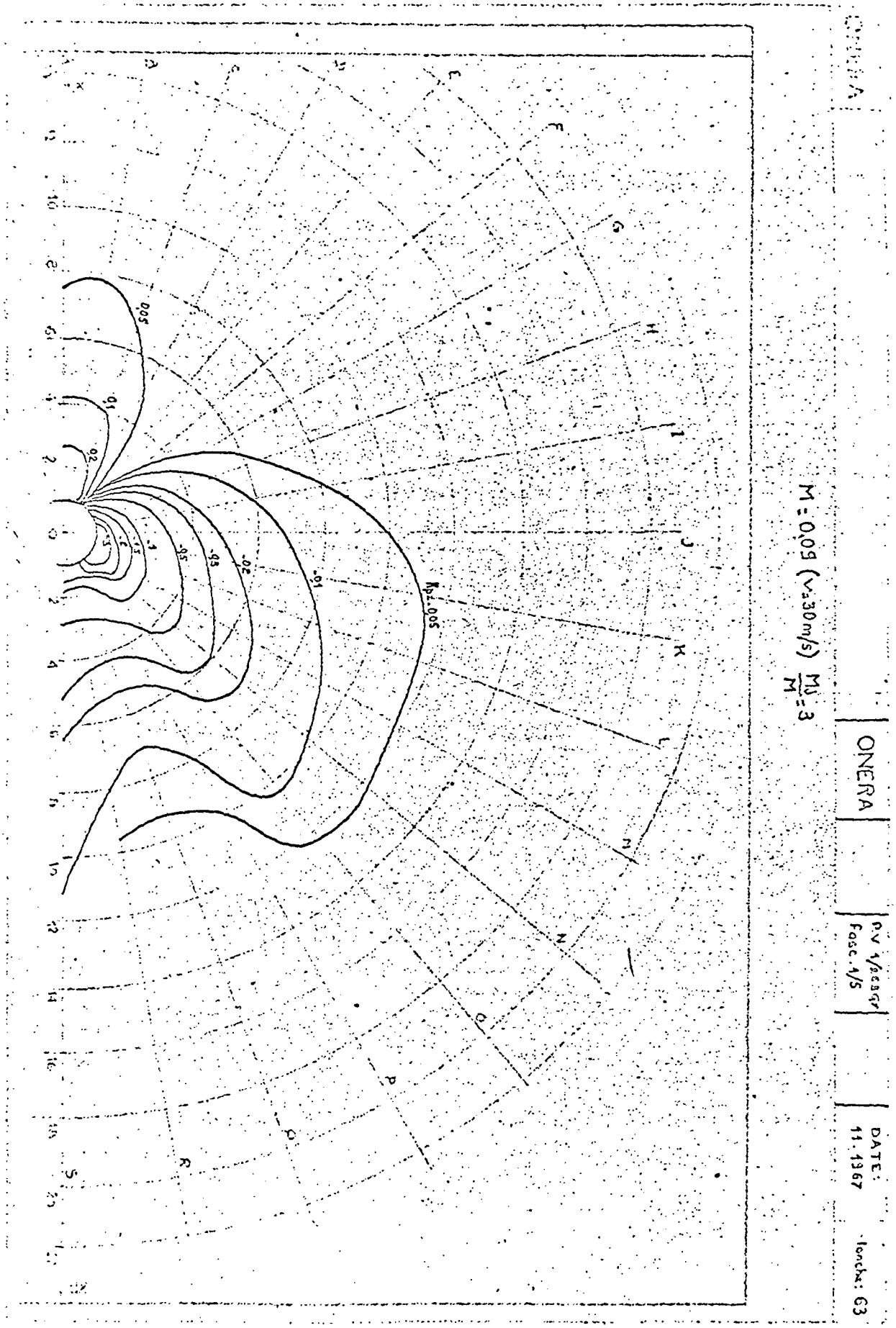

Figure 63. Jet interaction.

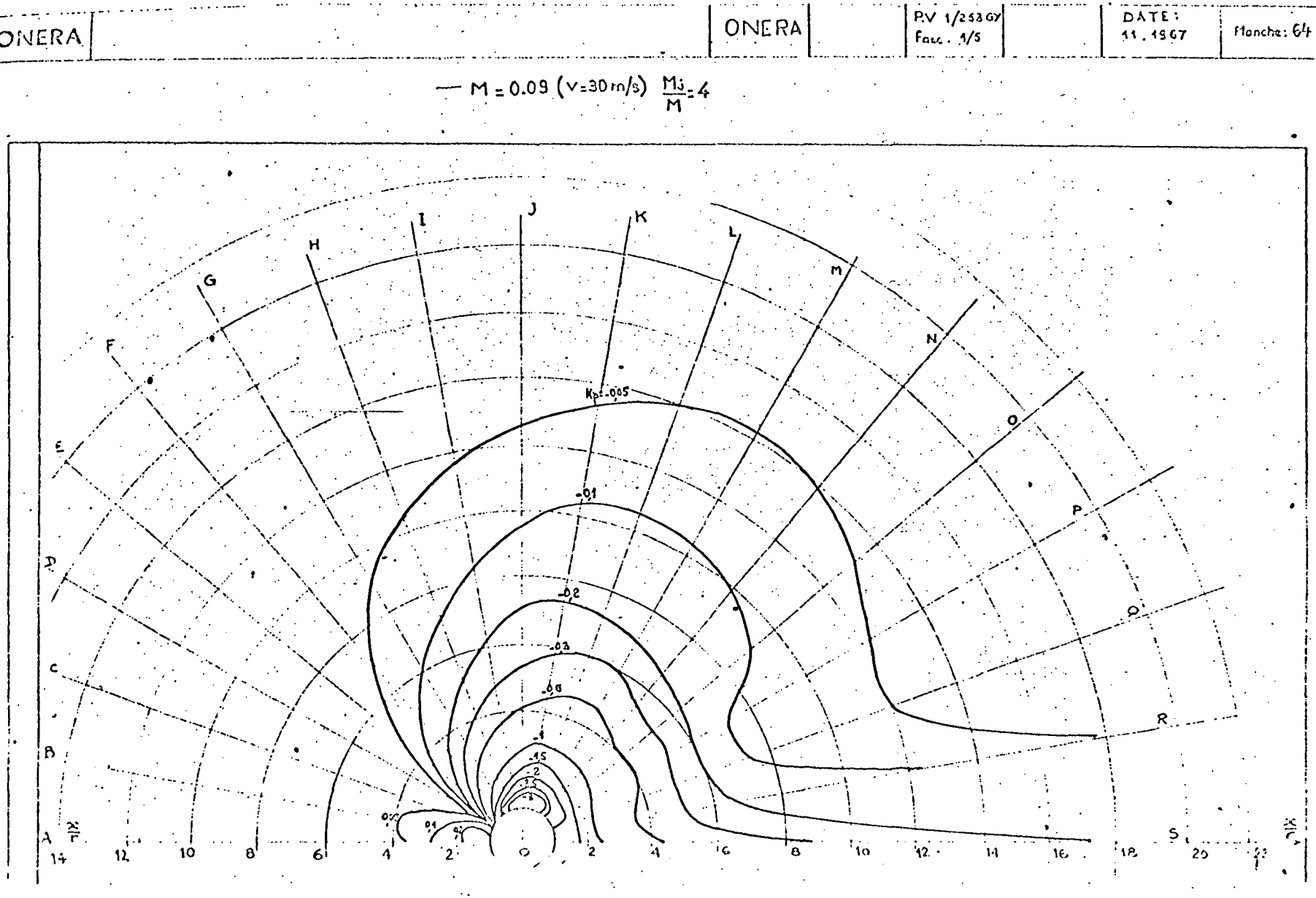

Figure 64. Jet interaction.

$M = 0{,}09$ ($V = 30$ m/s) $\frac{Mj}{M} = 7$ Test in unheated state. "Ideal" standard nozzle.

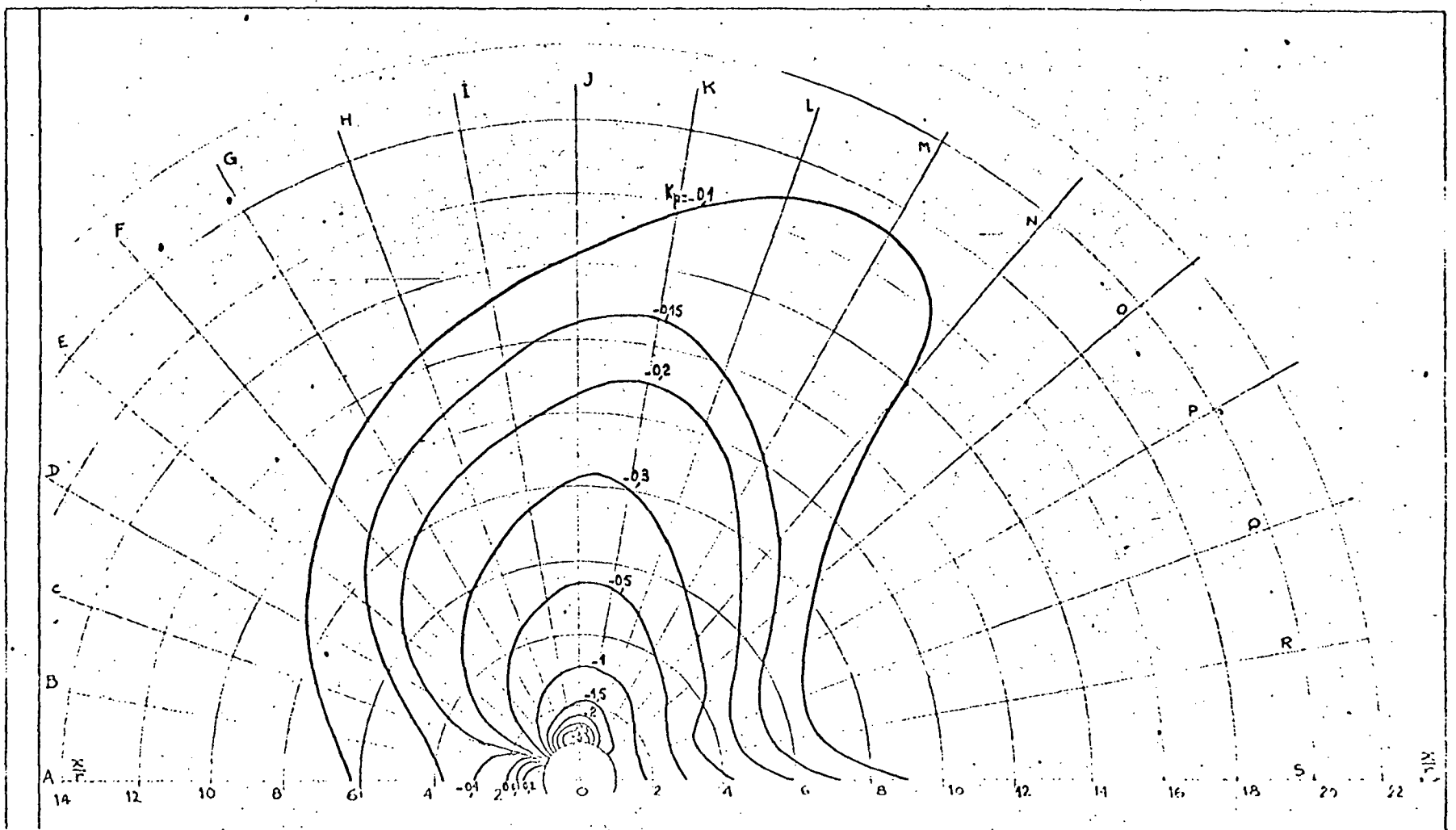

Figure 65. Jet interaction.

$M = 0,09$ ($V = 30$ m/s) $\frac{Mj}{M} = 10$ Test in unheated state. "Ideal" standard nozzle

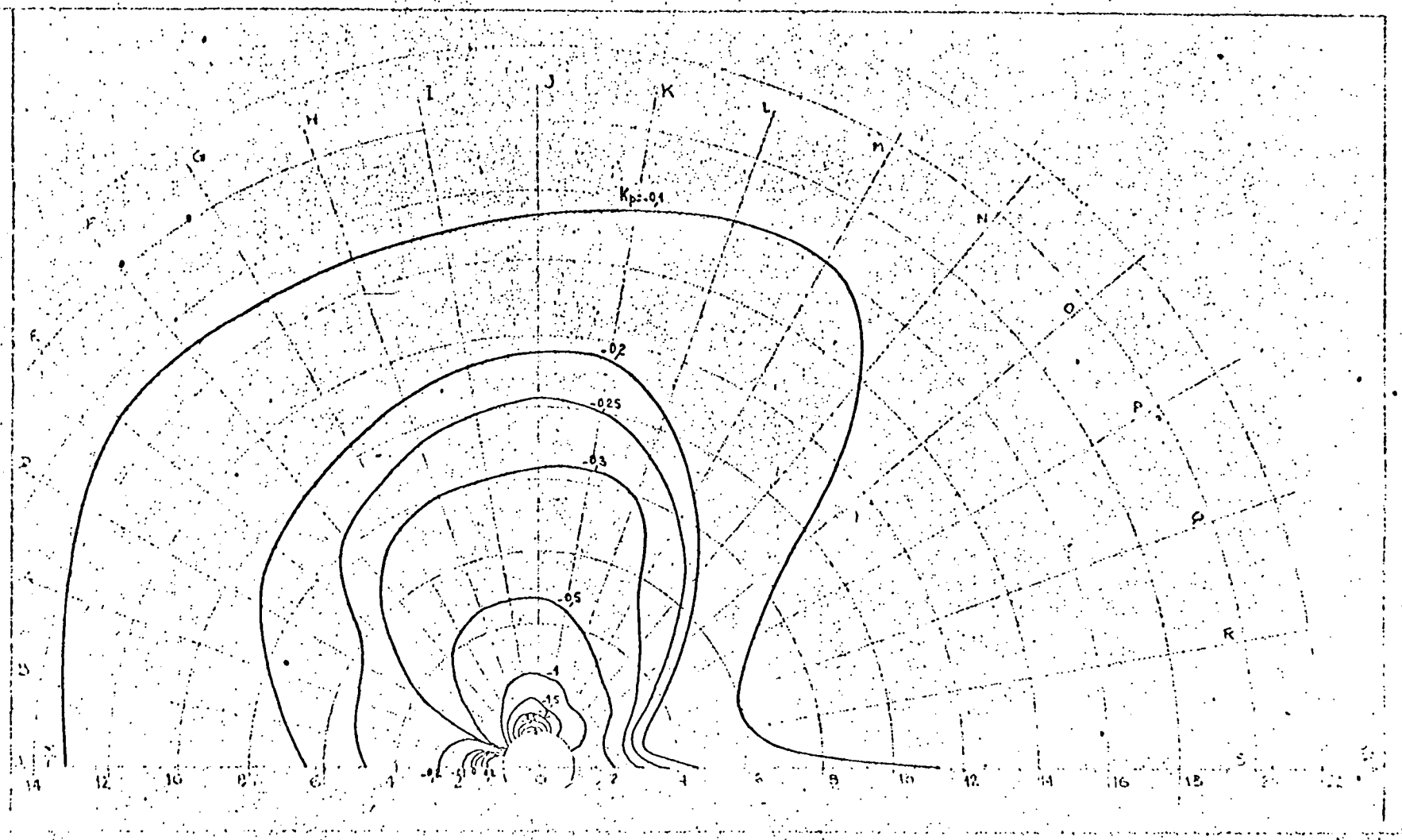

Figure 66. Jet interaction.

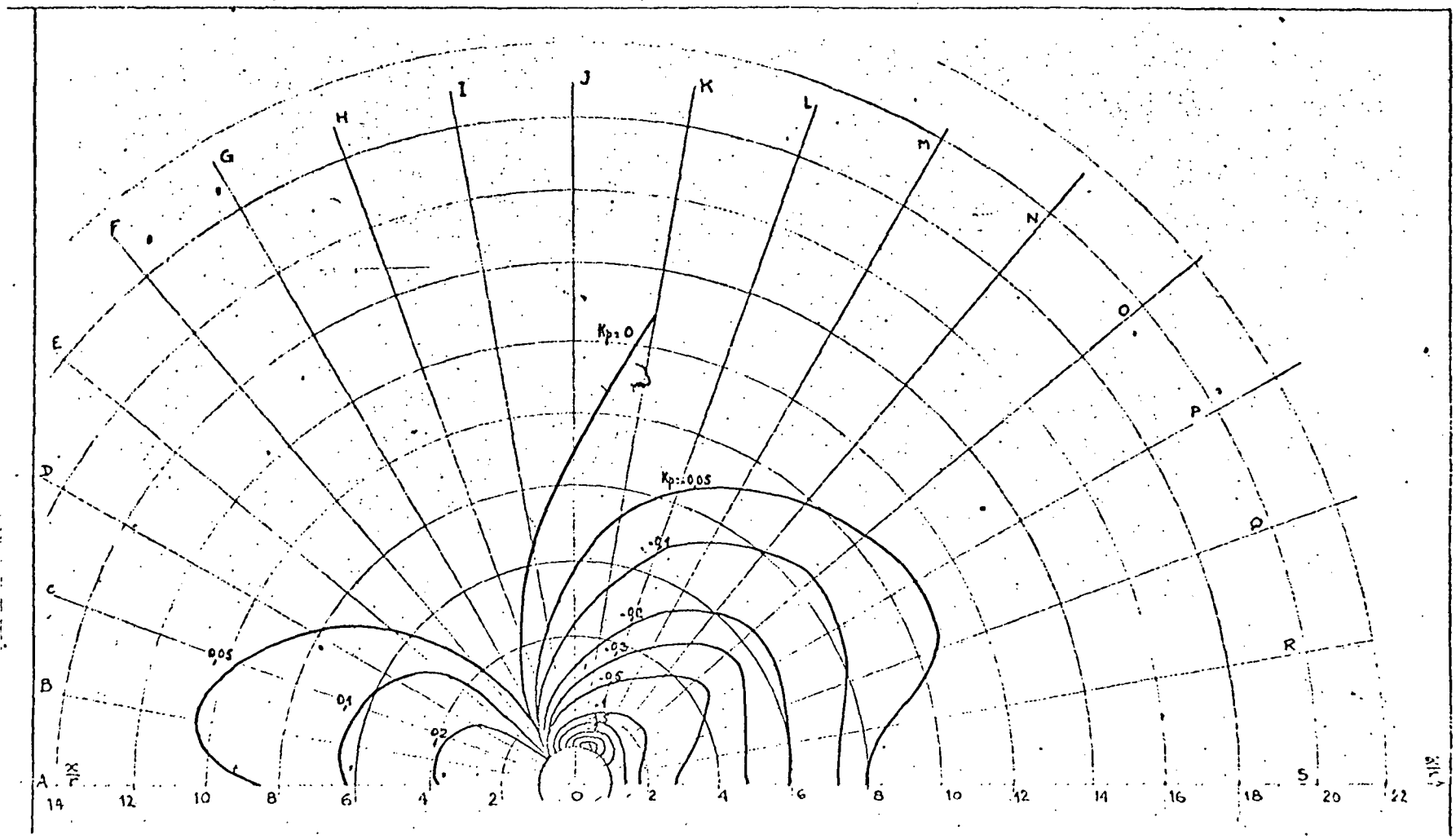

Figure 67. Jet interaction.

ONERA		ONERA		P.V. 1/2830Y fasc. 1/5		DATE: 11.1967	Planche : 68

$M=0,18$ ($v=60$ m/s) $\frac{M_j}{M}=3$

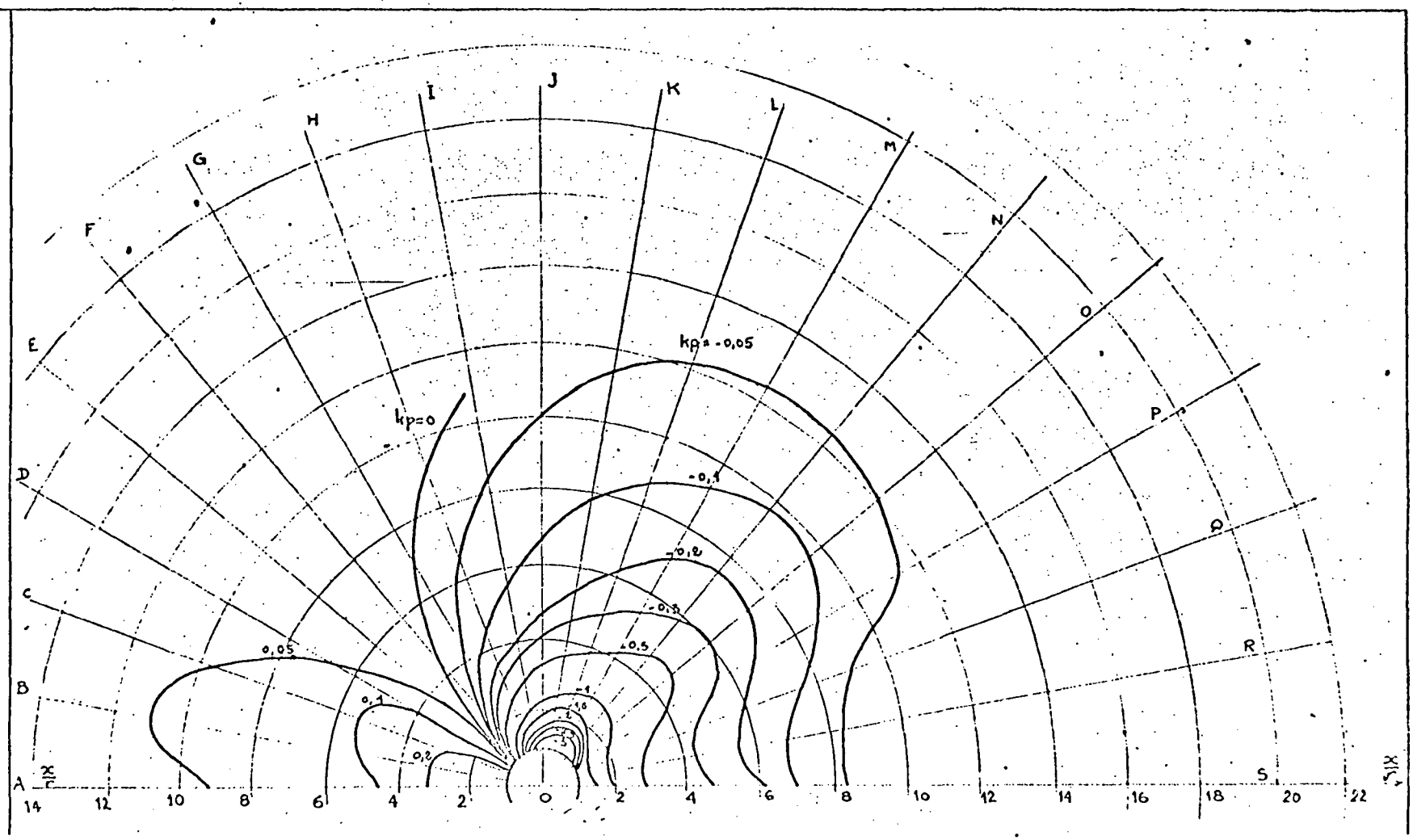

Figure 68. Jet interaction.

$M = 0{,}18$ ($v = 60$ m/s) $\frac{M_j}{M} = 4$

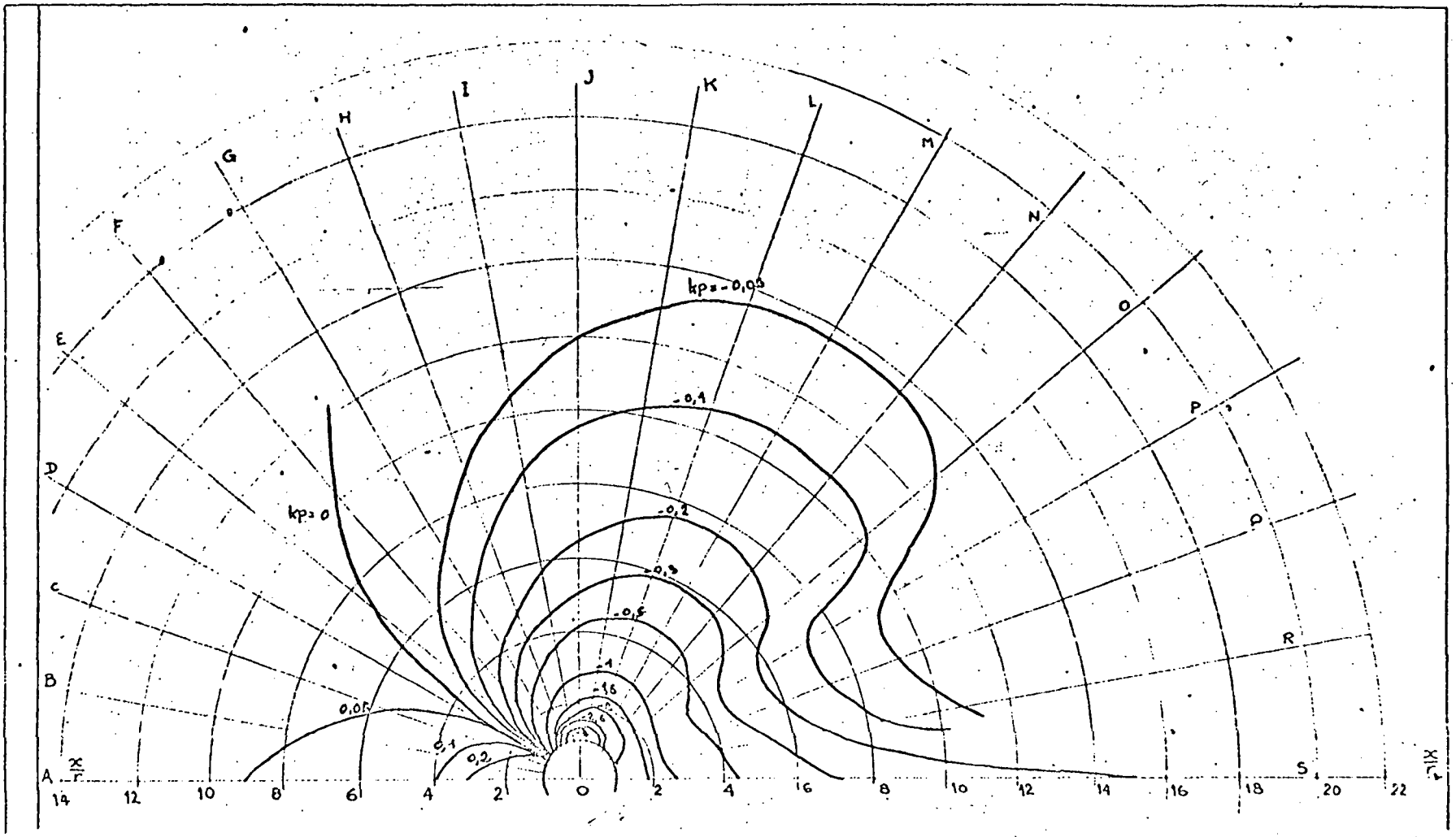

Figure 69. Jet interaction.

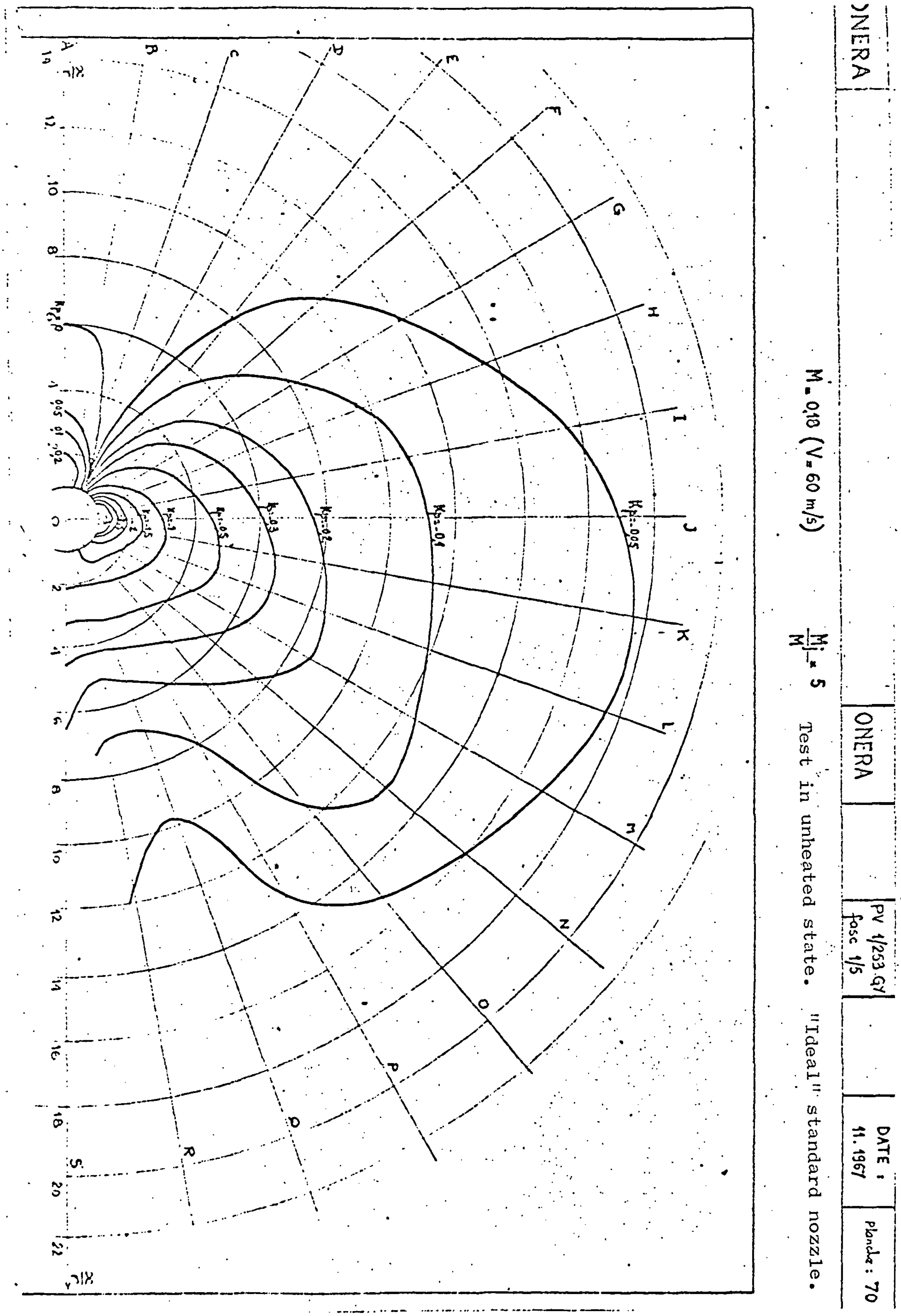

Figure 70. Jet interaction.

$M = 0{,}27$ ($v = 90$ m/s) $\frac{M_j}{M} = 2$

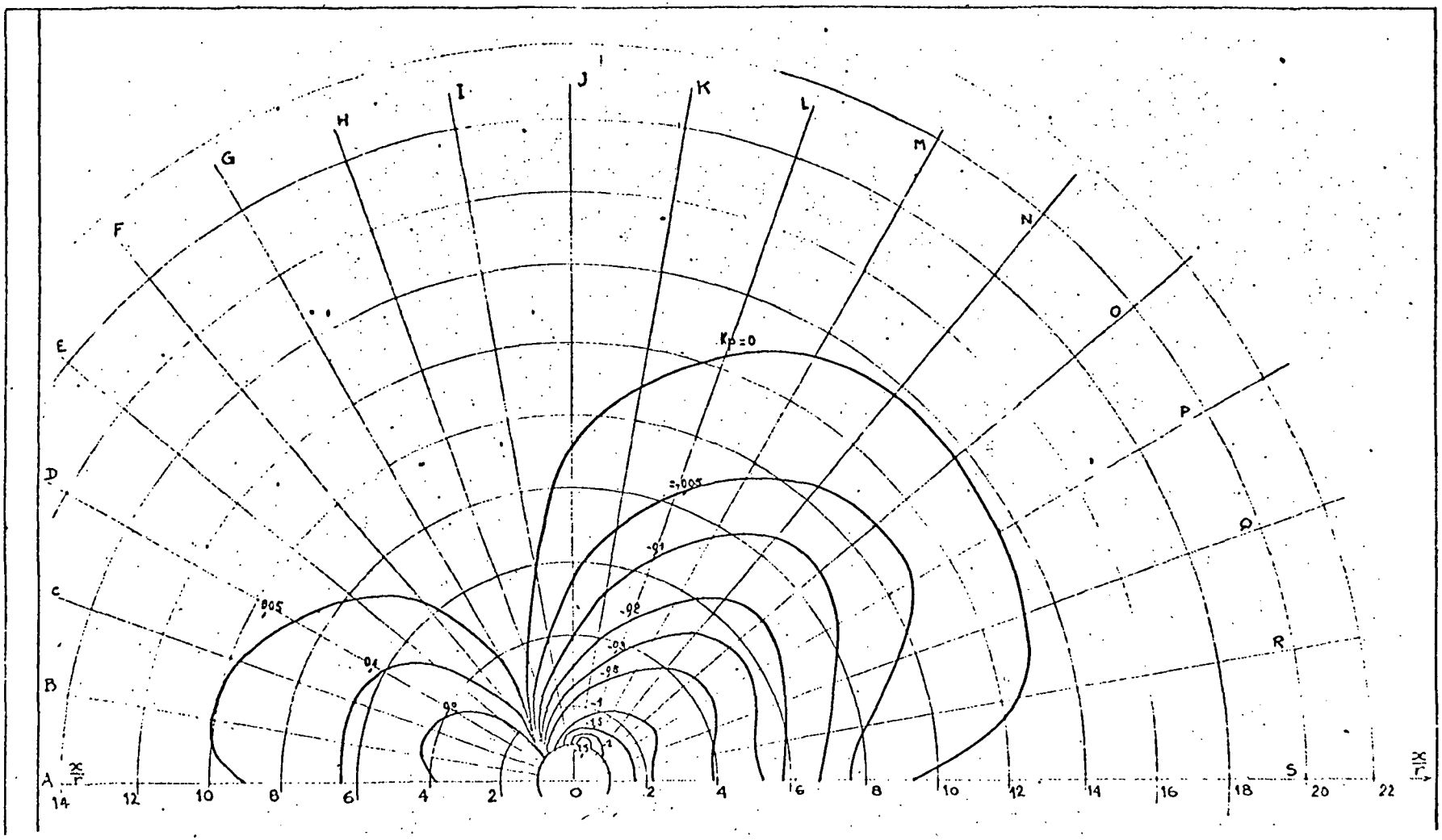

Figure 71. Jet interaction.

$M=0.27$ ($V=90$ m/s) $\frac{Mj}{M}=3$

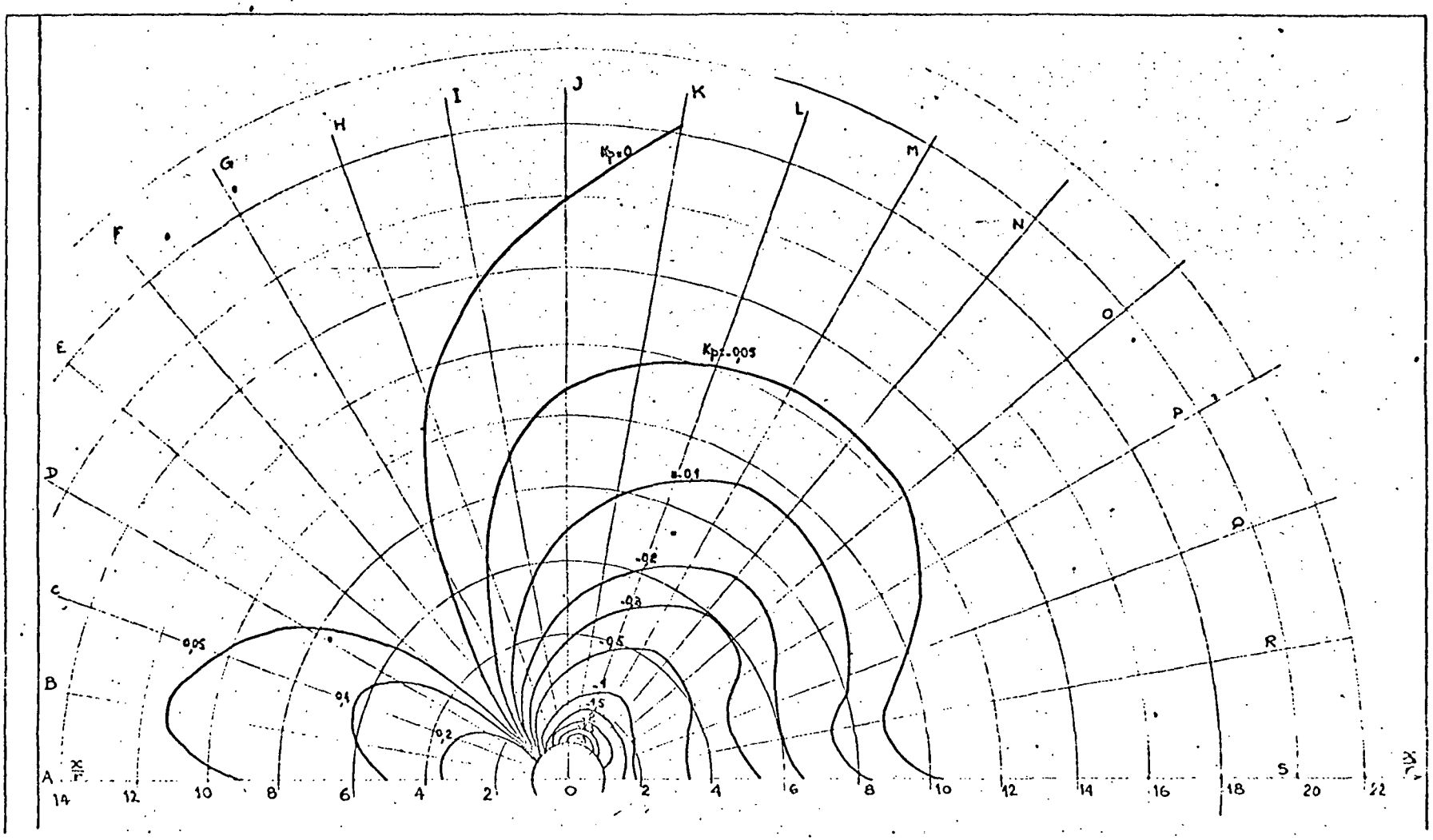

Figure 72. Jet interaction.

$\frac{Re = 5.3 \times 10^6}{}$ M = 0.27 (V = 90 m/s) $\frac{M_j}{M} = 2$

$\frac{Re = 4.5 \times 10^6}{}$ M = 0.18 (V = 60 m/s)

$\frac{Re = 2.3 \times 10^6}{}$ M = 0.09 (V = 30 m/s)

Effect of wind tunnel velocity.

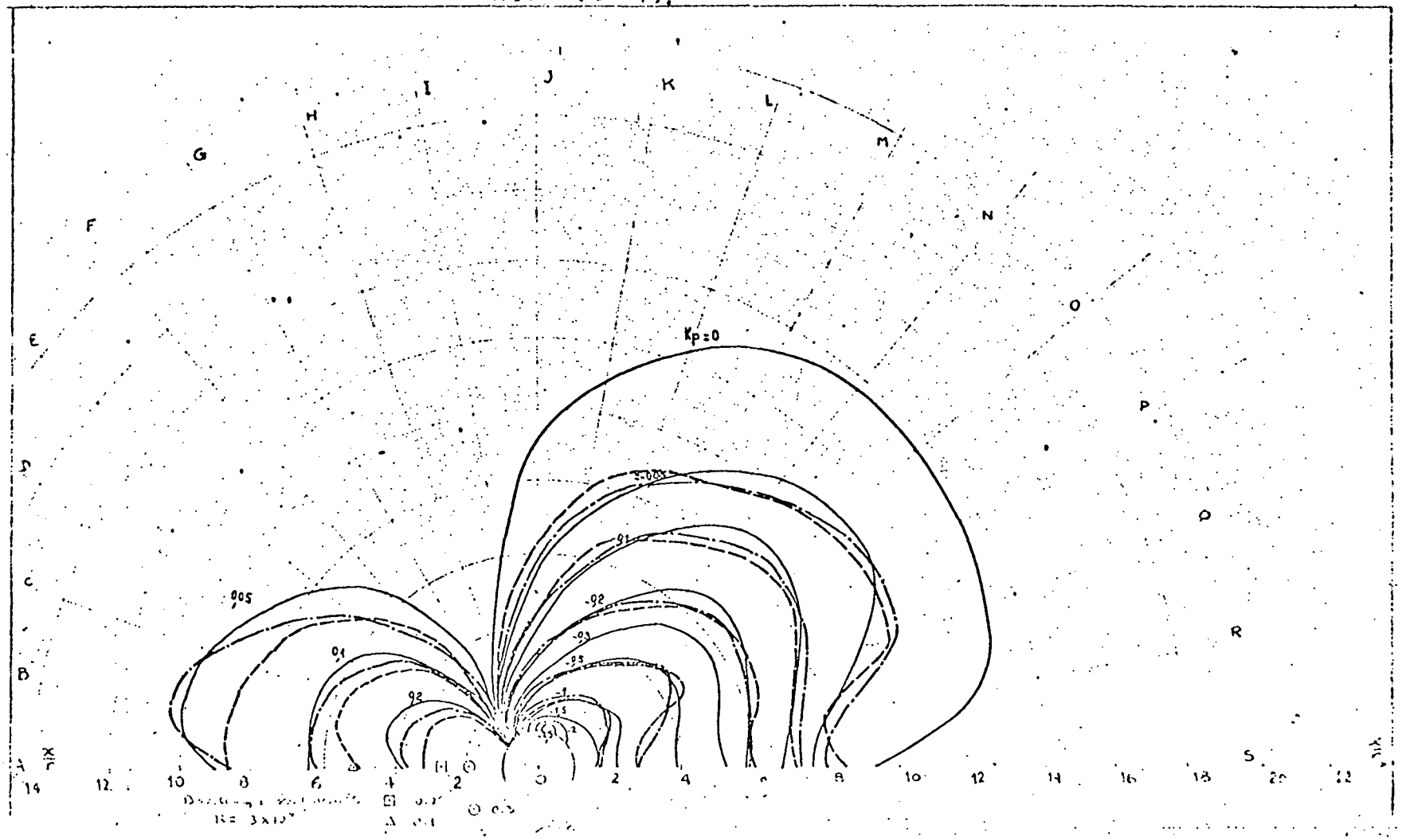

Figure 73. Jet interaction.

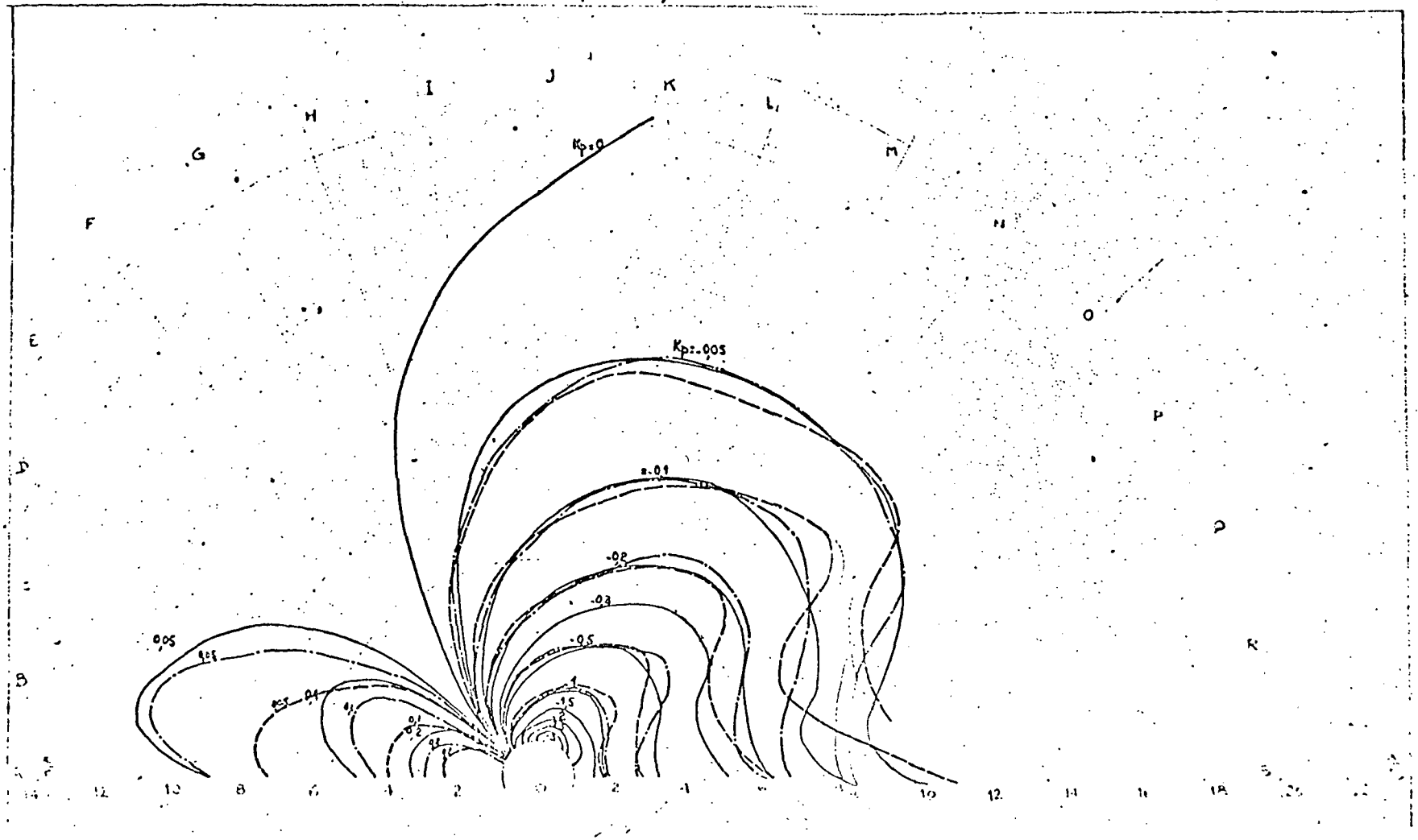

Figure 74. Jet interaction.

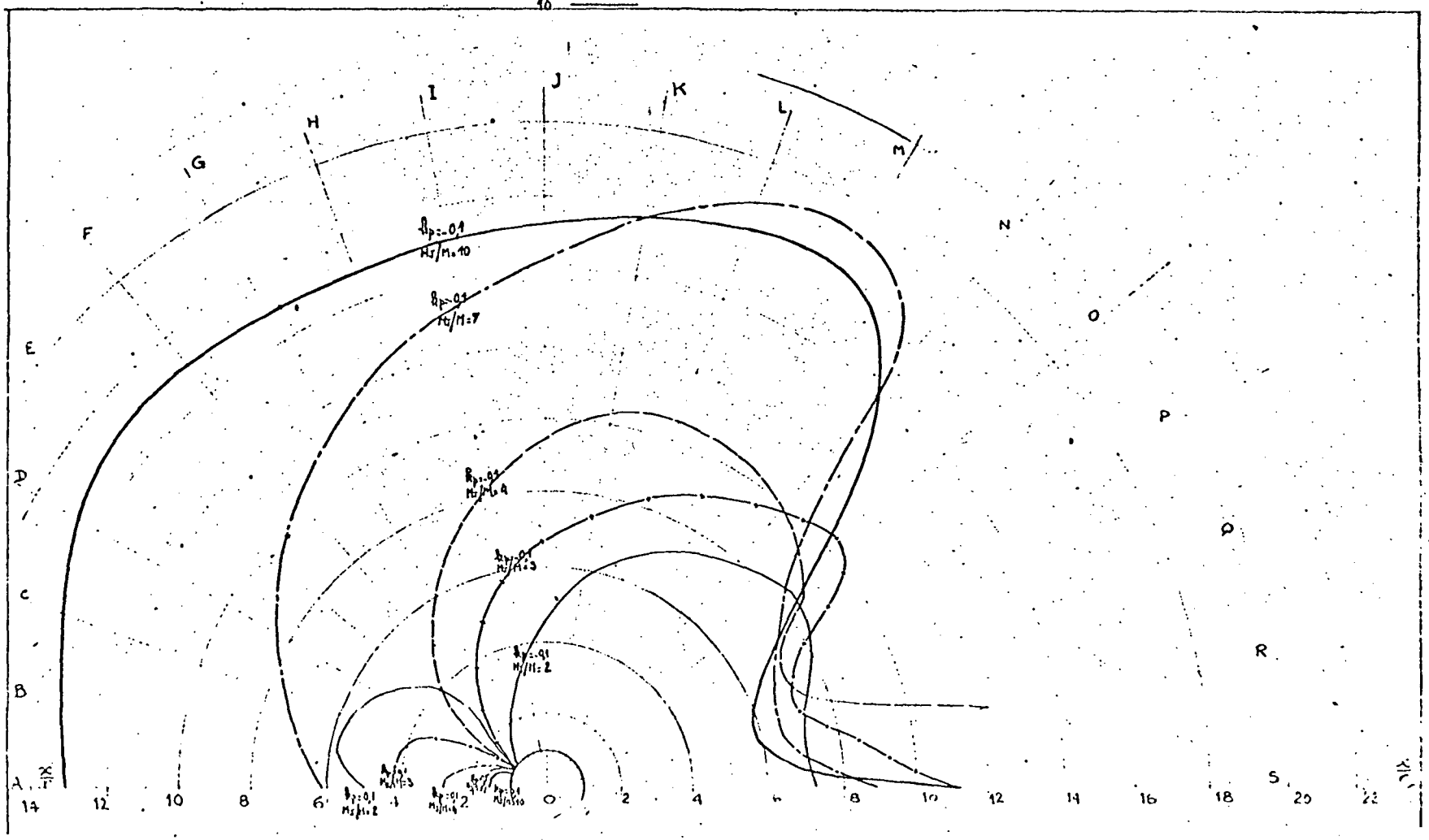

Figure 75. Jet interaction.

ONERA | | PV 1/253 GY fasc 1/5 | | DATE: 11.1967 | lancha: 76

$M = 0{,}09$ ($V = 30$ m/s) $\frac{M_j}{M} = 10$ ——— $\frac{M_I}{M} = 2$ —·—·—

Effect of jet velocity.

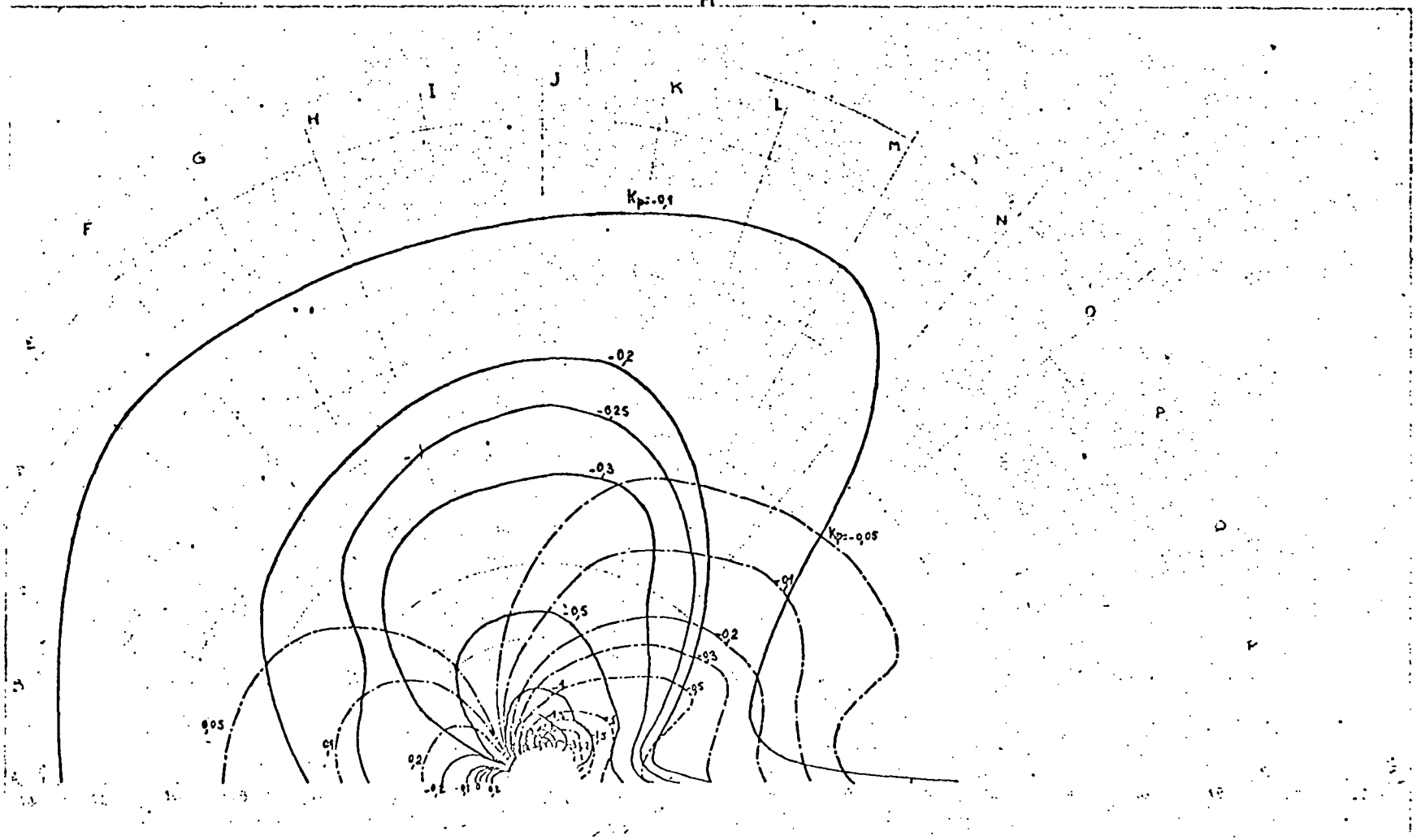

Figure 76. Jet interaction.

LIFT AND PITCH MOMENT RELATED TO THE INTEGRATION SURFACE

N° Point	M	$\frac{M_j}{M}$	S = 1,251 m²	l = 1,790 m	S = 0,588 m²	l = 1,230 m	S = 0,157 m²	l = 0,645 m
			Δ 100 C_z	Δ 100 C_m	Δ 100 C_z	Δ 100 C_m	Δ 100 C_z	Δ 100 C_m
921	0,09	0	0	0	0	0	0	0
922		2	- 4,6	0,8	- 9,1	2,1	- 26,6	6,6
923		3	- 8,4	0,9	- 15,8	2,1	- 41,0	5,8
924		4	- 12,1	1,1	- 21,4	2,1	- 53,1	5,4
925		7	- 17,3	0,2	- 27,6	0,3	- 54,9	1,4
926		10	- 20,8	- 0,5	- 29,2	- 0,7	- 48,3	- 0,5
927		11,11	- 23,1	- 0,8	- 30,7	- 1,1	- 48,1	- 1,2
928		7	- 19,1	- 0,2	- 27,8	0,1	- 53,8	0,8
930	0,18	0	0	0				
931		2	- 5,5	1,0				
932		3	- 8,4	1,2				
933		4	- 11,5	1,2				
934		5	- 13,7	0,9				
935		5,55	- 15,1	0,7				
936		4	- 12,0	1,2				
937	0,27	0	0	0				
938		2	- 4,2	1,0				
939		3	- 7,3	1,1				
940		3,3	- 8,1	1,1				
941		3,7	- 9,4	1,3				
942		2	- 5,1	0,9				

Commas represent decimal points.

Figure 77.

LIFT AND PITCH MOMENT RELATED TO THE DISCHARGE SECTION OF THE JET

$$S = \frac{\pi d^2}{4} = 0{,}0113\ m^2 \qquad l = d = 0{,}12\ m$$

N° Point	M	$\frac{M_j}{M}$	Integration surface 1,251 m^2		Integration surface 0,588 m^2		Integration surface 0,157 m^2	
			ΔC_z	ΔC_m	ΔC_z	ΔC_m	ΔC_z	ΔC_m
921	0,09	0	0	0	0	0	0	0
922		2	-10,2	26,4	- 9,4	22,4	- 7,2	9,9
923		3	-18,6	29,7	-16,4	22,4	-11,4	8,7
924		4	-26,8	36,3	-22,3	22,4	-14,8	8,1
925		7	-38,4	6,6	-28,8	3,2	-15,2	2,1
926		10	-46,1	-16,5	-30,4	- 7,5	-13,4	-0,7
927		11,11	-51,2	-26,4	-32	-11,7	-13,4	-1,8
928		7	-42,4	- 6,6	-29	1,1	-15,0	0,1
930	0,18	0	0	0				
931		2	-12,2	33,0				
932		3	-18,6	39,6				
933		4	-25,5	39,6				
934		5	-30,4	29,7				
935		5,55	-33,4	23,2				
936		4	- 26,6	39,6				
937	0,27	0	0	0				
938		2	- 9,3	33,0				
939		3	-16,2	36,4				
940		3,3	-18,0	36,4				
941		3,7	-20,8	43,0				
942		2	-11,4	29,7				

Commas represent decimal points.

Figure 78.

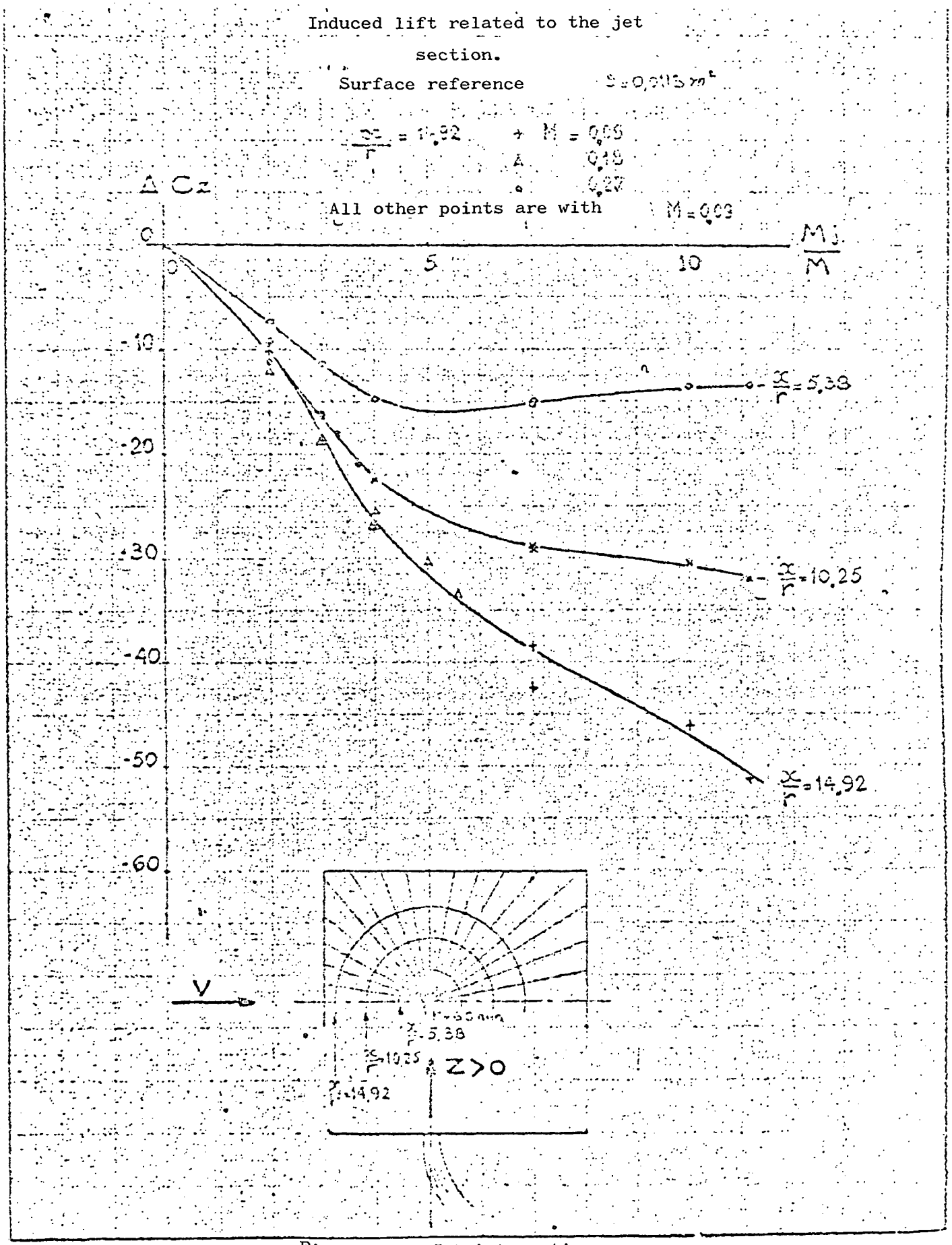

Figure 79. Jet interaction.

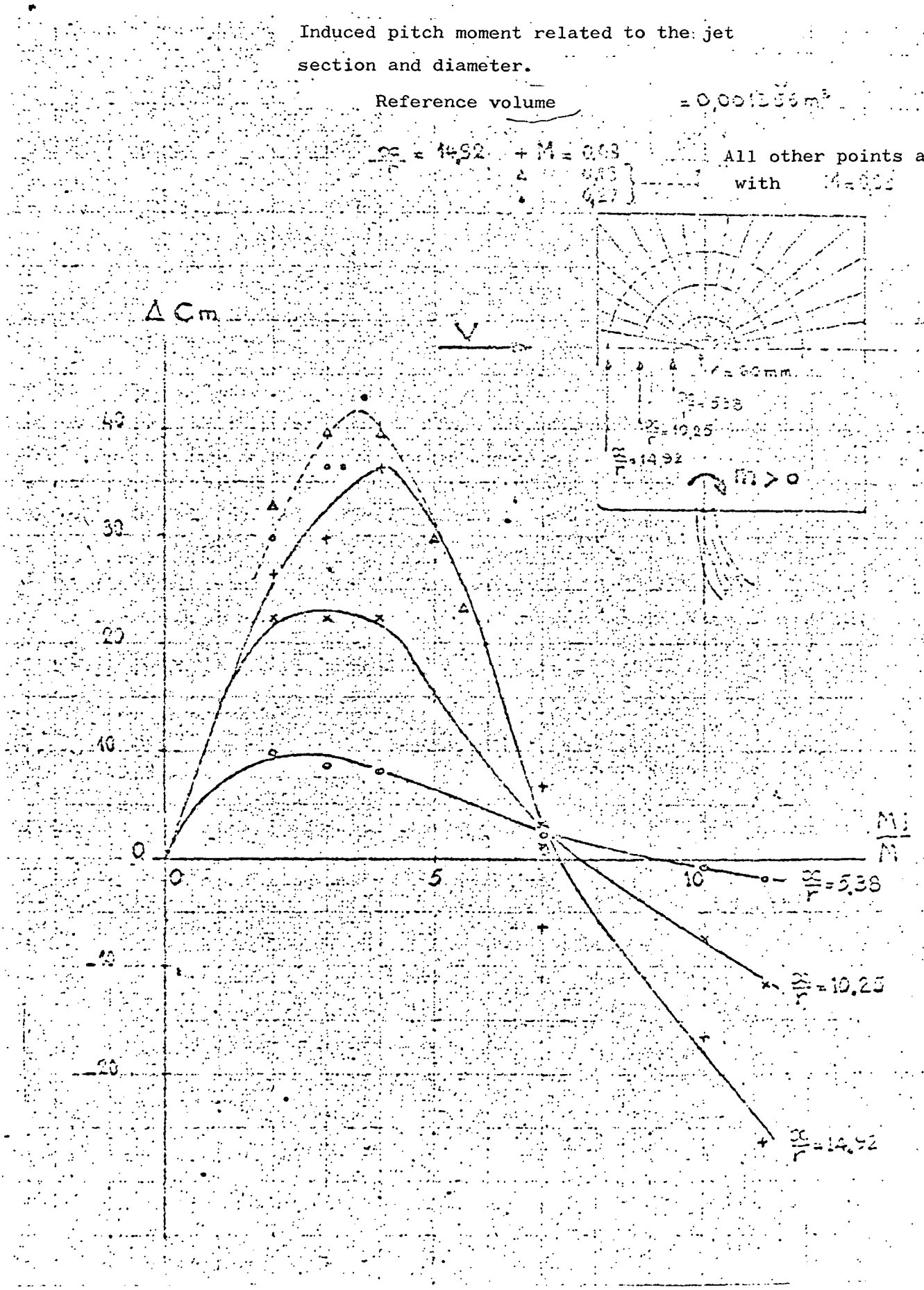

Figure 80. Jet interaction.

Translated for the National Aeronautics and Space Administration
under contract No. NASw-2038 by Translation Consultants, Ltd.,
944 South Wakefield Street, Arlington, Virginia 22204.